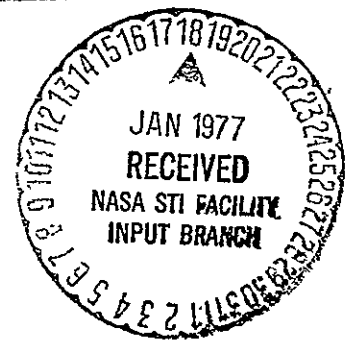# Analysis Of Rocket Engine Injection Combustion Processes

Final Report 31531 F-1
Contract NAS 8-31531
November 1976

Prepared For:

NASA

George C. Marshal Space Flight Center

Marshall Space Flight Center, Alabama 35812

By:

J.W. Salmon

Aerojet
Liquid Rocket
Company

FINAL REPORT

ANALYSIS OF ROCKET ENGINE INJECTION
COMBUSTION PROCESSES

NOVEMBER 1976

BY

J. W. SALMON

AEROJET LIQUID ROCKET COMPANY
SACRAMENTO, CALIFORNIA   95813

PREPARED FOR

· NATIONAL AERONAUTICS AND SPACE ADMINISTRATION

GEORGE C. MARSHALL SPACE FLIGHT CENTER
CONTRACT NAS 8-31531
K. W. GROSS, COR

FOREWORD

This report was prepared for the NASA George C. Marshall Space. Flight Center under Contract NAS 8-31531, by Aerojet Liquid Rocket Company (ALRC), Sacramento, California. The NASA Contracting Officer Representative was Mr. K. W. Gross. The study was performed during the period July 1975 to September 1976.

The ALRC Project Manager for this study was Mr. David L. Kors, Manager, Analytical Design Section, Design and Analysis Department. Mr. Larry B. Bassham was the Program Manager responsible for all fiscal and contracting functions. Mr. Jeffery W. Salmon served as Project Engineer, Principal Investigator, and the author of this program final report. The author is grateful for the valuable technical support offered by Mr. David Saltzman during the Task II development of a new mixing methodology for the LISP subprogram of the DER computer model.

TABLE OF CONTENTS

LIST OF TABLES

LIST OF FIGURES

List of Figures (cont.)

List of Figures (cont.)

I   SUMMARY

The scope of this program was to include a thorough critique of the JANNAF sub-critical propellant injection/combustion process analysis computer models and application of the models to correlation of well documented hot fire engine data bases. These programs are the Distributed Energy Release (DER) model for conventional liquid propellant injectors and the Coaxial Injection Combustion Model (CICM) for gaseous annulus/liquid core coaxial injectors. The critique would identify model inconsistencies while the computer analyses would provide quantitative data on predictive accuracy. The program was comprised of three tasks; Task I - Computer Program Review and Operation, Task II - Analysis and Data Correlations, and Task III - Documentation.

There were three objectives of Task I. (1) Critique of the DER and CICM Computer Programs, (2) Correction of coding errors, updating of inadequate formulations, and addition of diagnostic printout statements, and (3) Identification of inconsistencies between the analysis computer programs and the JANNAF prediction procedures documented in CPIA 246. The results of the DER and CICM reviews are comprehensively reported in Appendices A and B, respectively. Complete summaries of the corresponding conclusions and recommendations of the reviews are contained in Section III, Computer Program Review and Operation. There were two major conclusions resulting from the DER review. First, the intended predictive accuracy of the JANNAF rigorous performance evaluation procedure (to within 1 percent for predicted specific impulse) is, in general, currently out of the question for a priori performance prediction with DER. Secondly, the DER analysis originally planned to be conducted during program Task II should rather be concerned with improvement of a DER technical shortcoming. The primary conclusion of the CICM review was that the applicability and accuracy of the model is currently limited by the absence of an intra-element coaxial gas/liquid mixing model. This limitation not only makes the mixing loss calculation dependent on correct application of empirical cold flow mass distribution data, but hinders the development of general program coaxial jet atomization and drop size constants that control the program vaporization calculation.

I   Summary (cont.)

There were originally three primary objectives of Task II. (1) Provide
information on the present prediction capabilities of the JANNAF DER and CICM
injection-combustion computer analysis techniques, (2) Identify conditions
where reliable predictions can be obtained, and (3) Identify areas requiring
further improvement and research. The CICM analysis task was completed as
originally planned. The results of the CICM analysis are reported in Section
IV, CICM Analysis and Data Correlations. The CICM analysis was performed by
establishing the existing M-1 H_2/O_2 engine data base, executing a nominal
operating point CICM analysis, correlating the CICM prediction with the test
data, conducting two off-nominal test point analyses to determine the influence
of velocity ratio changes on injector performance, and identifying prediction
ranges and required model improvements. The CICM analysis results verified
the accuracy of the CICM vaporization model for the case where injector intra-
element mixing losses are negligible.

The objective of the DER Phase of Task II was altered based on the
recommendations of the Task I DER computer model review. Improvement of the
LISP subprogram ZOM plane mass distribution and mixing methodology was
selected as the new Task II DER goal. This task was conducted in four parts.
(1) An a priori ZOM plane prediction model was formulated that accounts for
combustion gas acceleration effects on inter-spray fan mixing, (2) A subscale
test data base was developed for analysis and the ZOM model was used to predict
mixing performance for each test, (3) The model predictions were correlated
with the hot fire test results, and (4) Recommendations for continuation of
model development were formulated. The primary discovery of this initial
ZOM model development work was that a physically mechanistic near-zone model
that will predict the ZOM mixing plane location must account for both gas
acceleration and reactive stream ("blowapart") forces on droplet spray fan
formation and mixing.

Task III of the program resulted in eleven monthly status letters
and this comprehensive final report containing explicit recommendations for
improvement of the JANNAF performance prediction computer programs. The

I   Summary· (cont.)

English system of units has been exclusively employed in·this report since
SI units have yet to be adapted to the JANNAF system .of computer programs.
The program COR has concurred with and approved this choice.

II   INTRODUCTION

The ICRPG (now JANNAF) Performance Standardization Working Group was formed in 1965 for the purpose of improving and recommending methodology for the analytical and experimental evaluation of the performance of liquid propellant rocket engines. In 1968, the working group published a Performance Evaluation Manual (Ref. 1) which described the procedures and computer programs recommended for the prediction, correlation, and extrapolation of the performance of liquid propellant thrust chambers. The scope of this first effort was limited to assembling, into a compatible overall system, the best relevant analytical and experimental techniques existing throughout the industry at that time. During this effort, it was concluded that the energy release phenomenon could not be adequately described or predicted by existing analytical techniques. As a result, an interim empirical procedure was adopted.

Since this first attempt at achieving a standard performance evaluation model, a semi-empirical, but mechanistic, computer model has been developed for the analysis of the liquid injector-combustion chamber energy release process. This model, termed the Distributed Energy Release (DER) model (Ref. 2) has reached the stage of development where it is being incorporated into the Improved JANNAF Performance Evaluation Methodology (Ref. 3). DER is composed of two major programs which link the atomization, vaporization and mixing processes within the combustion chamber. The first is the Liquid Injector Spray Patterns (LISP) program which calculates propellant mass and mixture ratio distributions at a specified chamber cross-sectional plane (ZOM) downstream of the injector face. The second is the Stream Tube Combustion (STC) program which calculates the propellant vaporization, reaction and acceleration from the LISP specified collection plane to the combustion chamber throat plane. Additionally, a third JANNAF recommended program has been developed for the specialized case of injector elements containing central circular orifice liquid propellant injection surrounded by annular gaseous injection. The Coaxial Injection Combustion Model (CICM) (Ref. 4) is designed to replace the DER LISP subprogram for this injector type.

II   Introduction (cont.)

While these programs provide analytical methods for evaluation of the energy release process, the program developers have identified analysis parameters which are critical to the accuracy of the resulting performance predictions. These include specification of propellant mass median droplet diameters and the LISP Spray distribution correlation coefficients, which have been established over limited ranges of element type and design conditions. Additional studies using DER have shown that the specification of the LISP-STC interface plane (ZOM) is also critical to the end performance prediction.

The objective of this program was to develop quantitative data on the present prediction capabilities of the JANNAF sub-critical propellant injection/combustion process analysis programs (LISP, STC, and CICM). The desired program end product was identification of conditions for which reliable predictions could be conducted and areas which need further improvement and research.

Future attainment of a broader overall objective was continued with conductance of the Injection Processes Program. The JANNAF Performance Standardization Working Group has the purpose of improving methodology for analytical design modeling of rocket engines. The current and future economics of rocket development do, and will certainly, make it imperative that cost saving analytical methods replace more expensive hardware development and test programs. Of course, such tools are only cost effective if they model the applicable physical processes realistically and accurately. The Injection Processes program and other related efforts have provided information on the state of JANNAF model development through application to real rocket engine systems. During this program the CICM computer program was used to correlate performance data obtained with the M-1 1 million lbf. hydrogen/oxygen engine. The DER computer program has been successfully applied to design analysis of the Orbital Maneuvering System (OMS) engine for Space Shuttle, the Improved Transtage Injector Program (ITIP) currently being conducted by the USAF, and an advanced development monomethyl hydrazine/

fluorine-oxygen engine tested by the NASA. Each of these efforts has resulted in constructive criticism of the computer models that, when applied, results in further advancement of the state-of-the-art of rocket engine analytical design. The final end product of programs that support the JANNAF predictive methodology will someday be a capability to eliminate major hardware development technology programs through verified standardized analysis techniques. A superior development procedure would be constituted of initial JANNAF model analysis, fabrication and test of the full scale engine, re-analysis, full scale hardware modification, and final engine verification test. The Injection Processes. Program has made this seemingly optimistic goal a bit more achievable through a comprehensive evaluation of the DER and CICM models.

III COMPUTER PROGRAM REVIEW AND OPERATION

There were three primary objectives of the first program task.

(1) Critique of the JANNAF DER and CICM programs,

(2) Correction of coding errors, updating of inadequate formulations, and addition of diagnostic printout statements, and

(3) Identification of inconsistencies between the analysis computer programs and the JANNAF prediction procedures described in CPIA 246 (Ref. 3).

The complete results of the DER and CICM reviews are contained in Appendices A and B, respectively, of this report. The computer programs are introduced and their functions in the JANNAF performance prediction procedure briefly described in the following paragraph. A complete summary of the findings and corresponding recommendations of the computer model reviews follows the program descriptions.

A flow-chart showing the DER and CICM programs and their relationship to the JANNAF Two-Dimensional Kinetic (TDK) Computer Program (Ref. 5) is illustrated in Figure 1, taken from Ref. 3. DER is composed of LISP and STC, two major programs that link atomization, vaporization, and mixing processes within the combustion chamber. The Liquid Injector Spray Patterns (LISP) program calculates propellant mass and mixture ratio distribution at a specified chamber cross-sectional plane (termed ZOM) downstream of the injector face. LISP was developed for conventional (i.e., circular orifice) liquid/liquid injection elements. The Stream Tube Combustion (STC) program calculates propellant vaporization, reaction, and acceleration from ZOM to the combustion chamber throat plane. STC can provide direct computer input data for the TDK program that continues the multiple stream tube analysis through the supersonic expansion process. CICM replaces the LISP program for the analysis of gas/liquid coaxial elements. CICM is a highly specialized program that has currently only been applied to the analysis of injection elements with a central liquid O_2 circular core surrounded by a gaseous H_2 or H_2/O_2 combustion gas mixture annulus.
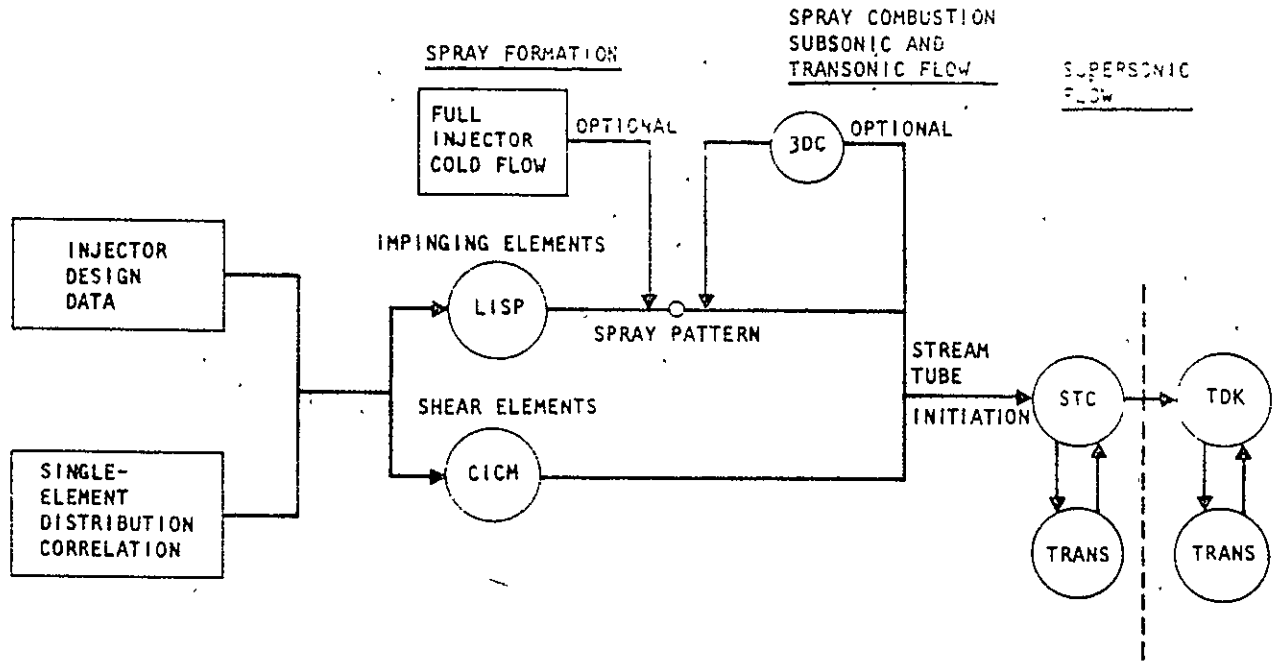
FIGURE 1.   JANNAF INJECTION AND COMBUSTION ANALYSIS PROCEDURES LOGIC STRUCTURE

III   Computer Program Review and Operation (cont.)

A.   DER. Computer Model Review Recommendations and Conclusions

Four subtasks were accomplished during the DER review.

(1)   Identification and Correction of Coding Errors,

(2)   Addition of Diagnostic Comment Cards and Print-Out Statements,

(3)   Identification of Inadequate Formulations and Model Technical Formulations, and

(4)   Review of the JANNAF Performance Prediction Procedures (CPIA 246) with Regard to Use of DER.

The review is applicable strictly the DER subcritical K-Prime version described in Ref. 2. The corresponding user's manual referred to in this report is Ref. 6.

The third subtask listed above was emphasized during the review for two reasons. The initial results of the review indicated that DER still requires major technical improvements and therefore subtasks (1) and (2) were considered to be of less current interest. Secondly, SDER, a new "standardized" version of DER (Contract FO 4611-75-C-0055),was developed concurrently with completion of this program. It was intended that the improved DER model be influenced by the findings summarized in this report; therefore the discovery of DER technical formulation shortcomings was considered to be of prime importance.

A major conclusion of the DER review was that the DER analysis originally planned to be conducted during program Task II should rather be concerned with improving a DER technical shortcoming. It seemed inappropriate to conduct the analysis with a computer model that possessed vaporization

and mixing models containing several questionable solution formulations, as summarized in the following paragraphs concerning review recommendations. Improvement of the LISP ZOM plane mass distribution methodology was selected as the new Task II DER analysis goal. The current status of the mixing model improvement work is described in Section V of this report. Key recommendations and conclusions, resulting from the DER review results detailed in Appendix A, are listed in the following four paragraphs corresponding to the previously described review subtasks.

1.   Identification and Correction of Coding Errors

a.   LISP Subprogram

(1)   An unsymmetrical pie section input problem was identified for the LISP program. It should be eliminated by adjusting the collected pie section mass flowrate to $\theta/360$ of the total injected flow of each propellant.

(2)   Inconsistencies between published DER drop size equations and those actually existent in the DER code must be resolved.

(3)   The DER code should be changed to eliminate a mass flux calculational error for triplet elements caused by an improper rotation of the ZOM collection plane around the normal x axis.

(4)   The ZOM mass distributions should consider the influence of baffle height.

b.   STC Subprogram

(1)   The STC program limits the number of radial and circumferential mesh lines to twenty; this limitation should be noted in the DER user's manual, or preferably removed.

2.   Addition of Diagnostic Comment Cards and Printout Statements

        The recommended statement additions and improvements are presented in Section B of Appendix A.

3.   Identification of Inadequate Formulations and Model Technical Shortcomings

        a.   Drop Size Prediction

        (1)   The inconsistencies cited, between referenced drop size correlations and those appearing in the DER code, must be resolved.

        (2)   It is recommended that the DER drop size equations be comprehensively reviewed with respect to available atomization correlations and their impact on DER performance prediction accuracy. A task performed during the SDER development program was to be concerned with such a review, although the results have not been published.

        (3)   Interim to release of SDER, all DER drop sizes should be user input and justified.

        b.   ZOM Plane Selection

        (1)   The ZOM point source flow assumption should be tested empirically. That is, it should be determined if the LISP spray distribution coefficients are a function of the cold flow collection plane distance.

        (2)   The ZOM mass distribution methodology should account for combustion effects such as gas acceleration and reactive stream separation forces. A proposed model approach is detailed in Section V of this report.

.   (3)   The LISP spray coefficient matrix should be expanded if the ZOM technique is retained in DER.

c.   DER Vaporization Sensitivity Study

(1)   The implications of the work of Bracco (Ref. 7) with respect to DER vaporization modeling should be evaluated.

(2)   The DER K-Prime vaporization model insensitivity to chamber pressure should be investigated. The argument suggested in Appendix A to be the source of this error should be evaluated.

(3)   The DER integration technique droplet downstream station velocity error should be eliminated. Additionally, the Euler predictor-corrector technique should be evaluated through a study using different calculational step sizes and number of corrective iterations. The possibility of developing a more efficient integration technique should be investigated.

(4)   The results of this study and the work of Bracco both indicate the importance of the droplet drag coefficient (C_D) assumption. The drag coefficient literature should be reviewed and the selected DER drag coefficient formulation justified.

(5)   The DER vaporization model should account for droplet heatup.

(6)   The DER user manual and CPIA 246 should include an expanded section on droplet size distribution input selection.

d.   Near-Zone Combustion and Monopropellant Flame Considerations

(1)   It is recommended that DER incorporate a monopropellant flame model for reasons cited in Section C.4. of Appendix A.

e.   Combustion Gas Acceleration and Reactive Stream
Separation (RSS) Effects on Cold Flow Mass
Distribution

(1)   It is recommended that a RSS model be
considered for DER.

(2)   The initial development of an a priori
ZOM plane selection methodology (See Section V) should be brought to fruition.

f.   Turbulent Mixing Model

(1)   The characterization of turbulent mixing
effects in DER would comprise a large step toward providing DER with the
desired a priori prediction capability. It is recommended that such a model
be considered for DER.

g.   Development of an A Priori DER Mixing Model

(1)   It is recommended that the current LISP ZOM
model be improved by incorporating the influences of combustion gas accelera-
tion, reactive stream separation, and turbulent mixing. As previously men-
tioned, an a priori ZOM calculational technique is also required. This topic
is expanded in Section C.7. of Appendix A.

4.   Inconsistencies Between JANNAF Procedures and DER
Computer Program Operations

The primary conclusion is that the intended predictive
accuracy of the JANNAF (DER) rigorous procedure (to within 1 percent for
predicted specific impulse) is currently out of the question for a priori
performance prediction. This directly relates to the program decision to
forego the originally planned Task II DER analysis and concentrate, instead,
on improvement of the ZOM plane mass distribution methodology.

III   Computer Program Review and Operation (cont.)

   B.   CICM Computer Model Review Recommendations and Conclusions

      The CICM review was accomplished in three subtasks.

      (1)   Identification of Operational Problems Including a Code
Review and Inclusion of Diagnostic Print-Out Statements,

      (2)   Identification of Inadequate Formulations and Model
Technical Shortcomings, and

      (3)   Review of the JANNAF Performance Prediction Procedure
(CPIA 246) with Regard to the Use of CICM and Identification of Inconsistencies.

The review is applicable to the CICM version described in Ref. 4, which also
contains the user's manual referenced continually in this report.

      The review was initiated by executing the program documented
sample case and attempting to interface the program output with the STC
subprogram of DER, as recommended in CPIA 246 for gas/liquid coaxial injector
rigorous performance analysis. It was determined that the current CICM
interface routine, DERINI, was incomplete and punched several improperly
formated cards for input to the STC subcritical K-Prime version. First
priority, during the review, was given to development of a new CICM/STC
interface procedure because of the need for an accurate and cost-effective
method of interfacing CICM and STC during the program Task II CICM analysis.
The resulting new procedure is detailed in Section C.3. of Appendix B. The
key recommendations and conclusions resulting from the CICM review results
detailed in Appendix B are listed in the following three paragraphs corres-
ponding to the previously described review subtasks.

      1.   Coding Errors and Diagnostic Statements

      It is recommended that the CICM calculational problem
that results in periodic "dropping" of drop size groups from the calculation
be investigated.

2.   Identification of Inadequate Formulations
        and Model Technical Shortcomings

The identification of inadequate CICM formulations and technical shortcomings was considered to be the next most important review task after improvement of the CICM interface procedure. CICM is a relatively new JANNAF program that has not been used extensively, except by the developers of the model. Therefore, it was considered important that basic model assumptions and analysis techniques be critically evaluated. The recommendations and conclusions resulting from the CICM technical formulations review are summarized below.

a.   A review of the CICM stripping rate correlation should be conducted. The derivation of the current, or any proposed alternate correlation, should be substantiated and be made open to critical review.

b.   A review of the CICM drop size correlation should be conducted. Such a study could also investigate the sensitivity of coaxial injector performance to the predicted jet mass median drop size. This would allow determination of the performance prediction uncertainty due to the availability of many different drop size correlation equations.

c.   The drop size distribution tabulated at the end of a CICM run is only the summation of several constant mass median diameter groups; each group being calculated over a particular axial step. This resultant distribution is quite different than a drop size group calculated with distributions typically used to model rocket combustor sprays (e.g., Nukiyama-Tanasawa, Logarithmic-Normal, etc.). It is recommended that the significance of this CICM model simplification be evaluated.

d.   It is strongly recommended that the CICM technique for accounting for intra-element mixing be improved. If the use of single element cold flow data to specify the intra-element mass distribution is continued, a standard measurement technique should be developed. A standard

methodology for interpreting and inputting the data to CICM is also required. Preferably, an intra-element mixing model should be developed for CICM. Applicable models have been derived from experiment for gas/gas coaxial element mixing. The first step in adapting such models would be to determine the feasibility of applying a gas/gas mixing model to the solution of gas/ liquid mixing.

     e.   All JANNAF engine analyses should record estimated manifold maldistribution performance losses, to build up a reference data base.

    3.   Inconsistencies Between JANNAF Procedures
        and Program Operations

     The new CICM/STC interface procedure was written during this review subtask. The recommendations and conclusions resulting from the review of CICM's role in the JANNAF performance procedures are listed below.

     a.   The original provision of the CICM/STC interface was for the supercritical DER program version. The new CICM/STC interface procedure described in Section C.3. of Appendix B should be used for sub-critical propellant analysis. This procedure should also be adopted for use in the new "standardized" DER program currently being developed.

     b.   The CICM and STC programs should be interfaced at a chamber axial plane where all the calculated oxidizer drop size groups have been heated to the chamber "wet bulb" temperature.

     c.   A standard JANNAF procedure or technique should be developed to predict single coaxial element intra-element mass distribution.

     d.   A procedure should be developed for allowing for the effect of diffusion mixing on face plane measured manifold mass distributions.

III   Computer Program Review and Operation (cont.)

e.   An accurate CICM mass distribution analytical model or empirical approach is required to allow JANNAF standard atomization coefficients (C_A and B_A) to be backed out from coaxial injector hot fire data.

The original objectives of Task II were: (1) Provide information on the present prediction capabilities of the JANNAF DER and CICM injection-combustion computer programs; (2) Identify conditions where reliable predictions can be obtained; and (3) Identify areas requiring further improvement and research. The CICM phase was completed as originally planned, while the DER phase of the task was rescoped (see Section V). The CICM model was applied to correlation of characteristic exhaust velocity efficiency (η_{c*}) for three tests conducted with the M-1 pressure fed 600,000 lbf (at 550 psia chamber pressure) hydrogen/oxygen engine. The CICM analysis was limited to tests with subcritical liquid oxygen inlet conditions. Excellent agreement was obtained between $\eta_{c*_{TEST}}$ and $\eta_{c*_{PRED}}$ from the JANNAF simplified prediction methodology for two of the three tests analyzed. The results of the analysis have verified the accuracy of the CICM model for the case where injector intra-element mixing losses are negligible.

A.   M-1 Engine Experimental Data Base

The data base selected for the analysis and correlation of the CICM computer program was that of the M-1 thrust chamber developed by ALRC under NASA Contracts NAS 3-2555 (Ref. 8) and NAS 3-11214 (Ref. 9). The M-1 engine was designed to utilize liquid oxygen/liquid hydrogen propellants and deliver 1,500,000 of thrust when operating at its nominal design conditions of 1000 psia chamber pressure and 5.49 mixture ratio. During development, the thrust chamber was tested with LO_2/GH_2 propellants with a low area ratio ablative combustion chamber over a range of chamber pressure (550-1050 psia), mixture ratio (4-6), and hydrogen inlet temperature (80-130°R). The CICM data base met all the pre-defined program requirements for the following eight reasons:

1.   Conventional injector element applicable to CICM (gas/liquid coaxial);

2.   Capable of direct modeling with CICM/DER;

3.   Subcritical propellant conditions (P_c = 550 psia);

4.   Propellants of future interest (O_2/H_2);

5.   Low area ratio test configuration (ε = 2:1);

6.   Simple wall boundary conditions (no mass addition, minimal fuel film cooling of 1/2 percent of the total flow rate);

7.   Test data at nominal and off-nominal operating conditions (O/F, hydrogen density variations);

8.   Element to element mass distribution cold flow data.

Detailed descriptions of all the M-1 test hardware, facilities, and data measurement techniques are contained within the JANNAF-Simplified Performance Prediction narrative of Appendix C. The S/N 012 injector analyzed during the study is pictured in Figure 2. The injector contained 3,248 elements with gaseous hydrogen being injected annularly around the oxidizer. A row of 360 orifices drilled through the porous rigimesh face were located around the injector periphery and provided the chamber wall film cooling. Approximately 3.7 percent of the total fuel flow rate was used for chamber wall film cooling. Total fuel element flow rate was 89.8 percent of the thrust chamber fuel flow-rate with a baffle fuel film cooling flow percentage of 3.9 percent. The remaining 2.6 percent of the fuel flowed through the rigimesh injector face. The coaxial element consisted of two basic components which were threaded together. An oxidizer tube was recessed within the fuel sleeve producing a fuel annulus between the two parts. The oxidizer tube was flared at a fifteen degree half angle and was recessed 0.231 inches from the injector face. Elements were arrayed in 33 concentric rows. The low area ratio combustion chamber used for testing with the M-1 injector was comprised of an outer steel shell and an inner ablative liner (tape wrapped silica-reinforced phenolic). The assembled combustion chamber (See Figure C-4 of Appendix C) consists of an upper fuel torous and a lower conical combustion chamber.

The test data that was reduced during the task data evaluation effort is tabulated in Table I. Nomenclature for Table I is shown in Figure C-1 of Appendix C. The three tests that were selected for CICM analysis are detailed in Table II. Test 009 was at the nominal operating point. Test 010 was analyzed to investigate the influence of mixture ratio on performance. Test 016 was analyzed to correlate the effect of injection velocity ratio change due to
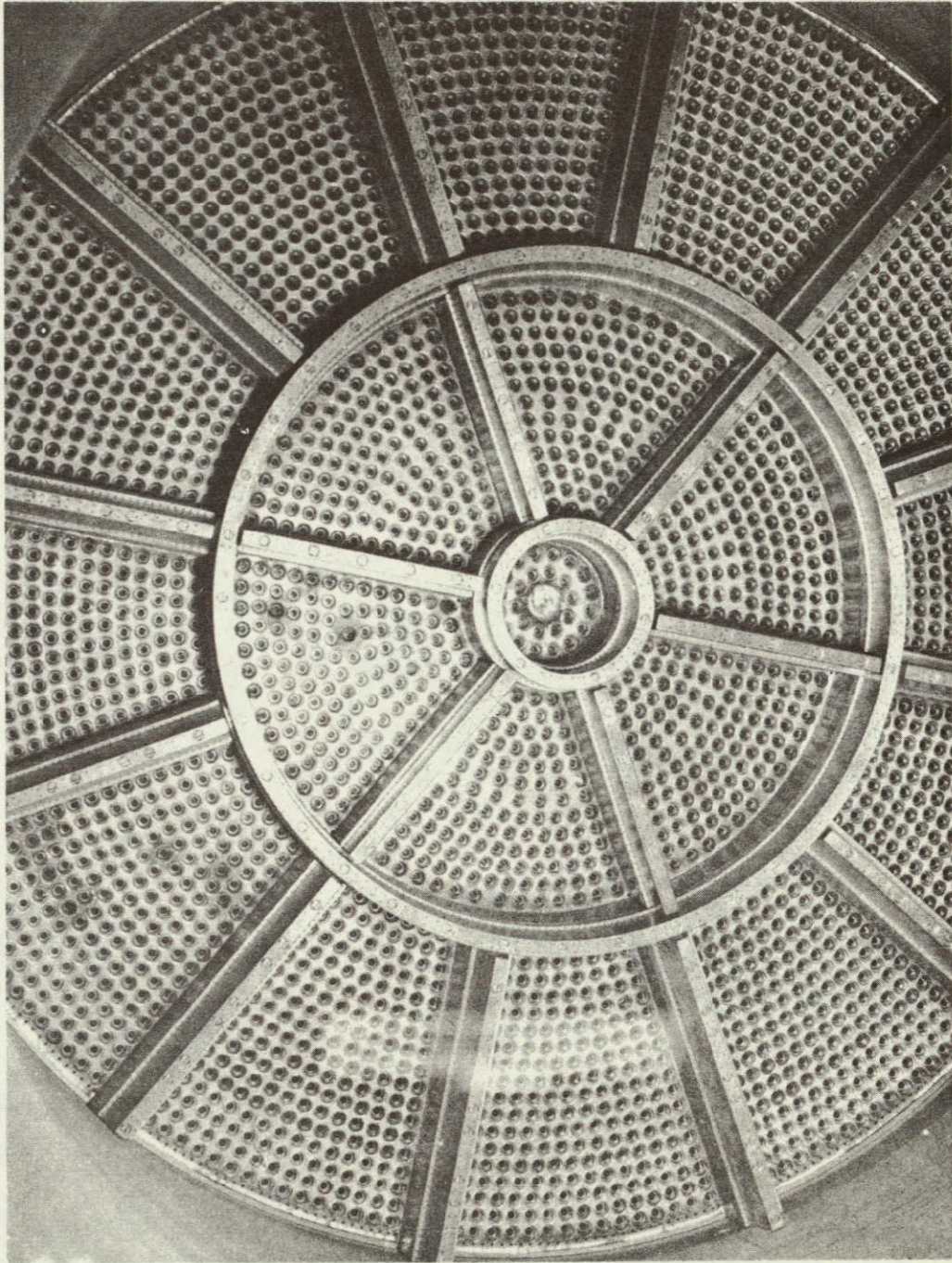
FIGURE 2.   INJECTOR S/N 012 SHOWING FACE AND BAFFLE PATTERN

-20-

TABLE I. SEA LEVEL SUB-CRITICAL TEST DATA

Test No.	Summary Time Start (sec)	Stop (sec)	Duration (sec)	Throat Area Pre (in²)	Post (in²)	Chamber Pressure (psia)	O/F	Thrust Meas. (lbs)	Isp Meas. (sec)	W_o (#/sec)	W_F (#/sec)	$W_{F(GH_2)}$ (#/sec)	W_{FT} (#/sec)	W_T (#/sec)
007	44.2	44.7	44.72	707.370	711.860	582.8	4.87	492840	305.0	1340.7	249.4	26.0	275.3	1616.0
009	44.3	44.8	44.81	728.269	735.994	556.6	5.46	495409	300.5	1393.4	220.2	35.0	255.2	1648.6
010	46.8	47.3	47.33	735.994	736.308	572.0	4.04	510096	310.4	1317.6	296.4	29.6	325.9	1643.6
014	46.8	47.3	47.38	706.495	722.048	541.1	5.30	481765	303.5	1335.4	213.4	38.6	251.9	1587.3
016	45.0	45.5	45.56	722.048	727.902	567.9	5.53	501304	301.7	1407.1	209.0	45.6	254.6	1661.7
017	46.3	46.8	46.89	727.902	728.368	571.0	4.76	506116	307.5	1360.1	245.7	40.1	285.7	1645.8
019	44.3	44.8	44.89	733.644	736.391	576.0	5.15	516590	304.4	1421.3	236.1	39.9	276.1	1697.3
020	46.5	46.5	46.5	736.391	748.222	569.4	5.07	510642	298.7	1428.1	240.0	41.6	281.5	1710.0

Test	PFT (psia)	PFFM-2 (psia)	PF_{MIX}-2 (psia)	PFTCV-1 (psia)	PFTCV-2 (psia)	PFJ-3A (psia)	TFFM (°R)	TFTCV-2 (°R)	TFJ (°R)	POT (psia)	POFM (psia)	POTCV-1 (psia)	POTCV-2 (psia)	POJ-2A (psia)	TOFM (°R)	TOTCA-2 (°R)	TOJ (°R)	PC4B-1 (psia)	PC4B-2 (psia)
007	805	731	722	719	703	624	44	102	84	749	729	729	724	680	171	186	173	482.4	482.6
009	808	748	740	741	720	619	44	117	97	750	732	729	737	674	168	181	169	464.4	463.8
010	878	773	761	763	742	638	45	89	82	749	737	734	737	685	173	177	174	477.5	476.9
014	832	778	758	763	746	523	45	116	110	730	720	717	705	662	173	180	174	451.5	450.1
016	872	823	805	808	788	646	44	127	122	769	750	746	734	686	173	181	174	474.0	472.3
017	897	831	804	812	787	652	45	108	106	759	686	742	732	686	170	181	171	476.7	475.4
019	899	830	811	816	792	658	45	117	110	788	769	762	740	700	171	179	172	480.4	478.3
020	900	832	814	816	793	656	44	115	107	787	769	762	753	706	169	180	170	475.3	473.7

TABLE II

M-1 TESTS SELECTED FOR CICM ANALYSIS

TEST	W_O (1bm/sec)	W_F (1bm/sec)	T_O (°R)	T_f (°R)	O/F	P_c (psia)	V_F/V_O	ΔV (ft/sec)	ρ_F (1bm/ft^3)	η_{C*}
009	1393	255.2	169	97	5.46	524	18.2	310	1.45	.959
010	1318	325.9	174	82	4.04	538	16.2	264	2.16	.964
016	1407	254.6	174	122	5.53	534	25.8	456	1.0	.980

009   Nominal Conditions

010   Effect of Fuel Gas Density at Constant ΔV

016   Effect of ΔV

IV   CICM Analysis and Data Correlations (cont.)

hydrogen density variation.

B.   M-1 Coaxial Injector Analysis with JANNAF Simplified
       Prediction Procedure

The procedures and results of the CICM analysis of the M-1
engine tests are summarized in the following three subsections, that describe
in turn: (1) calculation of test characteristic exhaust velocity efficiency;
(2) prediction of C* efficiency with the JANNAF simplified performance evaluation
tion methodology; and (3) determination of test measured C* uncertainties.
The JANNAF simplified prediction procedures described in CPIA 246 were utilized
to economize and speed the analysis.

Examination of the DER and CICM review results previously
presented in Section III can, admittedly, lead to the conclusion that the M-1
performance analysis described below has been conducted with inadequate models.
An important consideration was the fact that the M-1 thrust chamber design is
very similar to the J2-S design used to calibrate key CICM jet stripping rate
and drop size constants. (See Ref. 6 and J2-S sample case in CPIA 246). Also,
both the M-1 and J2-S engines posses extremely long chambers that eliminate
significant intra-element mixing losses. Therefore, the M-1 predictions were
not invalidated by assuming uniform intra-element mass distribution, as described
in a following paragraph. Additionally, using the STC subprogram of DER down-
stream of CICM was not considered an analysis weakness because STC utilizes
similar key vaporization model analytical techniques to those of CICM (e.g.,
both models use the same droplet drag coefficient model). It should be remem-
bered that a primary objective of the analysis was to verify that an independent
user of the CICM/STC JANNAF analysis methodology could obtain an accurate
performance prediction for a gas/liquid coaxial injector.

1.   Calculation of Test C* Efficiency

Test C* was calculated from the equation shown below,
taken from Section 2.1.2 of CPIA 245.

$$C^*_{TEST} = \frac{Pc_{eff} A_{T_{TEST}}}{\dot{M}_{T_{TEST}}} \qquad (1)$$

Pc_{eff} is the effective throat stagnation pressure, calculated from available chamber static pressure measurements. Two static pressure measurements were taken; at the Pc_5 and Pc_4 locations shown in Figure C-2 of Appendix C. The chamber combustion total pressure loss resulted from the CICM/STC computer run executed during the C* prediction analysis described in the next section. The CICM/STC calculated chamber static pressure profile correlated extremely well with the measured static pressures, as explained in Section IV.C.1. This correlation verified the CICM/STC calculated combustion (Rayleigh Line) total pressure loss. The test summary periods for analysis were selected to occur just prior to test FS2 so that the post-test ablative chamber throat diameter measurement would result in an accurate test throat area value.

Test C* efficiency is simply the ratio of the test C* to the theoretical ODE C* value at the test propellant inlet, mixture ratio, and chamber pressure conditions.

$$\eta_{C^*_{TEST}} = \frac{C^*_{TEST}}{C^*_{ODE}} \tag{2}$$

C* ODE was calculated with JANNAF TDK computer program (Ref. 5) at the test conditions indicated in Table III. The resulting test C* efficiencies are also shown in Table III.

2.   JANNAF Test C* Prediction

The JANNAF simplified performance prediction methodology described in Section 3 of CPIA 246 was utilized. Appendix C of this report contains a narrative of the application of the procedure to analysis of the selected M-1 tests and sample input for all the JANNAF computer programs executed. The predictive equation for C* is expressed in terms of efficiencies for the significant chamber loss processes.

$$\eta_{C^*_{Pred}} = \eta_{C^*_{HL}} \times \eta_{C^*_{TD}} \times \eta_{C^*_{KIN}} \times \eta_{C^*_{BL}} \times \eta_{C^*_{MIX}} \times \eta_{C^*_{VAP}} \tag{3}$$

TABLE III

TEST CONDITIONS FOR $\eta_{C*_{TEST}}$ CALCULATION

TEST	O/F	PC_{eff} (psia)	T_0 (°R)	T_f (°R)	H_{f_0} (cal/g-mole)	H_{f_f} (cal/g-mole)	$C*_{ODE}$ (ft/sec)	$C*_{TEST}$ (ft/sec)	η_{C*} TEST
009	5.46	514	169	97	−3027	−1827	7694	7376	.959
010	4.04	532	174	82	−2991	−1918	7960	7674	.964
016	5.53	534	174	122	−2991	−1733	7685	7529	.980

The purpose of the M-1 test data analysis was to verify the capability of the CICM model to calculate the $\eta_{C*_{MIX}}$ (mixing) and $\eta_{C*_{VAP}}$ (vaporization) efficiencies for a GH_2/LO_2 coaxial injector. The meaning of and the technique used to evaluate each of the efficiency terms are explained in the following six paragraphs.

a.   Heat Loss Efficiency $(\eta_{C*_{HL}})$

The chamber heat loss efficiency was assumed to be 1.0 for each test. This assumption was made for two reasons. (1) The thrust chamber wall was composed of an ablative silica-reinforced (tape-wrapped) phenolic that resulted in an effective adiabatic wall condition; and (2) Chamber heat loss to the injector face would be directly transferred to the propellants because of the plenum manifolds on the injector face backside.

b.   Two-Dimensional Flow Efficiency $(\eta_{C*_{TD}})$

The two-dimensional C* flow efficiency accounts for the reduction of the throat potential flow area due to inlet effects. The equation used is simply the inverse of the inviscid flow discharge coefficient.

$$\eta_{C*_{TD}} = \frac{\dot{M}_{ODE}}{\dot{M}_{TDE}} = \frac{1}{C_{D_{INV}}} \qquad (4)$$

The JANNAF ODE and TDE programs contained in TDK calculated the M-1 chamber $\eta_{C*_{TD}}$ value of 1.002 ($C_d = 0.998$). This high throat C_d value occurs because of the large M-1 chamber throat inlet radius ratio value of 2.132.

c.   Reaction Kinetic Efficiency $(\eta_{C*_{KIN}})$

The reaction kinetic C* efficiency was calculated with the ODK option of the TDK program. For all mixture ratios from 1.0 to 12.0 $\eta_{C*_{KIN}}$ was calculated to be 1.0 for the M-1 engine. This occurs because

of the high operating chamber pressure and thrust level of the engine (550 psia and 500,000 lbf, respectively).

d.   Boundary Layer Efficiency ($\eta_{C*_{BL}}$)

The C* boundary layer efficiency accounts for the displacement boundary layer effect on the throat potential flow area.

$$\eta_{C*_{BL}} = \frac{A_T}{A_T - 2\pi R_T \delta*_T} \qquad (5)$$

The TDK program was run at the Test 009 nominal O/F to establish edge conditions for a boundary analysis with the JANNAF BLIMP computer program (Ref.10). Wall temperature and calculated ablative chamber regression rates documented in Ref. 9 were used to establish input for BLIMP. BLIMP was executed by using the assigned wall temperature and assigned blowing rate input options, and edge gas properties for a mixture ratio of 2.5:1. This mixture ratio is the nominal Test 009 wall mixture ratio, based on M-1 injector manifold mass distribution results described in the next paragraph. The BLIMP calculated throat displacement thickness was -5. x 10^6 ft which resulted in $\eta_{C*_{BL}}$ of 1.000. Since the boundary layer effect on C* was found to be small, this value was assumed to be correct for all three tests analyzed.

e.   Mixing Efficiency ($\eta_{C*_{MIX}}$)

The purpose of the M-1 data analysis is to verify the capability of the JANNAF CICM computer program to predict energy release efficiencies for GH_2/LO_2 coaxial injectors. The C* energy release efficiency is composed of a mixing and vaporization term.

$$\eta_{C*_{ERL}} = \eta_{C*_{MIX}} \times \eta_{C*_{VAP}}$$

The C* simplified mixing efficiency definition is shown below.

$$\eta_{C^{*}_{MIX}} = \left. C^{*}_{\substack{ODE \\ INJ\ MR \\ MULTIZONE}} \middle/ C^{*}_{\substack{ODE \\ AVG\ INJ\ MR}} \right. \qquad (7)$$

CICM does not calculate intra-element (shear) or inter-element (diffusion) mixing, however, the program has the capability to accept multiple zones of varying mixture ratio and to calculate the corresponding effect on the LO_2 atomization and vaporization rates. Since CICM simply solves the equation shown above for $\eta_{C^{*}_{MIX}}$, this calculation was evaluated externally from the CICM program to allow inexpensive parametric evaluation of the M-1 injector mass distribution data.

The M-1 injector manifold radial mixture ratio distribution is shown in Figure 3. The three levels of mixture ratio are due to a segmenting of the fuel manifold at the location of two injector baffle rings. Because of symmetric inlet conditions, circumferential distributions were calculated to be within $\pm$ 2 percent of nominal, and thus were ignored for purposes of the $\eta_{C^{*}_{MIX}}$ calculation.

Intra-element maldistribution data was not available for the M-1 design configuration, therefore no intra-element mixing loss was calculated for the injector. The mixing efficiency term accounts only for manifold induced element-to-element mass maldistribution. The H_2/O_2 gas/gas empirically based mixing model developed in Ref. 11 was used to estimate the intra-element mixing efficiency for the M-1 injector. The model indicated that intra-element mixing losses would be insignificant because of the long (29.75 inch) M-1 chamber design.

A simple computer program was written to sum streamtube performance and to evaluate the injector manifold induced mixing loss; by solving the following equation.

$$C^{*}_{\substack{ODE \\ INJ\ MR \\ MULTIZONE}} = \sum_{i=1}^{i=n} \frac{\dot{W}_i}{\dot{W}_T} \times C^{*}_{\substack{ODE \\ ZONE\ MR}} \qquad (8)$$
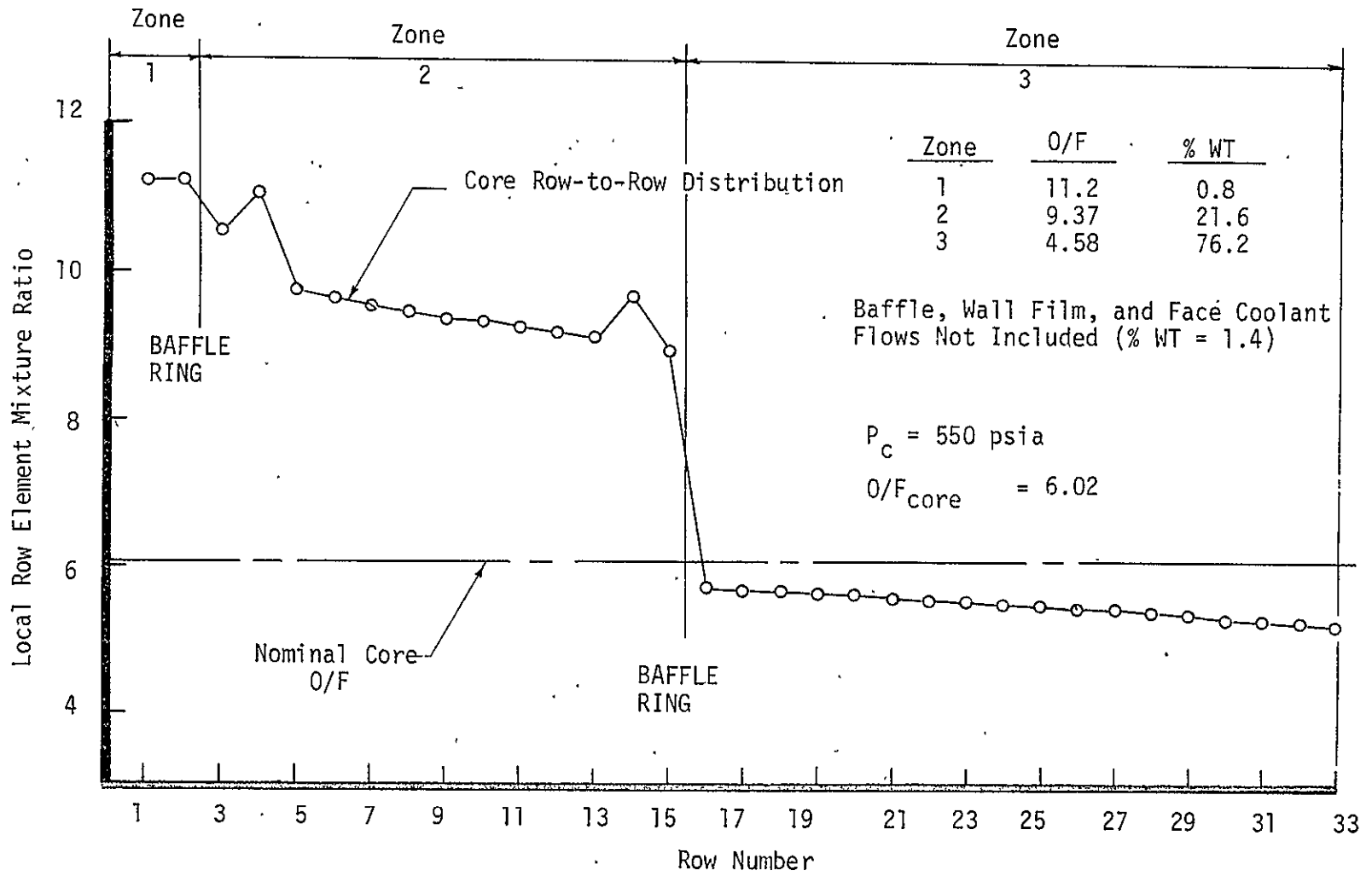
FIGURE 3.   M-1 INJECTOR CORE RADIAL MIXTURE RATIO DISTRIBUTION

Figure 4 indicates the results of the $\eta_{C*_{MIX}}$ evaluation. Calculations were made ranging from 1 to 36 streamtubes (33 injector rows plus two baffle ring and one outer film cooling row) to determine the influence of stream tube mass assignment on the $\eta_{C*_{MIX}}$ calculation. The calculated efficiency is seen to be extremely sensitive to the selected number of streamtubes for flow division. The $\eta_{C*_{MIX}}$ value decreases as the number of streamtubes is increased as would be expected. This sensitivity points out a general weakness of the JANNAF performance prediction methodology, that is, there are no standardized techniques for streamtube mass assignment in any of the JANNAF performance programs (i.e., CICM and DER). Since, as shown in Figure 3, the M-1 manifold design resulted in three distinct chamber flow field mixture ratio zones, a three zone $\eta_{C*_{MIX}}$ calculation was performed. This result is indicated by the dashed line in Figure 4 . The calculated value was equal to the case where a streamtube was assigned to each injector row. This $\eta_{C*_{MIX}}$ calculation technique was selected for analysis because it was consistent with the physical injection zones created by the injector baffle design. The calculated $\eta_{C*_{MIX}}$ ranged from 0.976 for tests 009 and 016 to 0.980 for the low mixture ratio test number 010.

.f.   Vaporization Efficiency ($\eta_{C*_{VAP}}$) .

The JANNAF CICM and STC computer programs were utilized to calculate the injector LO_2 vaporization efficiency. As explained in Appendix B, the recommended program interface technique,which was utilized during the analysis, is to run CICM until all LO_2 droplets have approached the chamber wet-bulb temperature. The CICM analysis was conducted by inputing required M-1 injector/chamber geometry and selecting the program user's manual recommended atomization rate (C_A) and vaporization rate (B_A) constants shown in Table IV. The test vaporization calculations are summarized in Table IV. CICM was run to a chamber axial location of 4.10 inches (wet bulb plane determined through one trial CICM run) from the injector face plane for all three tests. STC completed the calculation to the chamber throat plane axial location of 29.75 inches. One zone analyses (at the test mixture ratio) were executed
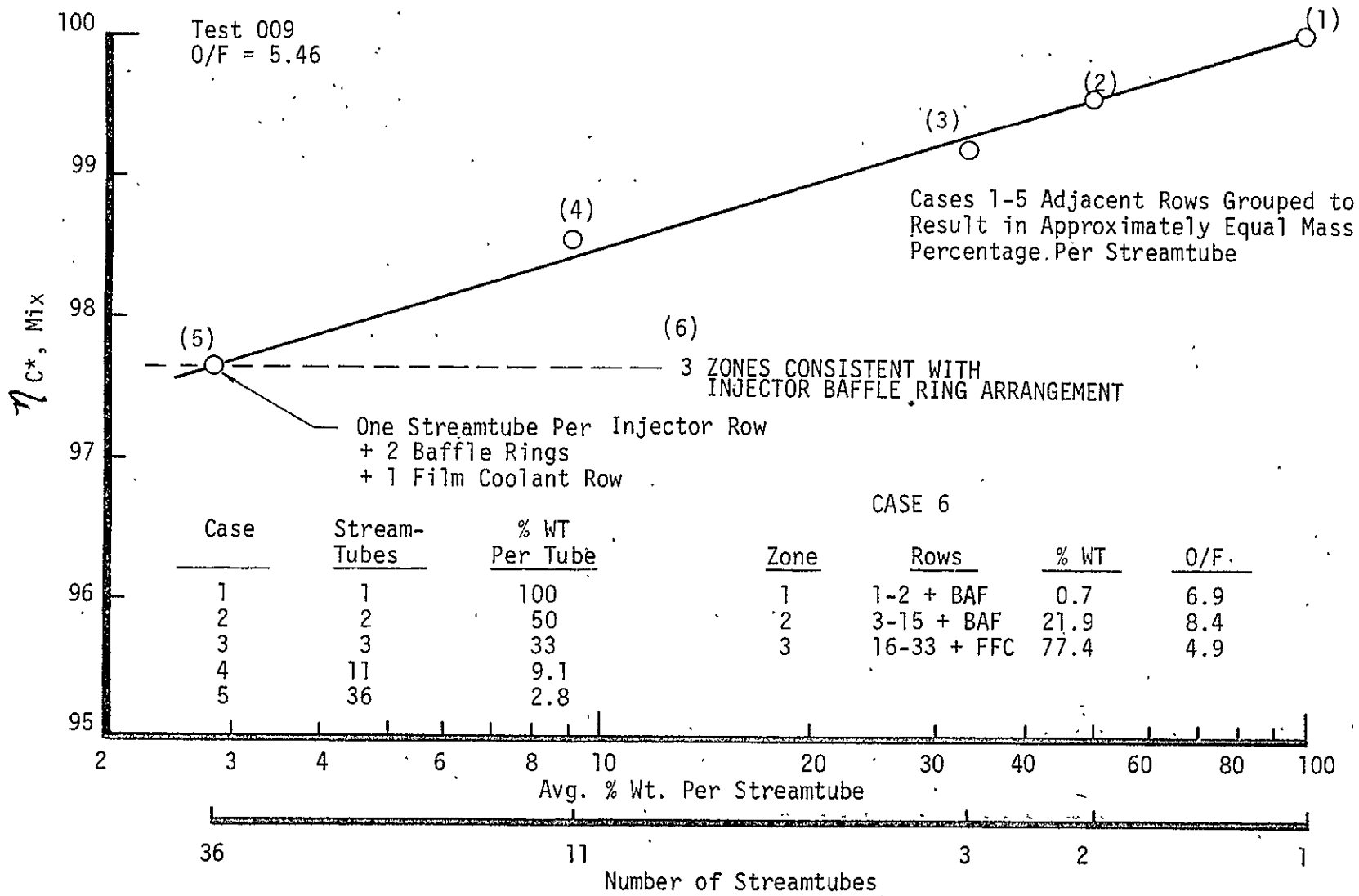
FIGURE 4. MIXING LOSS SENSITIVITY TO STREAMTUBE MASS DISTRIBUTION

TABLE IV

CICM/STC VAPORIZATION CALCULATION SUMMARY

RUN	TEST	PROGRAM	ZONES	O/F	CA	BA	$\%VAP_{OX}$	nc^*_{VAP}
1	009	CICM/STC	1	5.46	0.08	120	.973	.982
2	010	CICM/STC	1	4.04	0.08	120	.992	.994
3	016	CICM/STC	1	5.53	0.08	120	.997	.997
4	009	CICM only	1	5.46	0.08	120	~.98	~.99

for all three tests to calculate $\eta_{C^*_{VAP}}$. Multiple zone analyses were not conducted for two reasons. First, initial correlation of the test 009 C* prediction with the test value showed excellent agreement utilizing a one zone $\eta_{C^*_{VAP}}$ value. Secondly, approximately 75 percent of the injector mass flow is contained in the outer zone (rows 16-33, See Figure 3). All of these rows have mixture ratio values only slightly lower than the nominal injector core mixture ratio.

In addition to the three CICM/STC runs for each test, a CICM only run was conducted for test 009 to note any difference between a CICM/STC calculation and a complete CICM chamber calculation. The CICM run stopped at an axial station of 24 inches in the 29.75 inch M-1 chamber because of a continuity check error caused by improper input of the chamber throat area. For this reason, the corresponding efficiency values shown in Table IV were deduced through extrapolation. A complete discussion of the CICM and STC vaporization calculation results is included in the section on data correlation and analysis to follow. The CICM/STC $\eta_{C^*_{VAP}}$ calculations were utilized in the C* efficiency predictions summarized in the next subsection.

g.   C* Efficiency Prediction ($\eta_{C^*_{PRED}}$)

The calculated test C* efficiencies are tabularized below in Table V. A discussion on correlation of the predicted and test values follows the next section on test measurement uncertainties.

TABLE V

TEST η_{C^*} PREDICTION SUMMARY

TEST	$\eta_{C^*_{HL}}$	$\eta_{C^*_{TD}}$	$\eta_{C^*_{KIN}}$	$\eta_{C^*_{BL}}$	$\eta_{C^*_{MIX}}$	$\eta_{C^*_{VAP}}$	$\eta_{C^*_{PRED}}$	$\eta_{C^*_{TEST}}$
009	1.000	1.002	1.000	1.000	0.976	0.982	0.960	0.959
010	1.000	1.002	1.000	1.000	0.980	0.994	0.977	0.964
016	1.000	1.002	1.000	1.000	0.976	0.997	0.976	0.980

·3.   Test Measurement C* Uncertainties

The correlation of the test and predicted η_{C*} depend on the uncertainty of both values. The net correlation uncertainty is defined by CPIA 245 (Ref. 12) as:

$$U = \sqrt{S_{TEST}^2 + S_{PRED}^2} + B_{TEST} + B_{PRED} \tag{9}$$

The precision (S) and bias values (B) depend on a knowledge of measurement and prediction calibrations and trends. To correlate the M-1 prediction and test values the following simplifications were made, because of lack of data.

$$S_{PRED} = 0, \quad B_{TEST} = 0, \quad B_{PRED} = 0.$$

These assumptions indicate that the only uncertainty that can be accurately evaluated for the M-1 analysis is the precision of the test data C* measurement. The following C* measurement 2σ data uncertainties were known.

Total Weight Flow	$\pm 0.8\%$
Chamber Pressure	$\pm 0.4\%$
Ablative Throat Area	$\pm 0.7\%$

The resultant uncertainty in test-measured C* is $\pm 1.1\%$. Therefore, even by assuming zero uncertainty in the C* prediction and no measurement or prediction bias the agreement between measured and predicted C* (See Table V) is well within the accuracy of the test data, except for test 010. This result is discussed in the next section.

C.   Data Correlation and Analysis

The results of the M-1 test data correlation will be discussed in two parts: (1) a discussion on the results of the CICM/STC and CICM computer model combustion chamber energy release predictions; and (2) results of the correlation of the JANNAF simplified prediction procedure C* efficiencies with the test values.

IV   CICM Analysis and Data Correlations   (cont.)

1.   Vaporization Model Results

The CICM/STC calculated chamber pressure profiles for
the three tests analyzed are shown in Figure 5. The analytically calculated
profiles pass closely to the test measured static pressure values, indicating
that the chamber energy release characteristic is being realistically modeled
with CICM. These good correlations verified the use of the CICM/STC calculated
chamber total pressure loss for the determination of the $P_{c_{eff}}$ value for each
test, as previously described in Section IV.B.1.

As previously mentioned, a CICM only run was executed
for test 009 to determine if the use of the simpler STC vaporization model of
DER was compromising the accuracy of the vaporization calculation. The LO_2
vaporization profiles for each calculational method is shown in Figure 6.
The two calculations agreed within one to two percent over the entire
chamber length. The CICM only calculation was extrapolated beyond the 24-
inch axial station because of an input throat area error described in the next
paragraph.

The test 009 chamber pressure profiles calculated by
CICM/STC and CICM only are compared in Figure 7. As displayed, the pressure
profile agreement is excellent. The slight differences are attributable to the
incorrect throat area input to CICM for the CICM only calculation. This input
error resulted in a continuity check error as the throat plane was approached.

2.   Correlation of Predicted and Test C* Efficiencies

The predicted and test C* efficiencies summarized in Table
V are graphically compared in Figure 8. Agreement was excellent for tests 009
and 016, while there was a 1.4 percent difference (compared to a test measurement
uncertainty of ± 1.1 percent) between prediction and test for test 010.

The test conditions are compared in Table II. The primary
operating difference between test 016 and the nominal test 009 is an increase
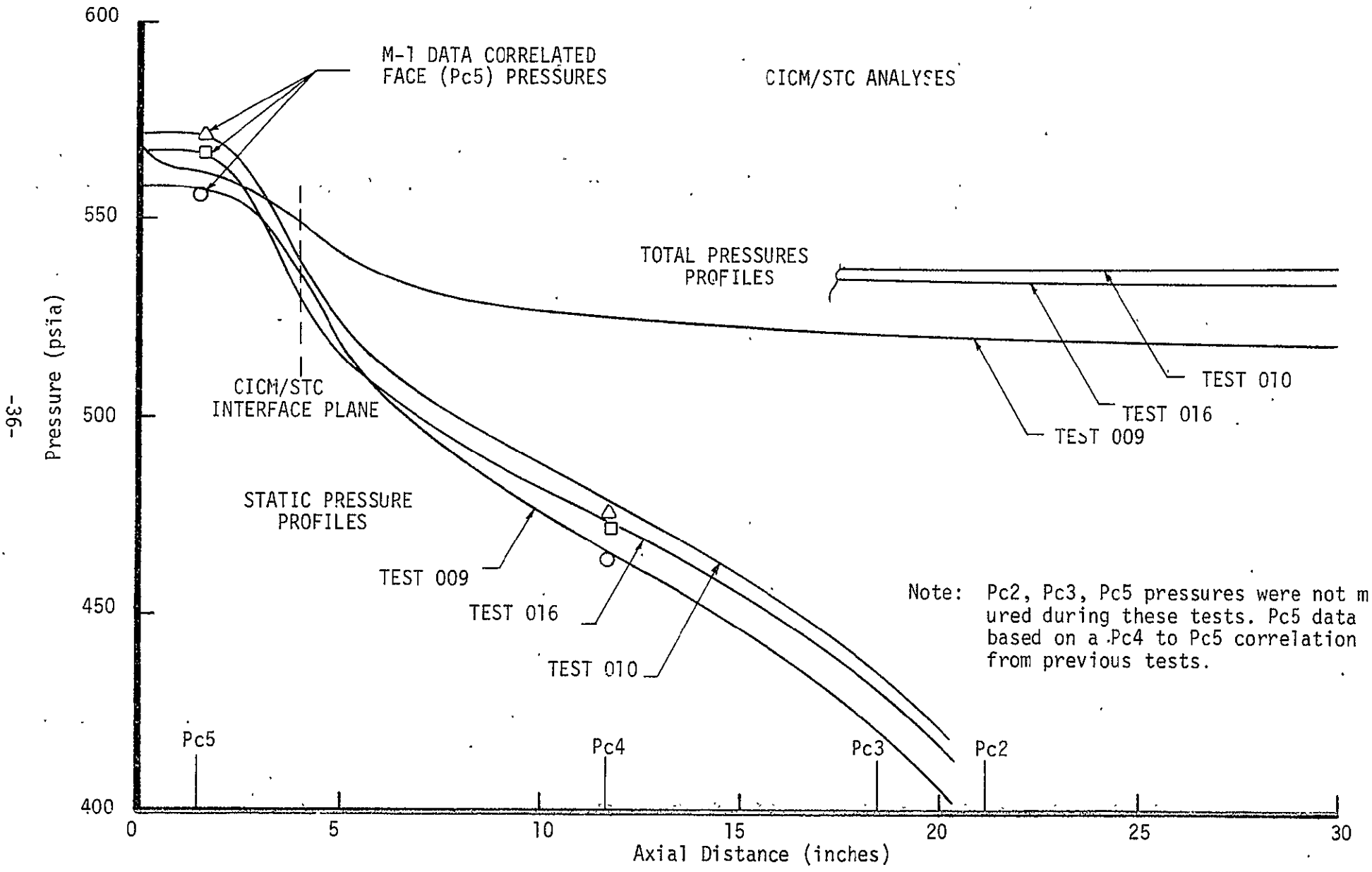
FIGURE 5. MEASURED AND CALCULATED CHAMBER PRESSURE PROFILES
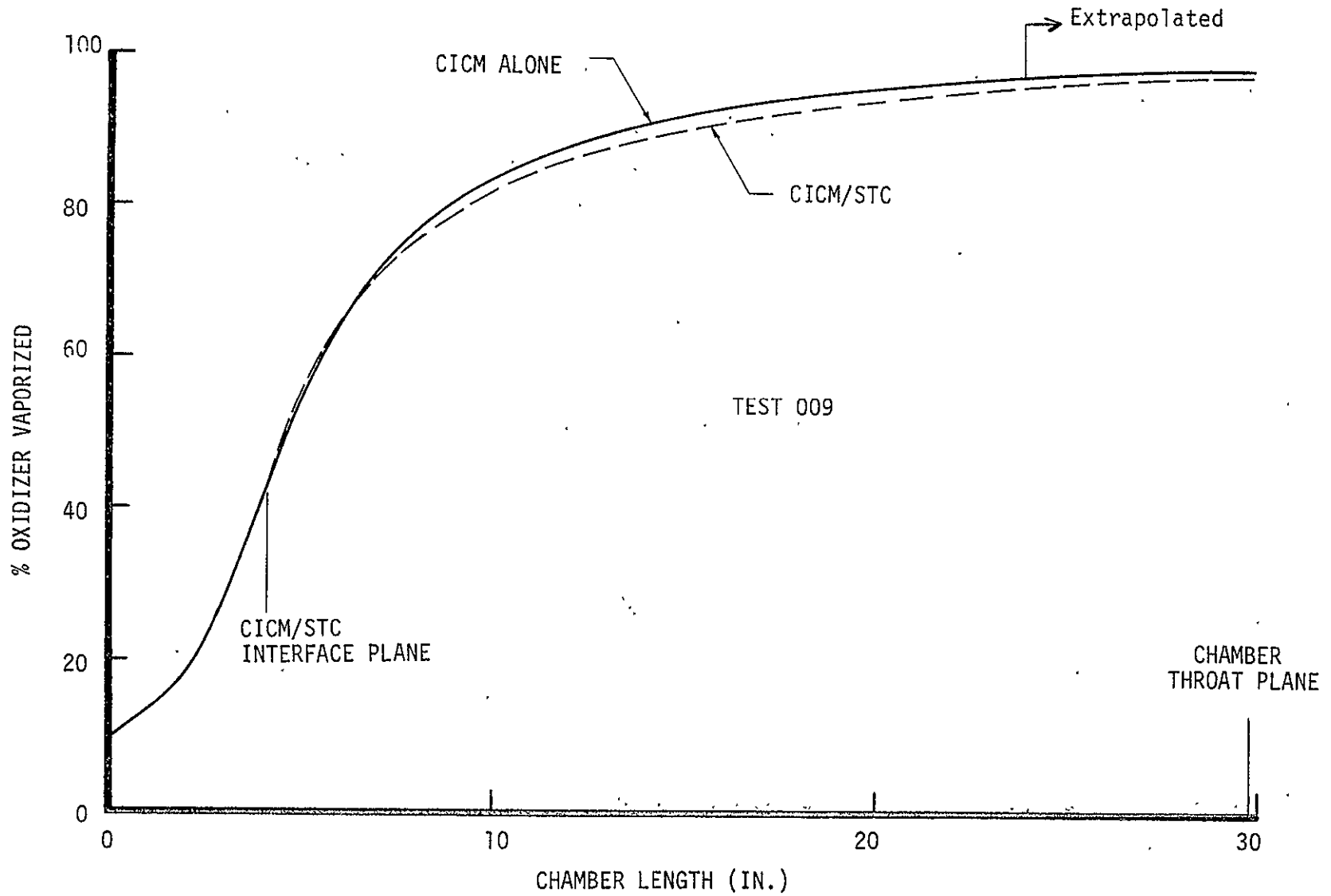
FIGURE 6. COMPARISON OF CICM AND STC OXIDIZER VAPORIZATION PROFILES
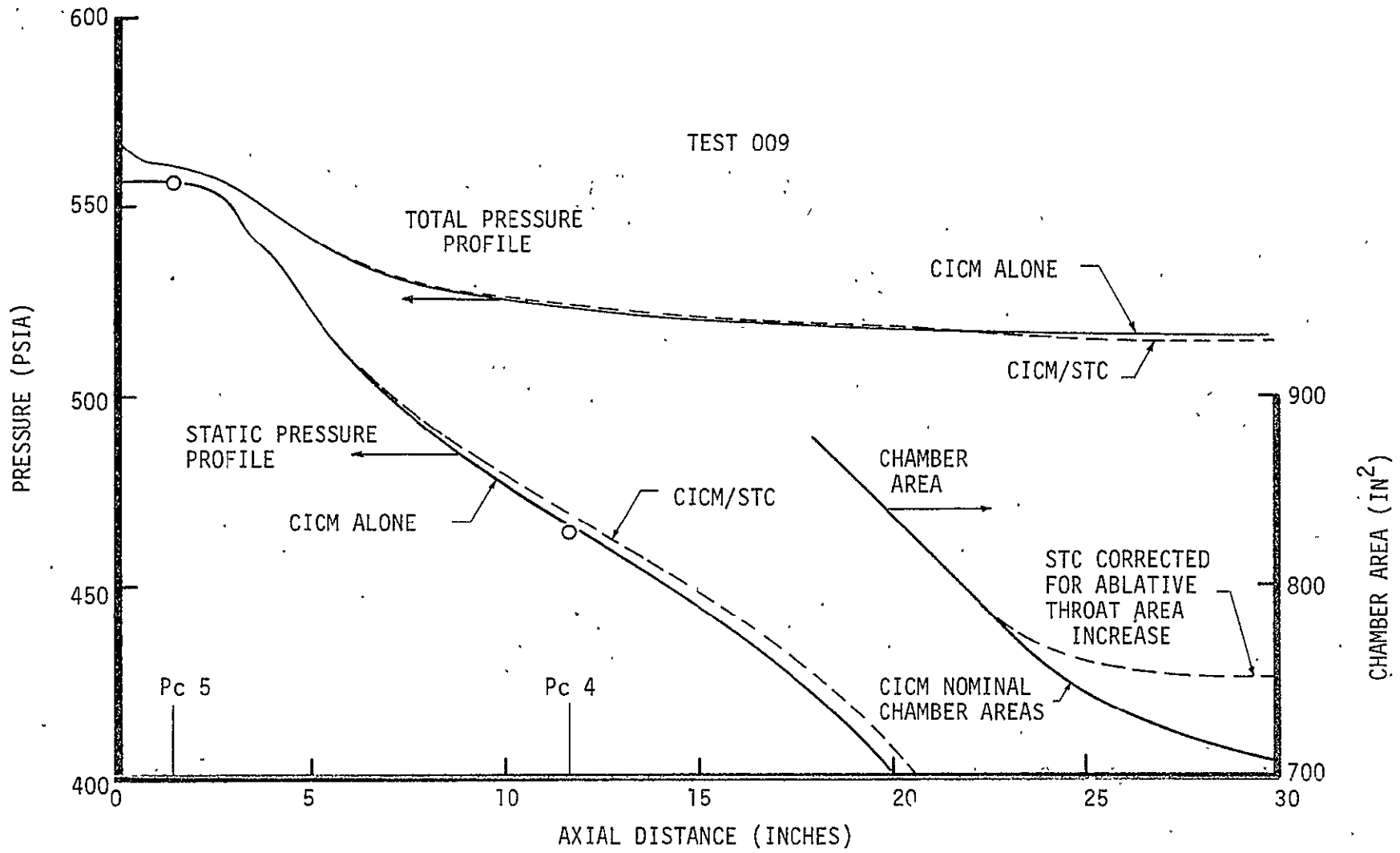
FIGURE 7. COMPARISON OF CICM AND STC PRESSURE PROFILES

-38-
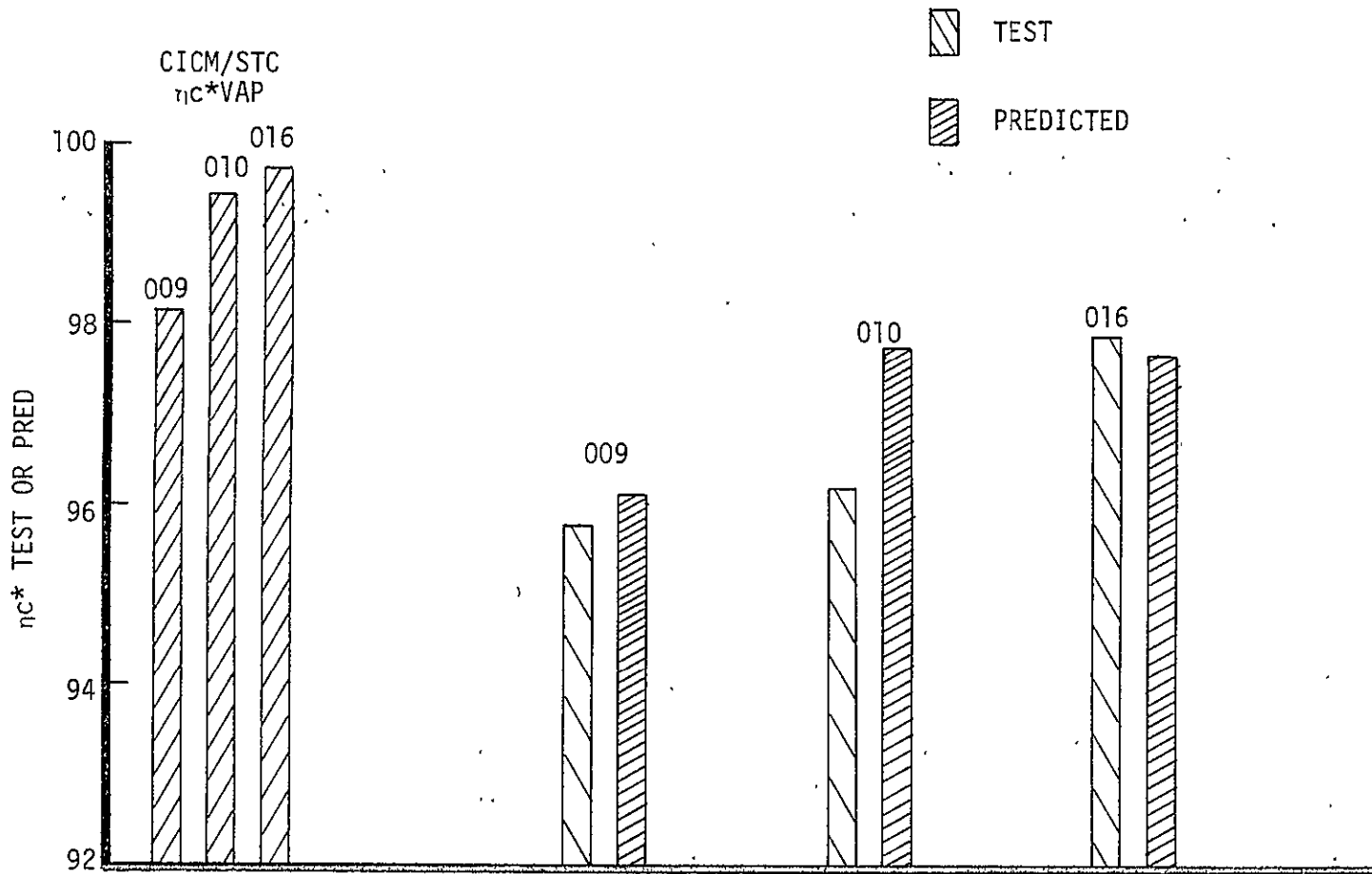
FIGURE 8.   CORRELATION OF PREDICTED AND TEST ηc^*'s

in the injection velocity difference of from 310 to 456 ft/sec. The increase occurs because of the fuel density decrease associated with increasing the fuel inlet temperature from 97°R to 122°R. The CICM equations accurately predict the performance increase due to the smaller drop sizes produced by a higher velocity difference between the gaseous H_2 annulus and the liquid O_2 core. This inverse relationship is evident from the CICM mass median drop size correlation equation shown below.

$$D_j = B_A \left[\frac{\mu_j \, (\sigma_j/\rho_j)^{1/2}}{\rho_g \, U_r^2} \right]^{2/3} \tag{10}$$

The JANNAF/CICM η_{C*} prediction for test 010 was 1.4 percent higher than the test value. As protrayed in Figure 8, the test performance for test 010 is only slightly higher than the nominal test 009 value. Referring again to Table II, it can be seen that a test 010 increase in fuel flowrate is offset by a higher fuel density that results in a net decrease in the gas to liquid jet relative gas velocity. This effect should lower predicted performance. However, the higher H_2 inlet density increases predicted performance as can be seen from equation (10). The mass median drop size is inversely proportional to the fuel gas density (ρ_g) raised to the 2/3 power. As described in Section B.2 of Appendix B, this CICM correlation dependency on the gaseous annulus density is much more severe than predicted by the other empirically based circular jet drop size models that has correlated a gas density influence. The model of Ingebo (Ref. 13) shows drop size to·be inversely proportional to gas density raised to the 3/10 power. It is therefore suggested that CICM overpredicts the performance of test 010 because the gas density term is too significant in the equation (10) drop size relationship.

The following two observations, that resulted from the CICM analysis, are reiterated here to help clarify the results of the M-1 data correlation work. (1) The M-1 thrust chamber design is very similar to the J2-S design used to calibrate key CICM jet stripping rate and drop size constants.

(See Ref. 4 and J2-S sample case in CPIA 246). This is a definite reason for the success of the M-1 performance predictions. (2) Both the M-1 and J2-S engines possess extremely long chambers that eliminate large intra-element mixing losses. Therefore, the M-1 predictions were not invalidated by assuming uniform intra-element mass distribution.

D.   Conclusions and Recommendations

1.   Conclusions

The following conclusions have resulted from the JANNAF/ CICM analysis of the M-1 thrust chamber.

a.   The CICM model has been verified for high performing thrust chambers with negligible intra-element mixing losses.

b.   The CICM mass median drop size dependency on the gaseous annulus density is overly significant. It must be noted that changing the equation would most likely result in the requirement of recorrelating the key drop size constant, B_A.

c.   The primary weakness of the CICM model is the simplified methodology for calculation of intra-element and inter-element (manifold induced) mixing losses.

2.   Recommendations

The following recommendations are made based on the above conclusions regarding the M-1 analysis.

a.   An intra-element mixing model should be developed for CICM.

b.   CICM should be applied to correlation of test data obtained with a short chamber coaxial injector thrust chamber with a finite intra-element mixing loss.

c.   Reformulation and verification of the CICM mass median drop size correlation equation should be considered.

V   DER MASS DISTRIBUTION MODEL IMPROVEMENT

The original objective of Task II was to provide information on the present prediction capabilities of the JANNAF DER and CICM computer programs through correlation of well documented hot fire data bases. DER was to be used to analyze a 6000 lbf like doublet pair injector developed on the OMS engine program while CICM was to be applied to the 500,000 lbf M-1 engine gas/liquid coaxial injector. The CICM analysis was completed as originally planned and is documented in Section IV of this report.

After a careful evaluation of the Task I DER Computer Program Review, it was concluded that the DER subcritical K-Prime program contains inadequacies in the analytical formulations that could produce invalid data when applied to the OMS thrust chamber analysis. It was decided that the originally considered funds for this task should rather be used to remove detected shortcomings in the model.

Improvement of the LISP ZOM plane mass distribution methodology was selected as the new Task II analysis goal for three reasons. First, the "standardized" DER (SDER) development program (Contract FO 4611-75-C-0055), conducted concurrently with this program, has concentrated on improvement of the DER vaporization modeling, but not on mass distribution and mixing modeling. Secondly, as discussed in Appendix A, the ZOM plane location is known to be a key DER input parameter which significantly influences the calculated chamber mixing performance efficiency. Lastly, recent empirical investigations have led to formulation of a model for calculation of the ZOM plane location on an a priori basis.

The current development status of the new ZOM mass distribution model is summarized in the following four paragraphs that concern, respectively, (1) an explanation of the hypothesized model, (2) presentation of the subscale like doublet pair injector data base used to correlate the predictions of the formulated model, (3) results of data analysis and model correlation effort, and (4) conclusions and recommendations of this initial model development work.

A.   Model Approach

During a recent development effort on the Space Shuttle OMS engine program subscale injectors were tested to model combustion stability response (Ref. 14). The test combustion chamber was densely instrumented with static pressure transducers to allow calculation of the local combustion gas flowrate and velocity through the use of isentropic flow relationships. Bracco (Ref. 15) has also utilized this technique and developed a method for accurately interpreting such measurements. The availability of the OMS test data has resulted in empirically based mass vaporization profiles that eliminate the uncertainty associated with calculating chamber gas profiles with DER or other available vaporization models. The uniquely accurate OMS data allowed calculations of the influence of near-zone combustion gas formation and acceleration on liquid spray fan profiles. The results of initial calculations indicated that these effects are significant, and that further investigation and formulation of an analytical model was warranted.

That the initial model development effort described in the following paragraphs of this section utilized empirical energy release rate data as the primary model input does not imply that such data will always be required. The test data was used instead of analytical predictions made with DER because accurate vaporization profiles near the injector face were required. DER does not account for monopropellant burning of hydrazine based fuels (the OMS subscale test propellant combination was NTO/MMH) that is known to significantly effect near zone energy release rates. (Monopropellant flame effects are discussed in Section C.4 of Appendix A). If the proposed model is ever adopted as a standard analytical procedure in DER it is probable that the DER vaporization models would have to account for monopropellant burning to result in accurate mixing loss predictions.

The originally proposed calculational technique is graphically portrayed in Figure **9**. The top plot in Figure 9 displays an empirically determined near zone (0-2 inches from the injector face plane) mass vaporization profile. Static pressure measurements included the five axial locations
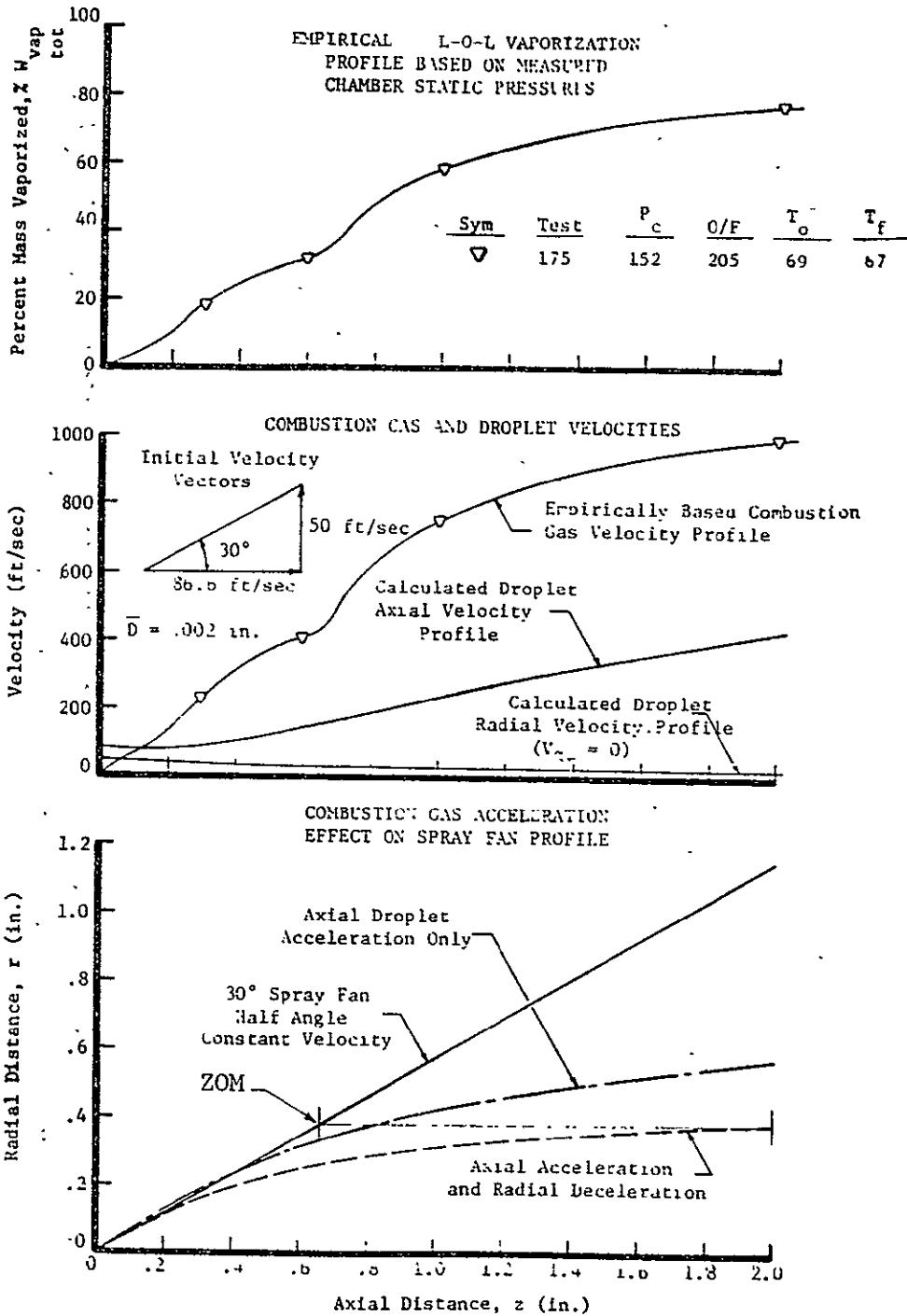
FIGURE 9. PROPOSED METHODOLOGY FOR ZOM GAS ACCELERATION
EFFECTS MODEL

shown; 0.0, 0.3, 0.6, 1.0 and 2.0 inches from the face. Isentropic flow
relationships were used to determine the local gas flowrate, resulting in
the plot of percent mass vaporized versus axial distance. The equations
used to develop gas flowrate (i.e., mass vaporization) profiles from chamber
static pressure measurements are detailed in Appendix D , taken from Ref. (15).

The local gas flowrates were then used to calculate a chamber
combustion gas axial velocity profile. Knowing the gas velocity profile
allowed calculation of droplet velocity profiles through use of the standard drag
equation and an assumed droplet drag coefficient model. These results are shown
in the middle plot of the figure. A mass median droplet with a constant dia-
meter of .002 inches was assumed to have an initial velocity vector as shown.
The droplet axial velocity increases as the combustion gas axial velocity
increases, because of axial aerodynamic drag. The droplet radial velocity
decreases because the combustion gas was assumed to have a radial velocity
component of zero.

The bottom plot on the figure shows the effect of combustion
gas acceleration on the trajectory of a propellant droplet assumed to be
on the outer spray fan streamline. Cold flow correlation techniques (e.g.
the DER ZOM mass distribution method) assume a constant droplet velocity
resulting, for the given initial droplet conditions, in the 30° spray fan
half angle shown. If gas acceleration effects are accounted for the droplet
trajectory, or spray fan profile, changes significantly. One of the corrected
trajectories shown in the figure assumes the droplet is accelerated in the axial
direction only. The other includes the effect of radial deceleration.

The results shown in the figure indicate that, for the case
considered, spray fan radial spreading becomes insignificant at distances
beyond 1.8 inches of the injector face. This result implies that little
interelement mixing would occur downstream, thus pinpointing the area for
selection of the correct value of the DER cold flow mixing plane, ZOM. The
initially proposed ZOM determination technique, indicated in the figure, was
to project the corrected spray fan radial dimension back to the cold flow case.
The hot fire spray fan mass distribution was assumed to be correctly charac-
terized by the cold flow mass distribution at the calculated ZOM plane location.

    A four part task was conducted to develop the proposed ZOM calculation technique.

    (1) Model Formulation

    The purpose of this task was to formulate the proposed model for calculation of a predicted hot fire ZOM plane location. The model was coded for the digital computer to allow rapid reduction of the test data to be correlated in the data analysis subtask.

    (2) Data Analysis

    A test data reduction program was written to calculate test $C*$ efficiencies and chamber axial gas velocity profiles. The ZOM prediction model used the gas velocity profile for each test to calculate the combustion corrected spray fan radial dimension and project back to the corresponding cold flow radial location to calculate the ZOM plane location.

    (3) Performance Data Correlation

    The DER LISP subprogram was used to predict $C*$ mixing efficiency ($\eta_{C*_{mix}}$) as a function of the ZOM plane location. An empirically determined $\eta_{C*_{mix}}$ value was backed out for each test knowing the measured $C*$ efficiency and analytically calculating the test vaporization efficiency. An empirical ZOM value was calculated for each test from the $\eta_{C*_{mix}}$ versus ZOM relationship calculated by LISP. Test determined ZOM values and trends were compared to those calculated by the analytical model.

    (4) Results and Recommendations

    The results of the initial model development effort were evaluated and conclusions reached. Recommendations for continuation of model development were formulated.

B.   OMS Subscale Injector Experimental Data Base

The OMS subscale injector test program documented in Ref. 14 provides a uniquely accurate and comprehensive data base for correlation of predictions of the new ZOM model. Sixty-eight multi-element combustion tests with intensive chamber pressure profile instrumentation were used to infer axially distributed combustion profiles for the various injector designs. The OMS engine utilizes NTO/MMH propellants at a nominal chamber pressure of 125 psia. Mixture ratio, chamber pressure, and propellant temperature variations were tested to gain quantitative data on the combustion response influences of these engine operating variables.

The combustion chamber design utilized during the testing is sketched in Figure 10. Pressure measurements were made at planes located 0., 0.3, 0.6, 1.0, 2.0, 3.5 and 5.4 inches from the injector face plane. The chamber was 8.0 inches in length, resulting in measured test C* efficiencies of 80 to 90 percent of theoretical. . The relatively low test C* efficiency for the coarse subscale injectors resulted in data that provided excellent insight into the effect of test variables on injector/chamber performance.

Two conventional circular orifice like doublet pair (quadlet) and four platelet injectors were tested. A quadlet injector design was selected for analysis because the DER LISP subroutine contains empirical spray distribution coefficients for only conventional circular orifice element types. The six element, 135 lbf thrust, quadlet injector is pictured in Figure 11. The fuel doublet is positioned nearest the wall and the oxidizer doublet is located inboard. A sketch of the quadlet element design is detailed in Figure 12. The quadlet tests selected for the ZOM model development effort are summarized in Table VI.
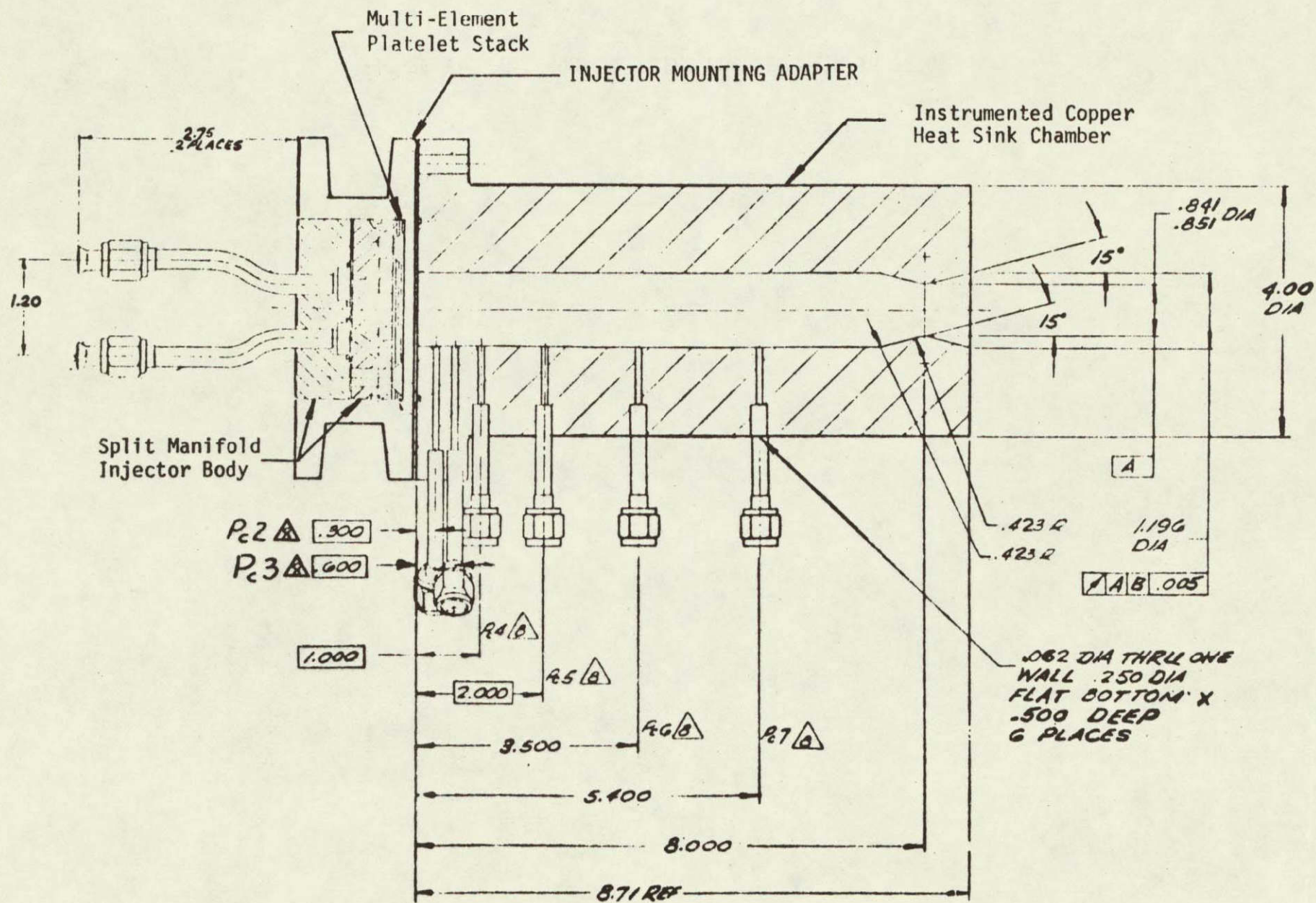
FIGURE 10. OMS MULTI-ELEMENT INJECTOR TEST COMBUSTION CHAMBER
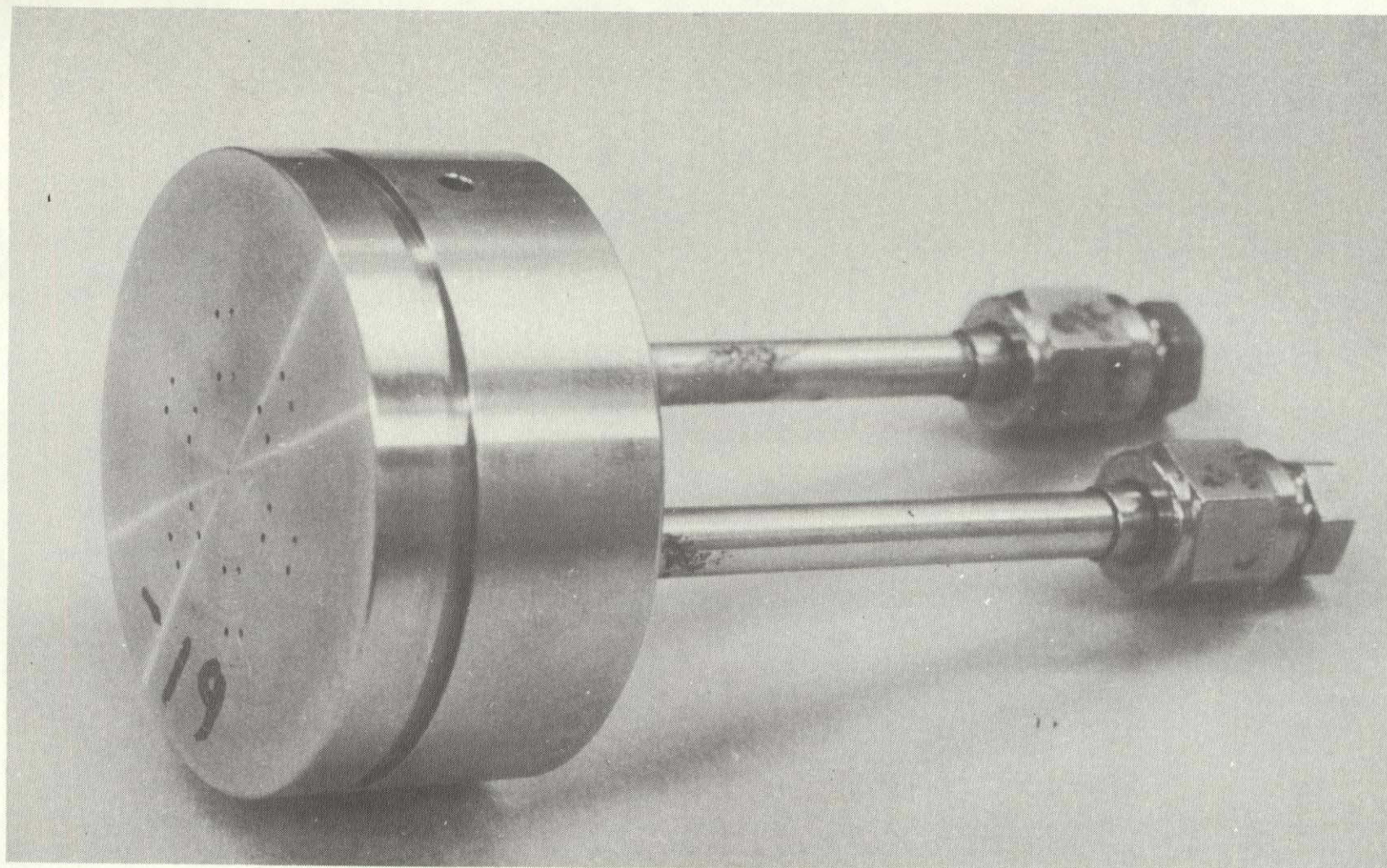
FIGURE 11.   OMS SUBSCALE LIKE DOUBLET PAIR INJECTOR
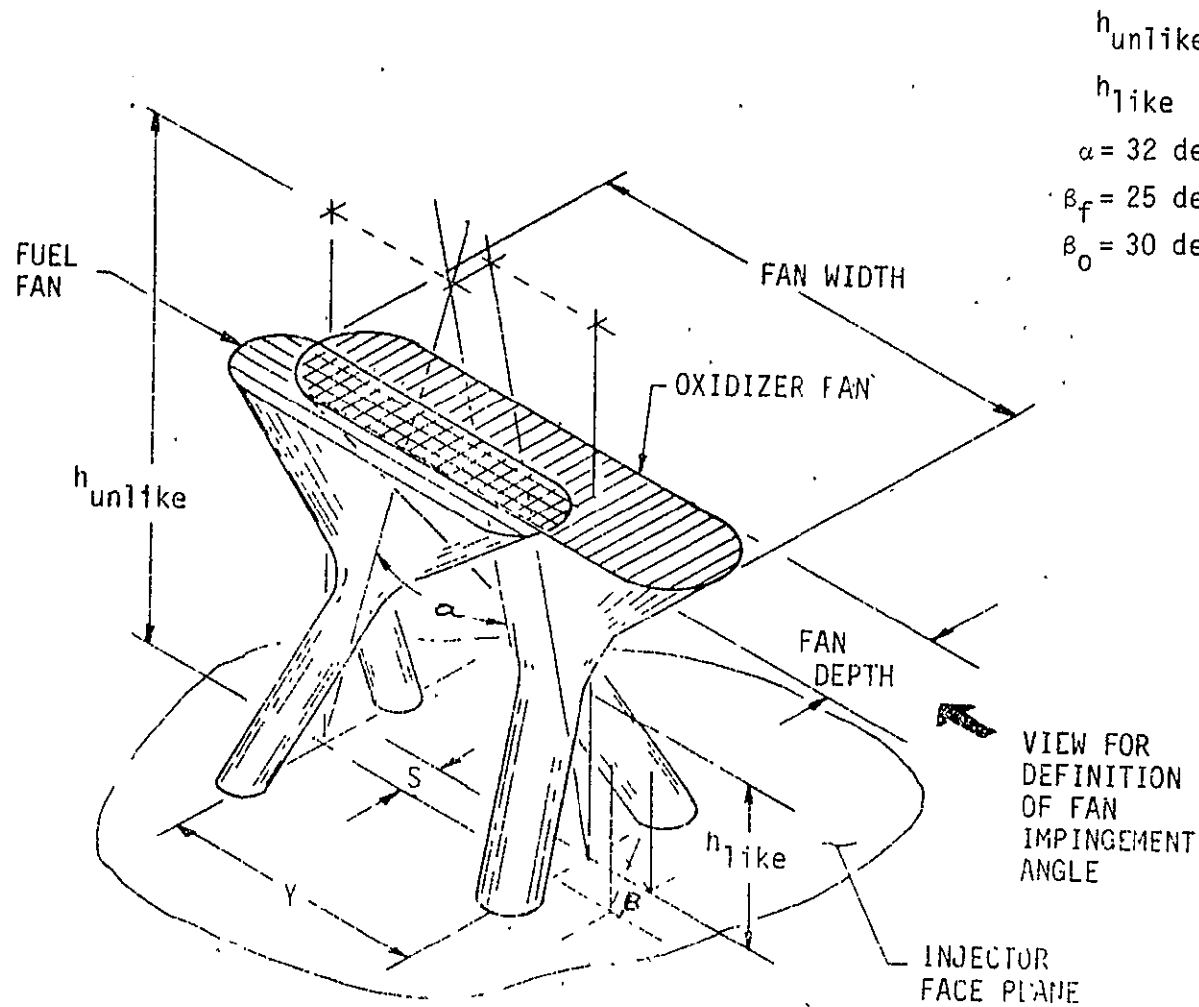
h_{unlike} = .350 in. D_o = .027 in

h_{like} = .100 in. D_f = .025 in

α = 32 deg

β_f = 25 deg

β_o = 30 deg

FUEL FAN

FAN WIDTH

OXIDIZER FAN

h_{unlike}

FAN DEPTH

α

S

Y

h_{like}

β

VIEW FOR DEFINITION OF FAN IMPINGEMENT ANGLE

INJECTOR FACE PLANE

FIGURE   12 .   QUADLET (LOL PAIR) ELEMENT DESIGN

TABLE VI

SUBSCALE QUADLET TEST SUMMARY

Test	O/F	P_c (psia)	T_o (°F)	T_f (°F)	η_{C*} (%)
175	2.05	152.5	69	77	89.3
176	1.87	120.7	69	77	88.9
177	1.60	120.8	69	75	87.4
178	1.59	97.6	71	75	88.9
179	1.69	99.3	72	75	88.8
180	1.71	79.9	73	75	90.2
181	1.66	141.0	74	76	87.0
182	1.70	142.1	75	75	86.4
183	1.64	121.5	73	190	86.5
184	1.67	123.9	69	184	87.2
185	1.72	124.2	69	217	86.6
186	1.72	123.1	141	215	85.1
187	1.68	141.1	137	283	86.3
188	1.73	146.3	130	271	84.3

Statistical characterization of C* efficiency and calculation of empirically determined combustion gas velocity profiles for these tests is detailed within the following section concerning model data analysis and correlation.

C.   Model Data Analysis and Correlation

1.   Quadlet Injector Test Data Reduction

A computer program was coded to reduce the quadlet injector tests selected for analysis and summarized in Table VI. The primary test variables input to the program are injector flow areas, chamber throat area, propellant flowrates, temperatures, and manifold pressures and the measured chamber static pressures.

A subroutine was included in the program that contained parametric NTO/MMH combustion gas properties as a function of chamber pressure, mixture ratio, and propellant temperatures. The one dimensional equilibrium (ODE) properties calculated with the routine included characteristic exhaust velocity (C*), molecular weight, stagnation temperature, dynamic viscosity, and the ratio of specific heats (γ). The ODE C* value was used to define test C* efficiency through comparison to the test calculated value. The remaining gas properties were used to compute throat effective chamber pressure and the test combustion gas velocity profile from the chamber axial static pressure measurements.

A sample output case of the test data reduction program is displayed in Figure 13. The gas velocity profile printed as a function of 0.1 inch axial chamber increments was generated by applying a 2nd order curve fit to the measured static pressure data. The primary program outputs used as input to the ZOM calculational model described in the next paragraph are the gas velocity profile and the calculated propellant injection velocities.

2.   ZOM Prediction Model Formulation

The ZOM prediction model approach introduced previously was coded for the computer to allow rapid reduction and correlation of the sub-scale quadlet injector tests. The function of the computer model is to integrate the basic equation for droplet acceleration based on input droplet size, injection velocity, spray fan half angle (i.e., the initial droplet trajectory) and the computed chamber gas velocity profile. The droplet acceleration equation is shown below.

$$\frac{dV}{dt} = -\frac{3}{4} C_D \frac{\rho_g}{\rho_1} \frac{(V_g - V_D)^2}{D} \tag{11}$$

The equation was converted to allow integration with respect to the axial chamber distance, x.

****** MULTIELEMENT LUL CORE ******

MEASURED VALUES	TEST TIME	PC1	PC2	PC3	PC4	PC5	PC6	PC7	PUJ	PFJ	TOJ	TFJ
	180	2.72	84.30	84.10	83.68	82.49	77.88	76.49	75.21	112.31	104.41	73.	75.

CALCULATED PERFORMANCE	PCU	DPOJ	DPFJ	KWO	KWF	WO	WF	WT	MR	C*	XC*
	79.92	28.01	20.11	.0278	.0247	.1767	.1035	.2801	1.71	5142.	90.24

CALCULATED VELOCITIES

VOX	VFL	VBAR
41.26	46.53	43.21

CALCULATED LOCAL PRESSURE, PERFORMANCE & GAS VELOCITY DATA

X	PCS (PSIA)	PERF	PVAP	VGAS (FT/SEC)
.00	84.30	.00	.00	.0
.10	84.26	4.69	4.23	58.7
.20	84.19	10.82	9.76	135.2
.30	84.10	16.74	15.10	209.2
.40	84.00	19.94	18.00	249.3
.50	83.86	21.08	19.03	263.5
.60	83.68	25.54	23.04	319.1
.70	83.42	29.88	26.97	373.4
.80	83.13	34.56	31.18	431.7
.90	82.82	38.81	35.02	484.8
1.00	82.49	42.98	38.78	536.8
1.10	81.90	49.65	44.80	619.8
1.20	81.33	55.41	50.00	691.5
1.30	80.80	60.32	54.43	752.6
1.40	80.29	64.77	58.45	- 807.8
1.50	79.82	68.69	61.98	856.5
1.60	79.37	72.22	65.17	900.3
1.70	78.96	75.43	68.06	940.0
1.80	78.57	78.29	70.65	975.4
1.90	78.21	80.87	72.97	1007.3
2.00	77.86	83.20	75.06	1036.2
2.20	77.68	84.63	76.37	1053.8
2.40	77.48	86.00	77.61	1070.7
2.60	77.29	87.31	78.79	1086.9
2.80	77.10	88.57	79.92	1102.4
3.00	76.92	89.76	81.00	1117.2
3.20	76.75	90.93	82.05	1131.5
3.40	76.58	92.04	83.05	1145.2
3.60	76.41	93.11	84.02	1158.4
3.80	76.26	94.13	84.94	1171.0
4.00	76.11	95.11	85.82	1183.0
4.20	75.96	96.04	86.66	1194.4
4.40	75.82	96.92	87.46	1205.3
4.60	75.69	97.76	88.22	1215.7
4.80	75.56	98.56	88.94	1225.5
5.00	75.44	99.32	89.62	1234.8

FIGURE 13. TEST REDUCTION PROGRAM SAMPLE OUTPUT

$$\frac{dV}{dx} = -\frac{3}{4} \quad C_D \quad \frac{\rho_g}{\rho_l} \quad \frac{(V_g - V_D)^2}{\overline{D} \; V_D} \tag{12}$$

The computer program utilized a special subroutine formulation of the Adams-Bashforth integration method. The Adams-Bashforth method is a extremely efficient predictor-corrector variable step size integration technique.

The Ingebo (Ref. 16) drag coefficient correlation was built into the computer model coding.

$$C_D = 27 \quad Re_D^{-0.84} \tag{13}$$

The influence of the drag coefficient assumption on the predictions of the ZOM model was not investigated during this initial development effort.

The model begins execution at a designated axial plane. A spray droplet of mass median diameter $\overline{D}$ is introduced at the initial plane with an input radial and axial velocity component. The droplet acceleration equation is integrated and the droplet trajectory calculated versus chamber axial distance. The calculation is terminated at the axial plane at which the droplet axial velocity vector is within 0.1 percent of the total droplet velocity vector. That is,

$$\frac{V_{axial}}{V_{Resultant}} \geq 0.999.$$

At this point droplet radial velocity forces that would induce inter-spray fan mixing are negligible. The final droplet trajectory point radial dimension is used to calculate the predicted ZOM value assuming a cold flow linear spray fan half angle consistent with the droplet initial radial and axial velocity components. This calculational process is explained in equation form below.

V · DER Mass Distribution Model Improvement (cont.)

$$\theta = \tan^{-1} \frac{V_{ri}}{V_{ai}} \quad (14)$$

$$ZOM = \tan\theta \times r_f \quad (15)$$
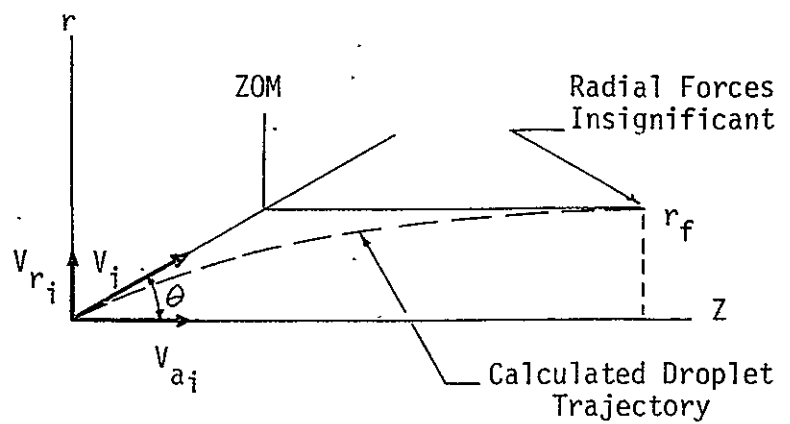
where:

V_{ri} = initial drop radial velocity vector

V_{ai} = initial drop axial velocity vector

r_f = final droplet radial location corresponding to point where axial droplet velocity forces are predominant ·

A sample case output of the ZOM prediction model is shown in Figure 14. The droplet location can be traced through the calculated axial and radial locations, X (1) and X (2), respectively. The calculated local axial and radial velocity components at these locations are V (1) and V (2) respectively. The ZOM value tabulated at the final calculational point is the model predicted cold flow spray fan ZOM value for mixing efficiency prediction with the LISP sub-program of DER.

3. Model Analysis and Data Correlation Results

·a. Statistical Evaluation of Quadlet Injector Test Data

The tests selected for analysis were subjected to a statistical evaluation to allow characterization of injector performance as a function of engine operating variables. A computer model was utilized that combines least squares curve fits with standard multiple regression and co-variance techniques. The primary test variables that were evaluated during the test program were chamber pressure and propellant temperature.

-56-

CASE	FUEL TEMP (F)	OXID TEMP (F)	PC (PSIA)	MR	INITIAL VEL (FT/SEC)	THETA (DEG)
180	75.	73.	84.	1.71	43.2	40.0

CSTARE (FT/SEC)	TGAS(R)	MOLECULAR WT	GAMMA	VISCOSITY (LB/FT-SEC)
5698.	5455.	20.66	1.23	.0000605

GAS VELOCITY

X1	VG (FT/SEC)
.000	.0
.100	58.7
.200	135.2
.300	209.2
.400	249.3
.500	263.5
.600	319.1
.700	373.4
.800	431.7
.900	484.8
1.000	536.8
1.100	619.8
1.200	691.5
1.300	752.6
1.400	807.8
1.500	856.5
1.600	900.3
1.700	940.0
1.800	975.4
1.900	1007.3
2.000	1036.2
2.200	1053.2
2.400	1070.7
2.600	1086.9
2.800	1102.4
3.000	1117.2
4.000	1183.0
5.000	1234.8

X(1)	X(2)	V(1)	V(2)	RE(1)	RE(2)	V(1)/V(RESULT)	ZOM(INCHES)	CD(1)	CD(2)
.313-05	.262-05	.331+02	.278+02	.407+01	.342+01	.766+00	.313-05	.830+01	.962+01
.560-01	.465-01	.320+02	.261+02	.158+00	.319+01	.774+00	.554-01	.127+03	.102+02
.101+00	.817-01	.326+02	.246+02	.328+01	.302+01	.798+00	.973-01	.996+01	.107+02
.152+00	.118+00	.353+02	.232+02	.764+01	.285+01	.836+00	.140+00	.489+01	.112+02
.203+00	.148+00	.402+02	.220+02	.119+02	.270+01	.877+00	.177+00	.336+01	.117+02
.254+00	.174+00	.466+02	.211+02	.161+02	.259+01	.911+00	.207+00	.262+01	.122+02
.306+00	.194+00	.539+02	.203+02	.194+02	.249+01	.936+00	.232+00	.224+01	.126+02
.350+00	.210+00	.614+02	.197+02	.211+02	.242+01	.952+00	.250+00	.208+01	.129+02
.402+00	.225+00	.687+02	.191+02	.222+02	.235+01	.963+00	.268+00	.199+01	.132+02
.453+00	.238+00	.754+02	.186+02	.221+02	.229+01	.971+00	.284+00	.200+01	.135+02
.504+00	.250+00	.816+02	.182+02	.225+02	.223+01	.976+00	.298+00	.197+01	.138+02
.555+00	.261+00	.876+02	.178+02	.251+02	.218+01	.980+00	.311+00	.180+01	.140+02
.606+00	.271+00	.941+02	.174+02	.280+02	.214+01	.983+00	.323+00	.164+01	.143+02
.651+00	.279+00	.101+03	.171+02	.302+02	.210+01	.986+00	.332+00	.154+01	.145+02
.702+00	.287+00	.108+03	.168+02	.328+02	.206+01	.988+00	.342+00	.144+01	.147+02
.754+00	.295+00	.115+03	.165+02	.356+02	.203+01	.990+00	.351+00	.134+01	.149+02
.805+00	.302+00	.122+03	.163+02	.383+02	.200+01	.991+00	.359+00	.126+01	.151+02
.856+00	.308+00	.130+03	.160+02	.407+02	.197+01	.992+00	.367+00	.120+01	.153+02
.901+00	.313+00	.137+03	.158+02	.428+02	.194+01	.993+00	.374+00	.115+01	.154+02
.952+00	.319+00	.145+03	.156+02	.449+02	.192+01	.994+00	.380+00	.111+01	.156+02
.100+01	.325+00	.152+03	.154+02	.475+02	.190+01	.995+00	.387+00	.105+01	.158+02
.105+01	.330+00	.160+03	.152+02	.517+02	.187+01	.995+00	.393+00	.982+00	.159+02
.111+01	.334+00	.168+03	.151+02	.559+02	.185+01	.996+00	.398+00	.919+00	.161+02
.115+01	.338+00	.177+03	.149+02	.591+02	.184+01	.996+00	.403+00	.877+00	.162+02
.120+01	.342+00	.185+03	.148+02	.624+02	.182+01	.997+00	.008+00	.839+00	.164+02
.125+01	.346+00	.194+03	.146+02	.652+02	.180+01	.997+00	.413+00	.808+00	.165+02
.130+01	.350+00	.203+03	.145+02	.678+02	.178+01	.997+00	.417+00	.782+00	.166+02
.136+01	.354+00	.211+03	.144+02	.703+02	.177+01	.998+00	.421+00	.758+00	.167+02
.141+01	.357+00	.220+03	.143+02	.726+02	.175+01	.998+00	.425+00	.739+00	.169+02
.145+01	.360+00	.229+03	.141+02	.744+02	.174+01	.998+00	.429+00	.724+00	.170+02
.150+01	.363+00	.237+03	.140+02	.763+02	.173+01	.998+00	.432+00	.708+00	.171+02
.155+01	.366+00	.246+03	.139+02	.780+02	.171+01	.998+00	.436+00	.695+00	.172+02
.160+01	.369+00	.254+03	.138+02	.796+02	.170+01	.999+00	.439+00	.683+00	.173+02
.166+01	.371+00	.262+03	.137+02	.811+02	.169+01	.999+00	.443+00	.672+00	.174+02
.170+01	.374+00	.271+03	.137+02	.823+02	.168+01	.999+00	.445+00	.664+00	.175+02
.175+01	.376+00	.279+03	.136+02	.836+02	.167+01	.999+00	.448+00	.656+00	.176+02
.180+01	.379+00	.287+03	.135+02	.848+02	.166+01	.999+00	.451+00	.648+00	.177+02
.185+01	.381+00	.295+03	.134+02	.858+02	.165+01	.999+00	.454+00	.641+00	.178+02
.191+01	.383+00	.303+03	.133+02	.868+02	.164+01	.999+00	.457+00	.635+00	.178+02

FIGURE 14.   ZOM MODEL SAMPLE OUTPUT

The results of the statistical analysis are plotted in Figure 15. The analysis indicated that chamber pressure and fuel temperature variances significantly influence injector C* efficiency. The statistical analysis resulted in the curve fit equation written below.

$$\eta_{C^*_{TEST}} = 95.36 - .05279\ P_c - .009468\ T_f \qquad (16)$$

As shown in the figure, the equation results in decreasing C* efficiency as chamber pressure and fuel temperature increase.

The statistical analysis results indicated real injector operating variable influences on performance that could, hopefully, be modeled with the ZOM prediction model. Also, the analysis indicated that the quadlet injector tests comprise a high quality, repeatable data base void of significant measurement error or bias influences.

b.   Model Analysis

The initial model analysis work concentrated on the influence of chamber pressure on test performance and evaluation of the model's capability to calculate the correct absolute magnitude of the ZOM plane location.

The data statistical analysis indicated a significant test performance efficiency sensitivity to chamber pressure. Examination of the test combustion gas velocity profiles calculated with the test data reduction program gave the initial indication that the model would accurately predict the chamber pressure influence trend. Figure 16 shows the empirically based gas velocity profile for a low Pc test (# 180) and a high Pc test (# 182). Both tests were conducted with ambient temperature propellants. As shown, the low Pc test resulted in a C* efficiency nearly 4 percent higher than the high Pc test. Interestingly, as displayed in the figure, the lower performing high Pc test actually possessed a significantly faster rate of near injector zone energy release, as reflected by the higher calculated combustion gas velocity. In other words, the test that exhibited high performance near the
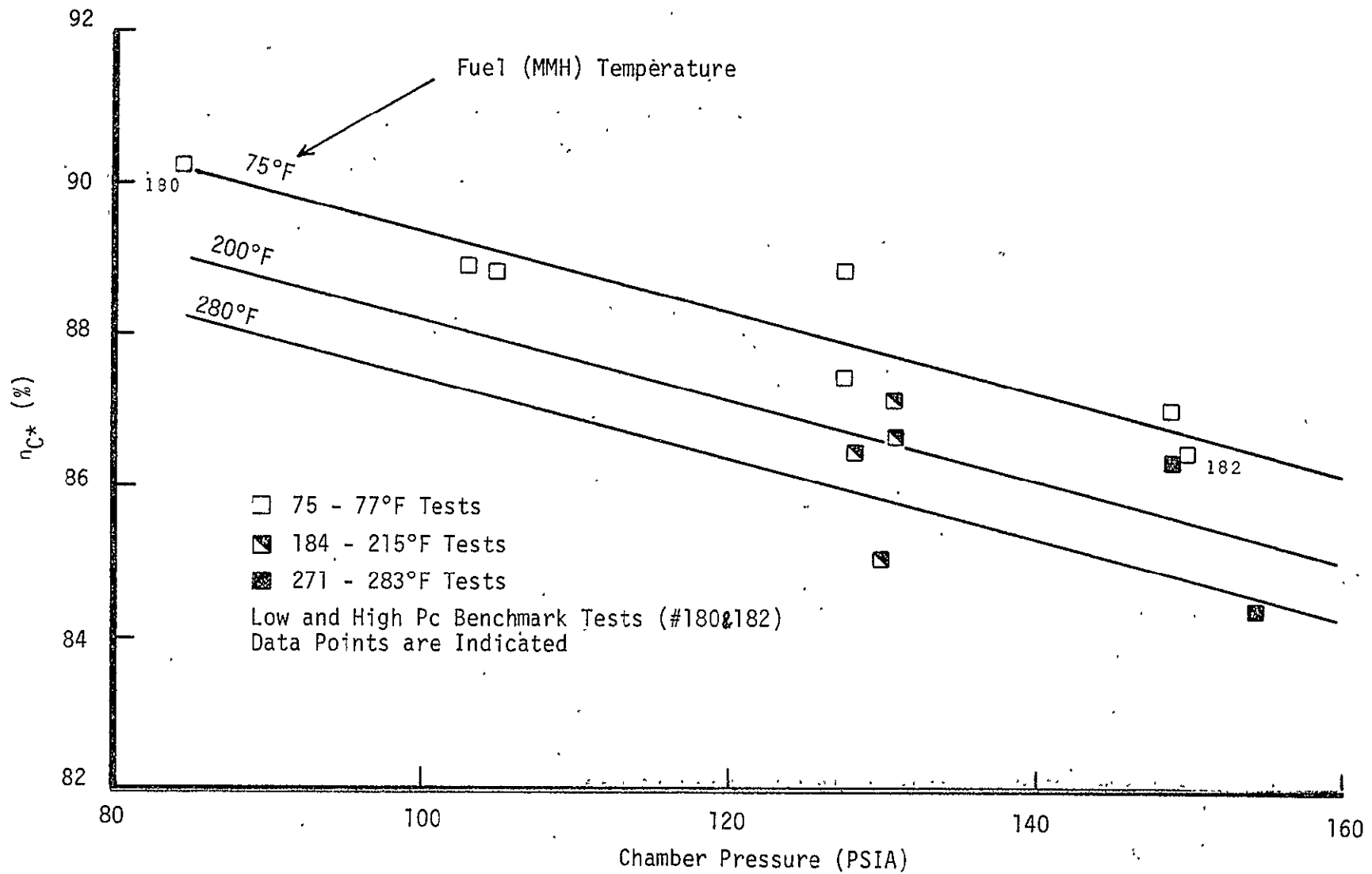
FIGURE 15.   PERFORMANCE CHARACTERIZATION FOR SUBSCALE
              QUADLET INJECTOR
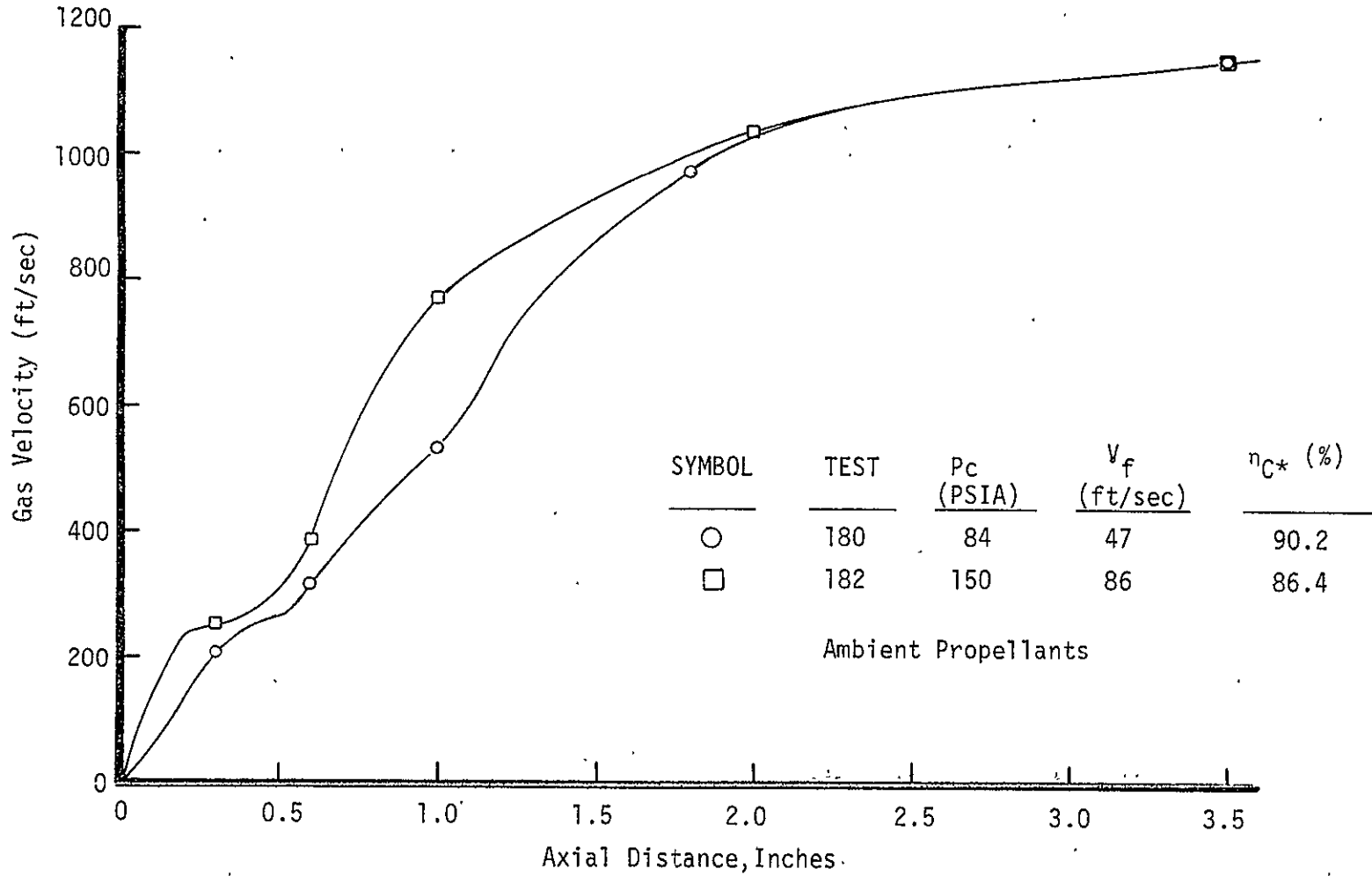
FIGURE 16. CHAMBER PRESSURE INFLUENCE ON GAS VELOCITY PROFILE

injector face (the area of spray fan formation and mixing) possessed lower overall performance. This result appears to mechanistically agree with the formulated ZOM prediction model for the following reason. The higher axial combustion gas velocity near the face results in more rapid axial acceleration of spray fan droplets, thus flattening the droplets trajectory. The more rapid attainment of an axially directed spray fan results in a lower calculated value of ZOM. A lower ZOM value results in a reduction in predicted mixing C* efficiency with the LISP computer model.

The initial ZOM model prediction results, for the calculational technique that will be termed the baseline model, are shown in Figure 17. In the baseline case radial velocity deceleration is calculated by assuming a combustion gas velocity component of zero in the radial direction, thus the droplet radial velocity component is reduced as the calculation proceeds axially down the chamber. The initial quadlet spray half angle was selected to be 40 degrees based on cold flow spray fan photographs and mass distribution measurements. The calculated ZOM value for each test is plotted versus test chamber pressure. To allow clear interpretation of the model predictive trend only the ambient propellant temperature test point predictions are plotted. The calculated trend is opposite from that expected; that is, the lower performing high pressure tests have high calculated ZOM values.

Model predictions were repeated for the same tests with varying calculational assumptions to ascertain the reason for the incorrectly calculated trend of ZOM versus chamber pressure. The results are displayed in Figure 18. The test data points were eliminated for clarity. The first calculational change (Case 2 in the figure) eliminated radial deceleration by assuming a constant droplet radial velocity equal to the injection radial component. The predicted trend of ZOM versus chamber pressure is the same but the absolute ZOM value is increased. ZOM increases because the constant radial velocity assumption results in a greater time to flatten the droplet trajectory because velocity is only changing in the axial direction. The second calculational change (Case 3 in the figure) was to initiate the calculation at an axial distance of 0.4 inches from the injector face plane (using the empirically calculated gas velocity consistent with this location). It was
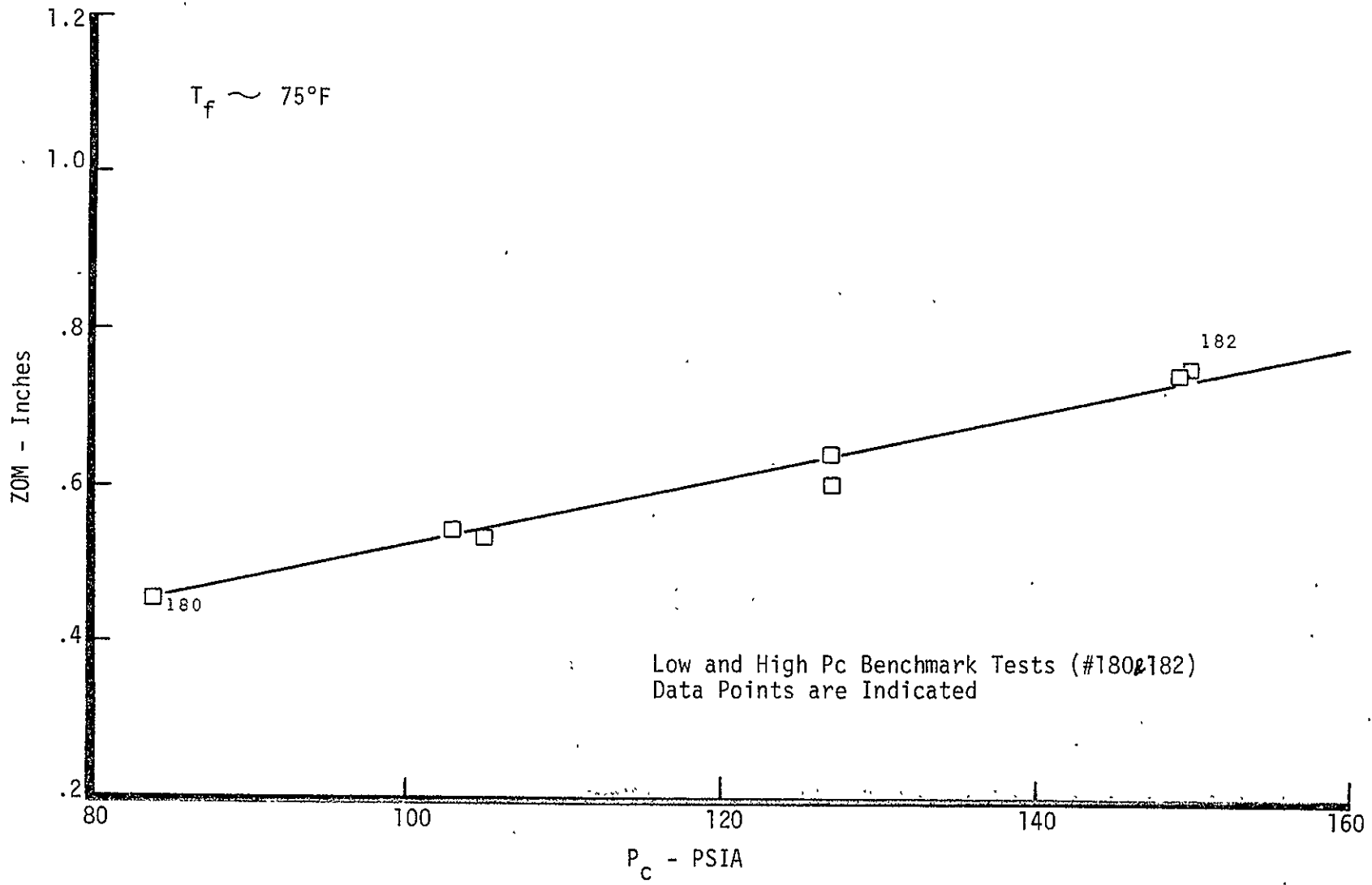
FIGURE 17.   CHAMBER PRESSURE INFLUENCE ON ZOM BASELINE MODEL
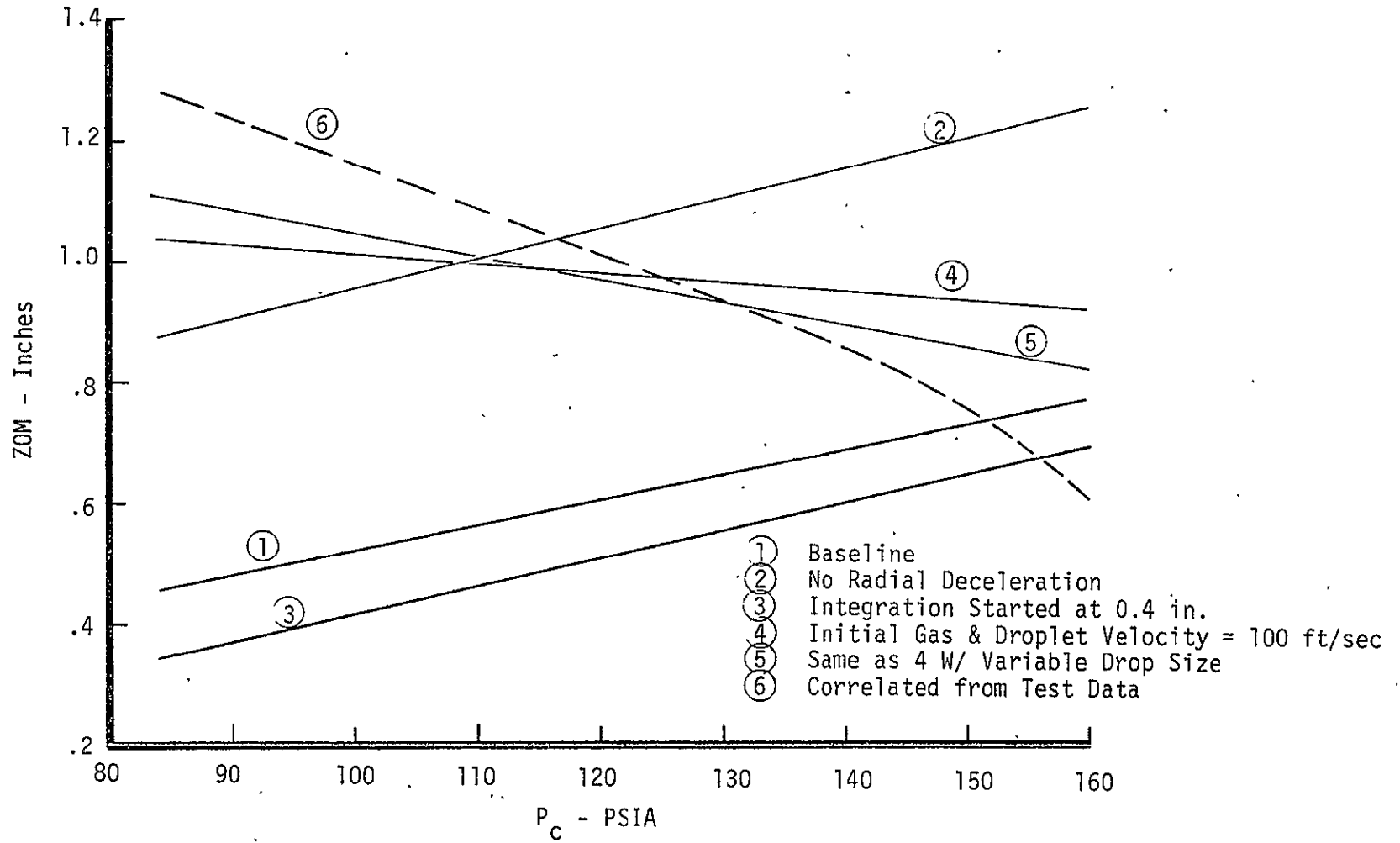
FIGURE 18. ZOM SENSITIVITY FOR DIFFERENT MODEL CALCULATIONAL ASSUMPTIONS

reasoned that since jet impingement and breakup require a finite time to occur the droplet acceleration calculation should begin at an axial plane consistent with initial development of atomized droplets. This calculational method did not significantly affect the trend or absolute magnitude of the predicted ZOM value. The third calculational change was based on the following observation. Although the tests at higher chamber pressure possessed higher near zone gas velocities that should flatten the droplet trajectory more rapidly they also result in higher initial injection velocities. The high initial radial velocity component is decelerated at a much slower rate than the axial component is accelerated. This results in the initial radial component predominating the calculation of the local droplet velocity vector as the droplet is marched downstream. Therefore, to verify this observation the third calculational change (Case 4 in the figure)was to assume an initial gas and droplet velocity for each test of 100 ft/sec. The droplet acceleration calculation was initiated when the empirically calculated gas velocity exceeded 100 ft/sec. The resultant ZOM trend is opposite to the previous cases because the influence of droplet injection velocity has been eliminated. This ZOM trend is consistent with the test data trend of decreasing C* efficiency with increasing chamber pressure. This method was varied only slightly in the final case 5 calculation by accounting for an influence of jet injection velocity on the atomized mass median drop diameter.

These initial model ZOM predictions were evaluated by "backing out" test ZOM values based on actual measured test C* efficiency. The test correlated ZOM trend is shown as curve 6 in Figure 18. This curve was developed through use of Figures 19 and 20. Figure 19 displays calculated test vaporization efficiency versus chamber pressure. The calculation was made with a "two-flame" modified version of the Priem L-General model (Ref. 17). Figure 20 shows the DER LISP subprogram predicted relationship between the ZOM plane location and mixing efficiency. This sensitivity curve of $n_{C*_{mix}}$ versus ZOM was based on quadlet mass distribution coefficients developed in-house at ALRC. The test "backed out" ZOM value was calculated knowing the measured test C* efficiency and the predicted test vaporization efficiency.
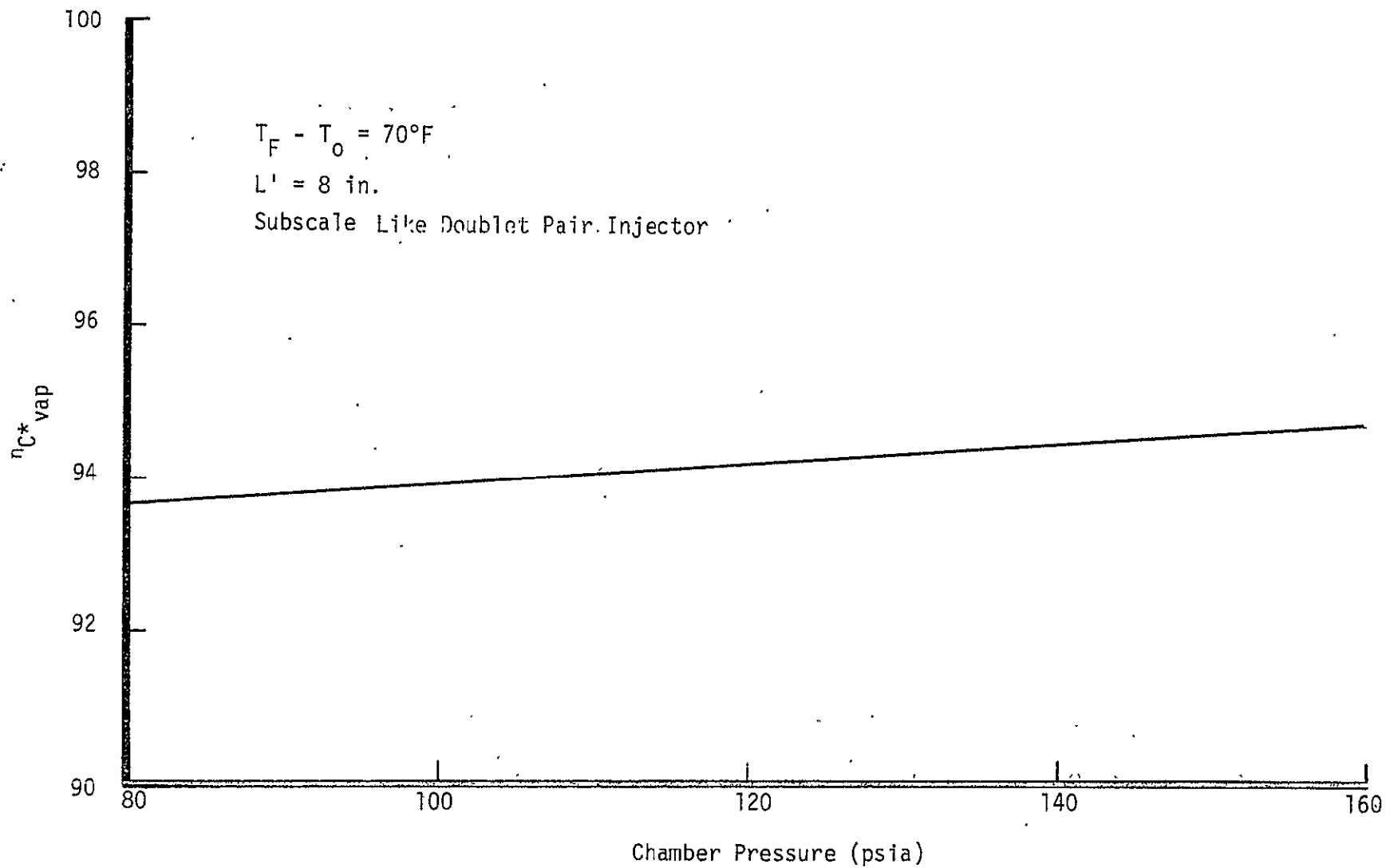
FIGURE 19.   VAPORIZATION EFFICIENCY SENSITIVITY TO CHAMBER PRESSURE

-65-
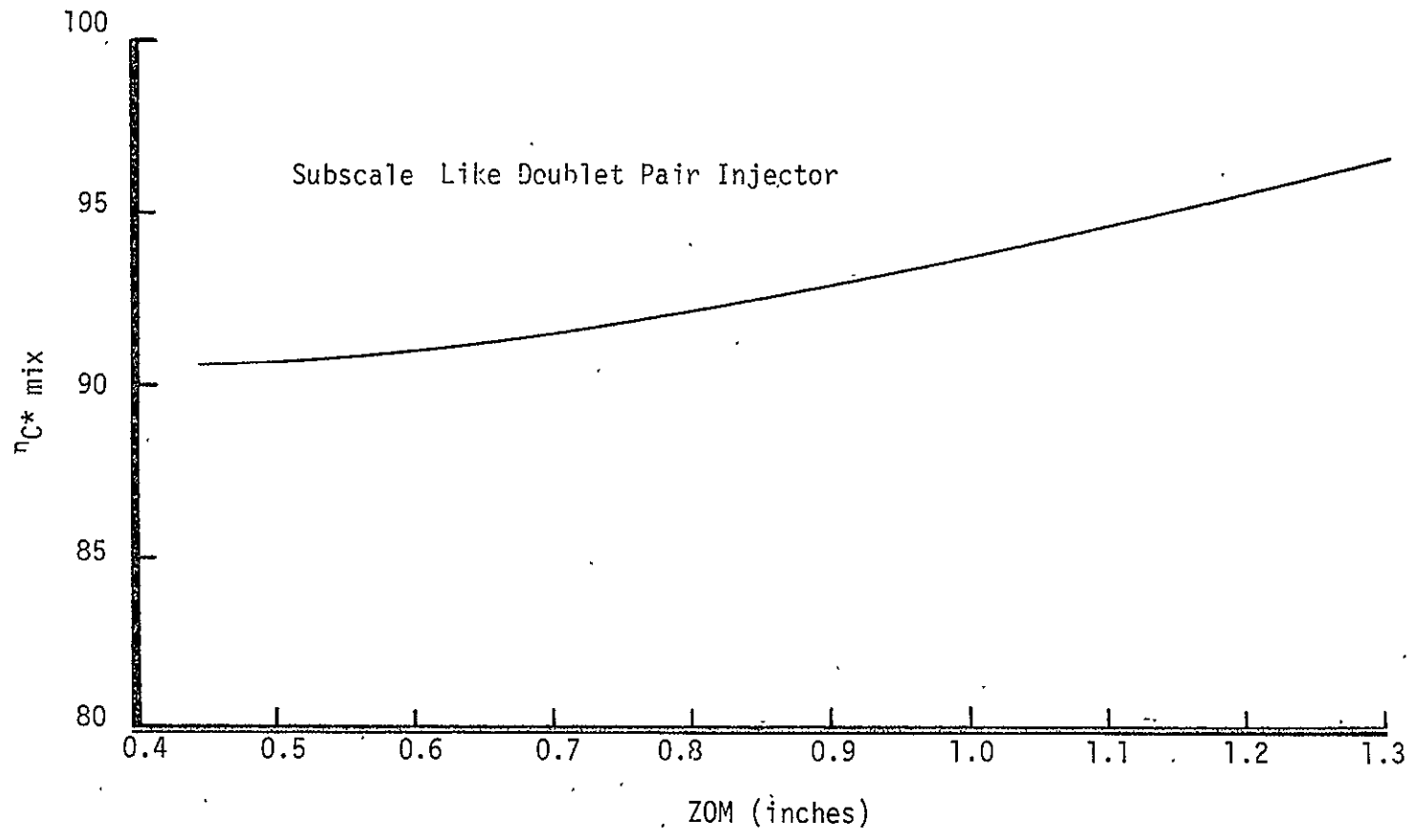
FIGURE 20.   C* MIXING EFFICIENCY SENSITIVITY TO ZOM PLANE

$$\eta_{C*_{mix}} = \eta_{C*_{test}} / \eta_{C*_{vap}} \qquad (17)$$

$$ZOM = f(\eta_{C*_{mix}}), \text{ from Figure 20} \qquad (18)$$

The absolute magnitude of the test ZOM value can be affected by error influences of the vaporization calculation, the LISP calculation, and the test C* efficiency measurement. However, the trend of test ZOM versus chamber pressure accurately reflects the actual test results of increasing performance with increasing test chamber pressure. Returning to Figure [18], it is encouraging that the model predicts ZOM values that have absolute values near those determined from the test data. However, it is apparent that only the case 4 and 5 ZOM calculational methods produce a trend approaching that deduced through "backing out" ZOM from the test data.

The correlations shown in Figure 18 resulted in the observation that droplet injection momentum forces dominate the ZOM calculation in a way that overshadows the influence of higher combustion gas velocity forces on droplet trajectories. Opposingly, the test data trend clearly reflects a test variable influence that affects measured performance to a greater degree than injection velocity. For this reason, the possibility that Reactive Stream Separation (RSS or "blowapart) forces affected quadlet injector performance was investigated. A discussion on RSS is included in Section C.5 of Appendix A. A recently completed subscale injector test investigation (Ref. [18]) indicates that RSS can be accurately modeled and predicted in terms of injector/chamber design and operating variables. The application of the Ref. [18] quadlet RSS model to the task test data base is shown in Figure [21]. The model predicts that the majority of the quadlet test data is in the separated operating mode. The previously presented ZOM model prediction results indicate that strong reactive forces, such as produced by RSS, are required to result in the measured quadlet test data trends. Encouragingly, for modeling purposes, the test data indicates that RSS is a continuous process (note the linear test η_{C*} trend versus chamber pressure in Figure [15] that does not result in step function changes in injector performance. The same conclusion was reached in Ref. [18] after reduction and correlation of several hundred tests conducted with many different injector
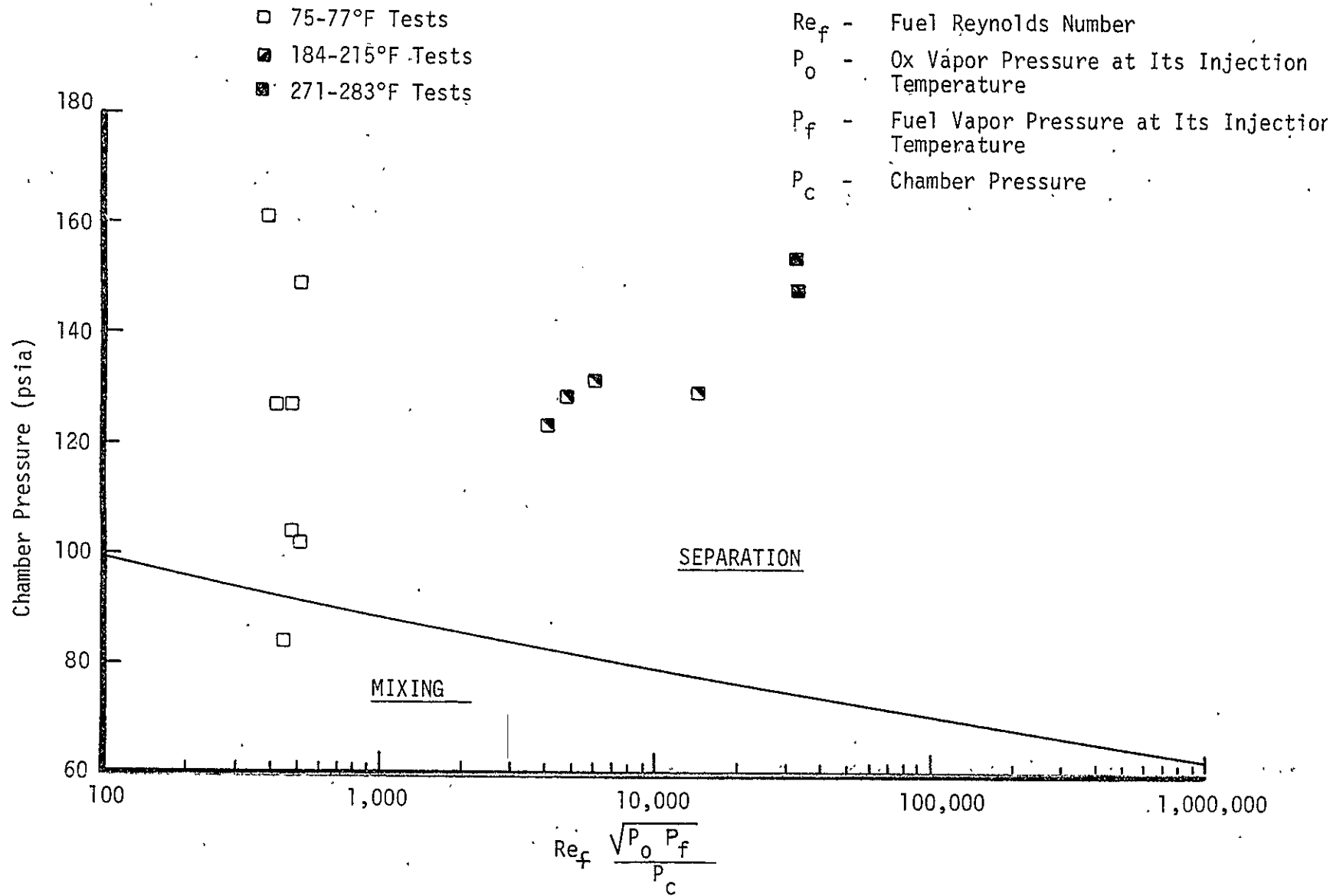
FIGURE 21. LIKE DOUBLET PAIR INJECTOR RSS CHARACTERIZATION

types and designs. Additionally, work has already been initiated towards the analytical modeling of the RSS phenomenon (Ref. 19).

The influence of fuel temperature on the ZOM prediction trends was also investigated to gain further data in support of the conclusions reached from the chamber pressure correlation effort. Figure 22 displays the influence of fuel temperature on test C* efficiency for six tests conducted at a chamber pressure of 130 psia. Test C* shows a significant decreasing trend as the fuel temperature is increased. The relationship between the empirically based combustion gas velocity profile for a low and high fuel temperature test is shown in Figure 23. Again, the higher performing test (Test #176) has a lower rate of energy release in the injector near zone. The ZOM model predictions for the six tests are presented in Figure 24. As before, an incorrect ZOM trend was produced with the baseline model. As fuel temperature increases the fuel density decreases resulting in increased injection velocity that again dominates the influence of increased axial acceleration forces. The fuel temperature correlations supports the previous results of the chamber pressure correlation effort.

D.   Conclusions and Recommendations

1. · Conclusions

The following conclusions have been reached from the initial a priori ZOM prediction model development effort.

a.   The OMS subscale test program (Ref.14) has resulted in an excellent data base for the investigation of near-zone combustion and mixing phenomenon.

b.   The formulated ZOM prediction model should be tested with a data set that is void of significant "blowapart" forces.

c.   The gas acceleration effects ZOM model calculates ZOM values on the level of those required to accurately predict injector mixing performance. Therefore, the model most probably accurately accounts for near zone injection and gas acceleration momentum forces.
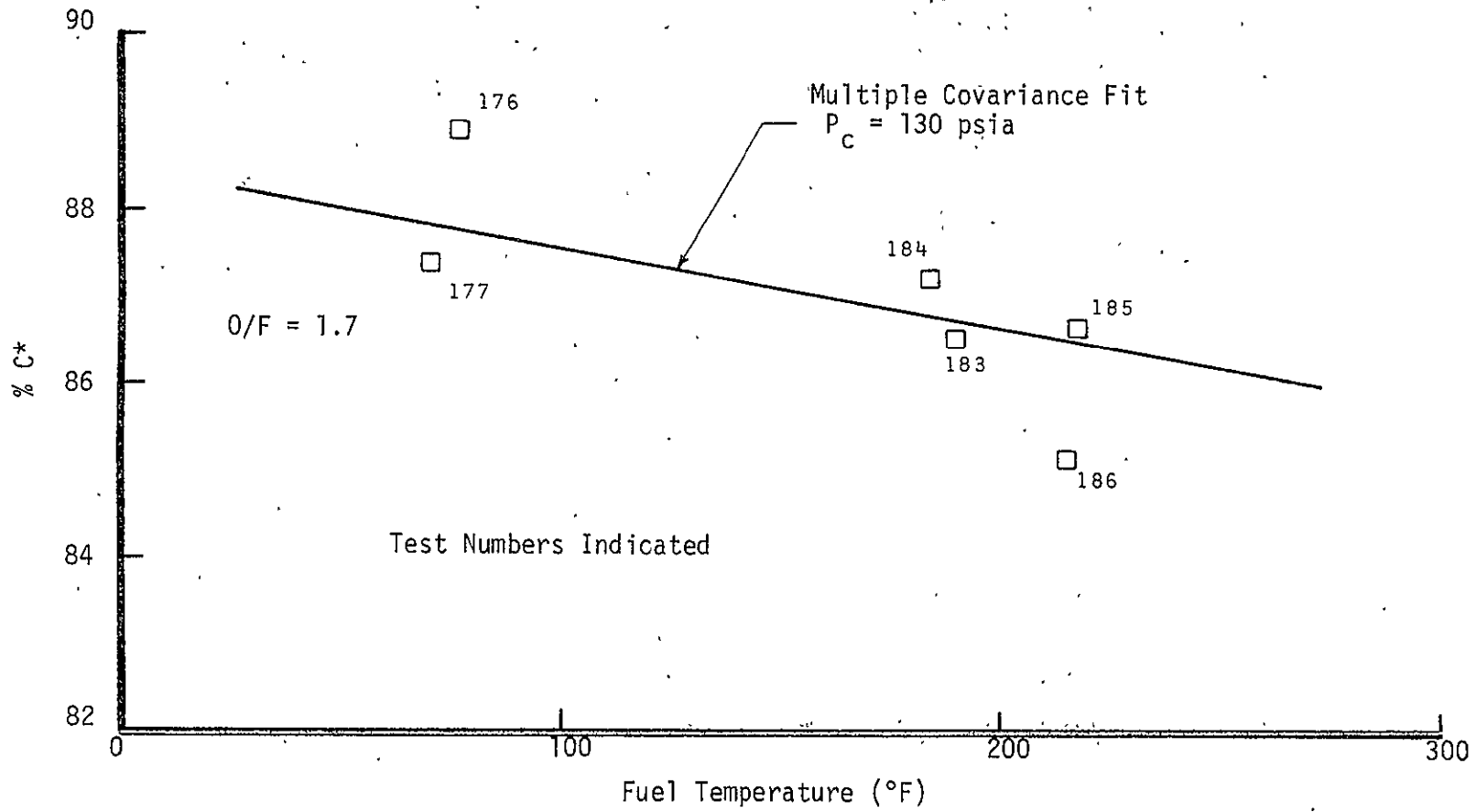
FIGURE 22.   FUEL TEMPERATURE INFLUENCE ON INJECTOR PERFORMANCE
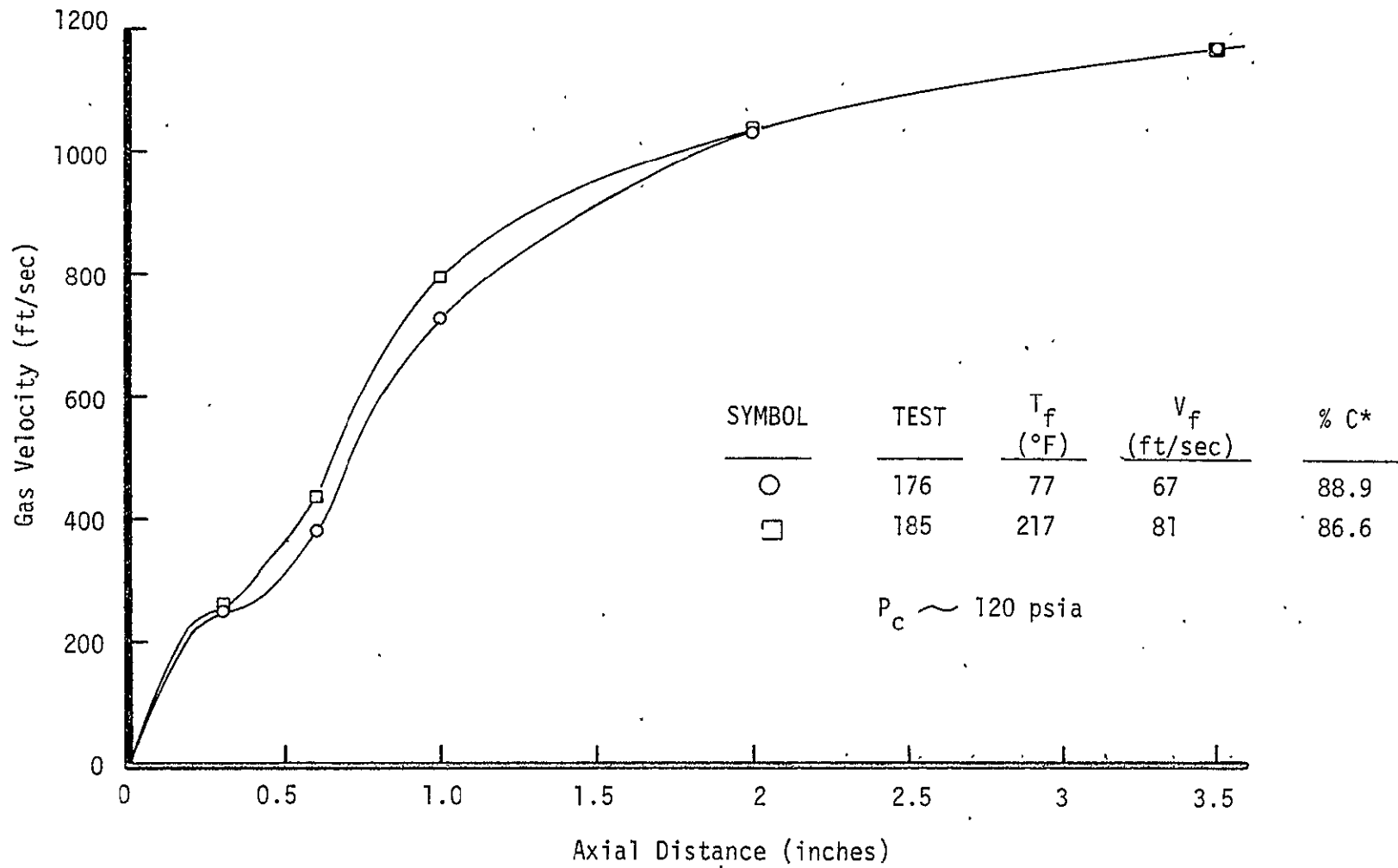
FIGURE 23.   FUEL TEMPERATURE INFLUENCE ON CHAMBER GAS VELOCITY PROFILE
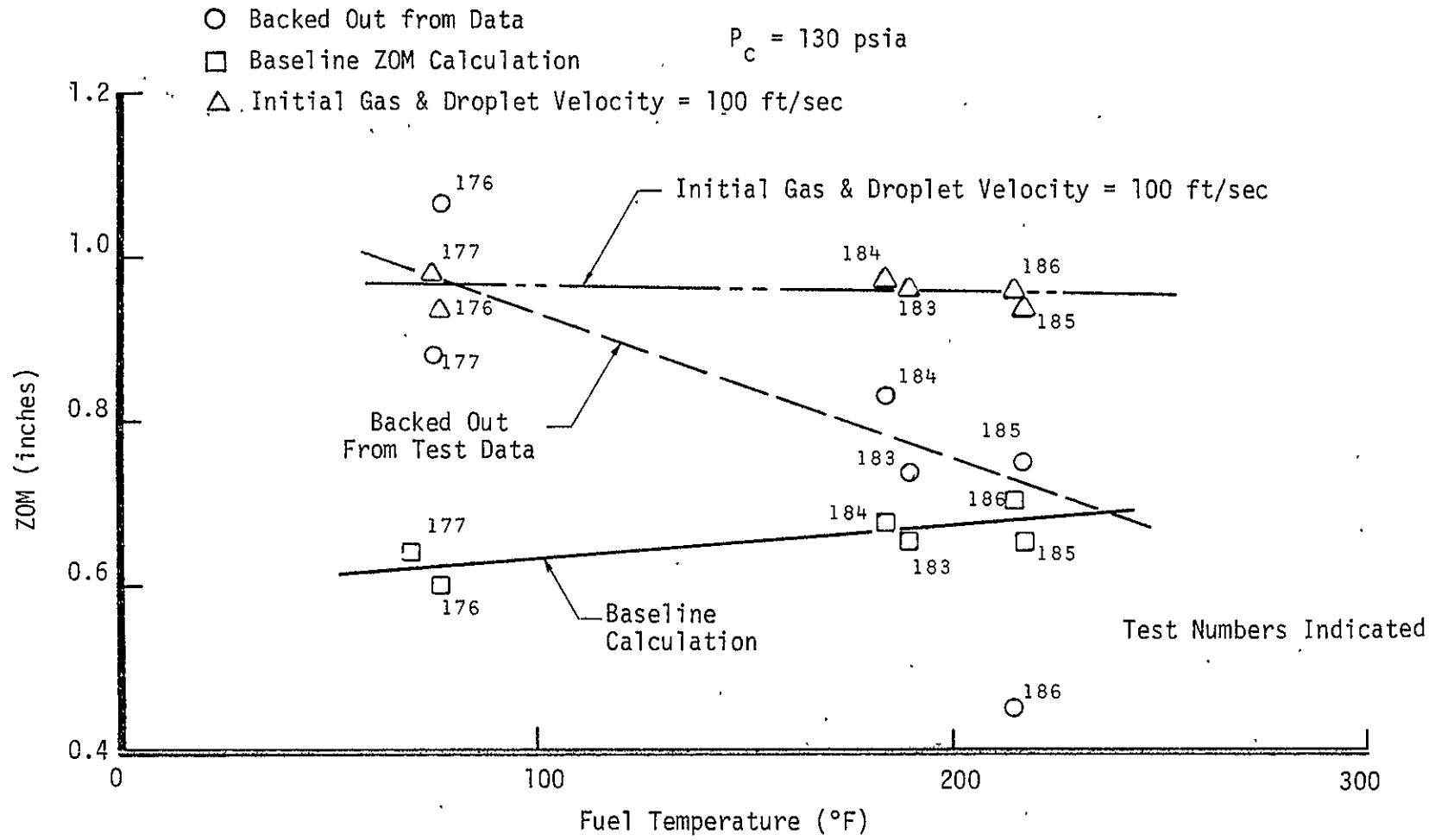
FIGURE 24.   FUEL TEMPERATURE INFLUENCE ON ZOM

d.   Combustion reactive forces due to the mechanism termed "blowapart" strongly alter droplet inertial forces.

e.   A physically mechanistic near-zone model that will predict the ZOM location must account for both gas acceleration and reactive stream forces on droplet spray fan formation and mixing.

2.   Recommendations

The following recommendations are made based on the above conclusions reached from the ZOM prediction model correlation task.

a.   The gas acceleration effects model should be further tested through application to a data base void of significant "blowapart" forces. Subscale (1K lbf) quadlet injector data, similar to the OMS data, was developed on the current Improved Transtage Injector Program. This data is at low chamber pressure and injection velocities and therefore is well suited for such an evaluation.

b.   The ZOM prediction model development effort should be continued with emphasis on the analytical modeling of reactive stream forces. The work initiated in Ref. 19 should be evaluated for application to the ZOM model.

VI   CONCLUSIONS

The major conclusions from this program were:

1.   The JANNAF Performance Evaluation Methodology is being advanced with regard to accuracy and applicability through conductance on this and other related technology programs. Such programs must continue based on resultant recommendations to end in valuable, standardized analytical prediction procedures.

2.   The intended predictive accuracy of the JANNAF rigorous prediction procedure(to within 1 percent for predicted specific impulse) is, in general, out of the question for a priori performance prediction.

3.   The generality of the CICM program is limited due to absence of an intra-element mixing model. If the use of single element cold flow data to specify the intra-element mass distribution is continued, a standard measurement technique should be developed. A standard methodology for interpreting and inputing the data to CICM is also required. Preferably, an intra-element mixing model should be developed for CICM.

4.   The CICM analysis results verified the CICM vaporization model for the case where injector intra-element mixing losses are negligible.

5.   The new ZOM mixing model development initiated during the program should be continued with the emphasis on the analytical modeling of reactive stream forces. A physically mechanistic near-zone model that will predict the ZOM location must account for both gas acceleration and reactive stream forces on droplet spray fan formation and mixing.

APPENDIX A

DER COMPUTER MODEL REVIEW RESULTS

APPENDIX A
DER COMPUTER MODEL REVIEW RESULTS

TABLE OF CONTENTS

This appendix details the results of the DER computer program review. The review was accomplished in four subtasks. (1) Identification and Correction of Coding Errors, (2) Addition of Diagnostic Comment Cards and Print-Out Statements, (3) Identification of Inadequate Formulations and Model Technical Shortcomings, and (4) Review of the JANNAF Performance Prediction Procedures (CPIA 246) with regard to use of DER. A complete summary of the recommendations resulting from the review are included in Section III.A. of this report.

A.   Identification and Correction of Coding Errors

A new "standardized" DER program is currently undergoing final development. General release is planned for the fall of 1976. This effort will result in a code considerably changed from the subcritical K-Prime version reviewed during Task I of the Injection Processes (IP) Program. For this reason no attempt was made to verify every formulation in the DER code. The results of the coding review are presented below. The majority of the comments do not concern errors, as such, but points that should be brought to the attention of the DER user to generate increased understanding of program limitations.

1.   LISP Unsymmetrical Pie Section Input Problem

The following must be true to result in an accurate total propellant flowrate integration calculation at the LISP collection plane (ZOM).

(a)   For an injector slice of θ degrees the slice must contain exactly $(\theta/360 \times 100)$ percent of the total number of injector elements. This requirement is sometimes difficult to achieve for fine patterns. If the above stipulation is met LISP will execute properly. However, the total flowrates used in STC will be in error unless the following is also true:

(b) θ must be a integer divisor of 360 degrees. That is, a θ value of 40 degrees will work, but a θ value of 39 degrees will cause an error in the STC total flowrate.

In the case of an unsymmetrical injector it is sometimes impossible to satisfy both points (a) and (b). An improved technique would be to adjust the collected pie section mass flowrate to $\theta/360$ of the total injected flow of each propellant.

2. <u>STC Mesh Point Dimensional Limits</u>.

LISP will execute properly if the total number of mesh points (NRML, constant radius lines x NTHML, constant θ lines) is equal to 400 or less. Any combination of NRML and NTHML will work. However, dimensional arrays in STC require that NTHML < 20 and NRWALL ≤ 20 (number of NRML to wall). Otherwise, the STAPE and SCRMBL routines will compute inaccurate streamtube flowrates. This STC limitation is not noted in the DER user's manual. It should be noted in the user's manual, or preferably removed to allow any NTHML-NRWALL combination in STC.

3. <u>Drop Size Equation Inconsistencies</u>

Examination of the drop size routine DSIZE indicated that two drop size equations differ from the equations given in DER documentation. The equations were inconsistent for (1) the center orifice of a Triplet or Pentad (4-on-1) element, and (2) the contraction ratio adjustment factor for secondary atomization of like doublet elements. The differences should be resolved, but basic questions concerning the validity of DER drop size prediction equations are a more important issue. The drop size equations are thoroughly evaluated in Section C.1. of this appendix.

4. <u>Triplet and Pentad Collection Plane Rotation Error</u>

An error exists in the LISP calculation of the ZOM mesh point mass fluxes for triplet and pentad elements. Inline triplet and pentad elements are symmetrical about both the face plane X and Y axis. The LISP subroutine SCOEF calculates a rotation of the ZOM collection plane around the normal X axis based on the relative fuel and oxidizer element momentum. For a regular symmetrical triplet or pentad the resultant spray fan will always be normal to the chamber longitudinal (Z) axis. The skewing of the collection

A-3

plane calculated by LISP results in incorrectly computed ZOM nodal point mass fluxes. This error can be eliminated by setting the variable ALFMOM equal to 0 in the triplet section of the SCOEF code.

5. LISP Infinite Baffle Height Assumption

When calculating mass distributions for injectors with baffles, the LISP subroutine BNDY assumes infinite baffle height. This technique results in large accumulation of mass at the baffle boundary. The ZOM mass distribution should be a function of baffle height. This limitation should be noted in the DER user's manual.

B. Addition of Diagnostic Comment Cards and Printout Statements

Error message requirements identified from Section A of this appendix and previous DER analyses are listed below. They are confined to the main LISP and STC routines.

1. LISP Error Messages

The main inconvenience for the user of LISP is that input errors that are detected do not have accompanying error messages that specifically pinpoint the problem.

(a) An error message is required to explain inconsistency between the program NTHML, NTHL, and NTHR inputs.

(b) An error message is required to identify input that assigns excessively high values to the NMESH, NEL, and NLSPEC program variables. NMESH is the total number of LISP nodal points, i.e., the product of the inputs NRML and NTHML. NEL is the total number of injector elements and NLSPEC the number of different element specifications input.

(c) An error message is required to specifically state the program failure associated with improper input of the Type 8 injector spray coefficients.

2.   STC Error Messages

        (a)   The limitation on the STC radial and angular mesh
lines has been alluded to (NTHML and NRWALL $\leq$ 20). If this limitation is not
removed an error message should be included in STC to identify the problem.

    C.   Identification of Inadequate Formulations and Model Technical
          Shortcomings

        Several inadequate formulations and shortcomings have been identi-
fied which limit the current predictive capability of DER. The purpose of
this subtask of the DER review was to identify model problem areas and, if
possible, to propose alternate approaches for improvement. Incorporation of
the improvements is, for the most part, beyond the scope of this program, but
their identification will provide a basis for future DER work. The model criti-
que is summarized in the following six separate sub-sections concerned with,
respectively; drop size predictions, ZOM plane selection, a DER vaporization
model sensitivity study, near-zone combustion and monopropellant flame consid-
erations, combustion gas acceleration and reactive stream separation effects
on cold flow mass distributions, and the need for a turbulent mixing model in
the STC subprogram. A seventh and final section contains a proposed approach
for combining ZOM plane, combustion gas acceleration, reactive stream separation,
and turbulent mixing considerations inot a physically realistic mass distri-
bution and mixing model for DER.

        1.   Drop Size Prediction

        The inaccuracy of the LISP drop size predictions has been
a major DER shortcoming identified by two studies that used DER to analyze
engine performance data (Refs. 20 and 21). The DER drop size correlations
were examined for coding accuracy and for reference DER equation predictions
were compared to those made with the empirically based drop size model of
Priem (Ref. 17). The drop size prediction equations for LISP element types
1-5 (unlike doublet, like doublet, like-doublet pair, triplet, pentad (4-on-1),
respectively) were included in the study. Several DER publications indicate.
that Ref. 22 includes a section showing all current DER drop size equations,
but examination of this report uncovered no such write-up.

a.   Unlike Doublet Drop Size Equations

The DER unlike drop size equations are presented in Ref. 23. They are shown below.

Unlike Doublet (larger Diameter Orifice)

$$\overline{D}_{HW} = 1.27 \left(\frac{D_{opp}}{D} \right)^{.38} \frac{1}{U_{D,opp}^{1.19} \, U_D^{.86}} \qquad (A-1)$$

Unlike Doublet (Smaller Diameter Orifice)

$$\overline{D}_{HW} = 2.29 \frac{D^{.27} \, D_{opp}^{.023}}{U_D^{.74} \, U_{D,opp}^{.33}} \qquad (A-2)$$

$\overline{D}_{HW}$ is the mass median drop diameter (inches) determined from molten wax atomization experiments (Ref. 24). $\overline{D}_{HW}$ is corrected in the DER code to account for secondary (aerodynamic) break-up with the following general equation (developed in Ref. 25).

$$\overline{D} = \frac{1}{\dfrac{J_A}{\overline{D}_{HW}} + B} \qquad (A-3)$$

For unlike doublets DER uses values of .8 and 250 for J_A and B, respectively.

In Figure A-1 drop size predictions made with the DER like doublet equations are shown. The predictions shown were made for equal orifice diameters ($D_{large} = D_{small}$) for orifices from .01 inch to .1 inch in diameter (a typical orifice design range). There are four apparent anomalies with the equations. The first peculiarity is that for the same jet size and velocity the large orifice and small orifice $\overline{D}_{HW}$ equations predict drop sizes one order magnitude different. Secondly, whereas the secondary break-up correction reduces the predicted small orifice drop size significantly, the correction actually increases the large orifice drop size prediction. The

A-6
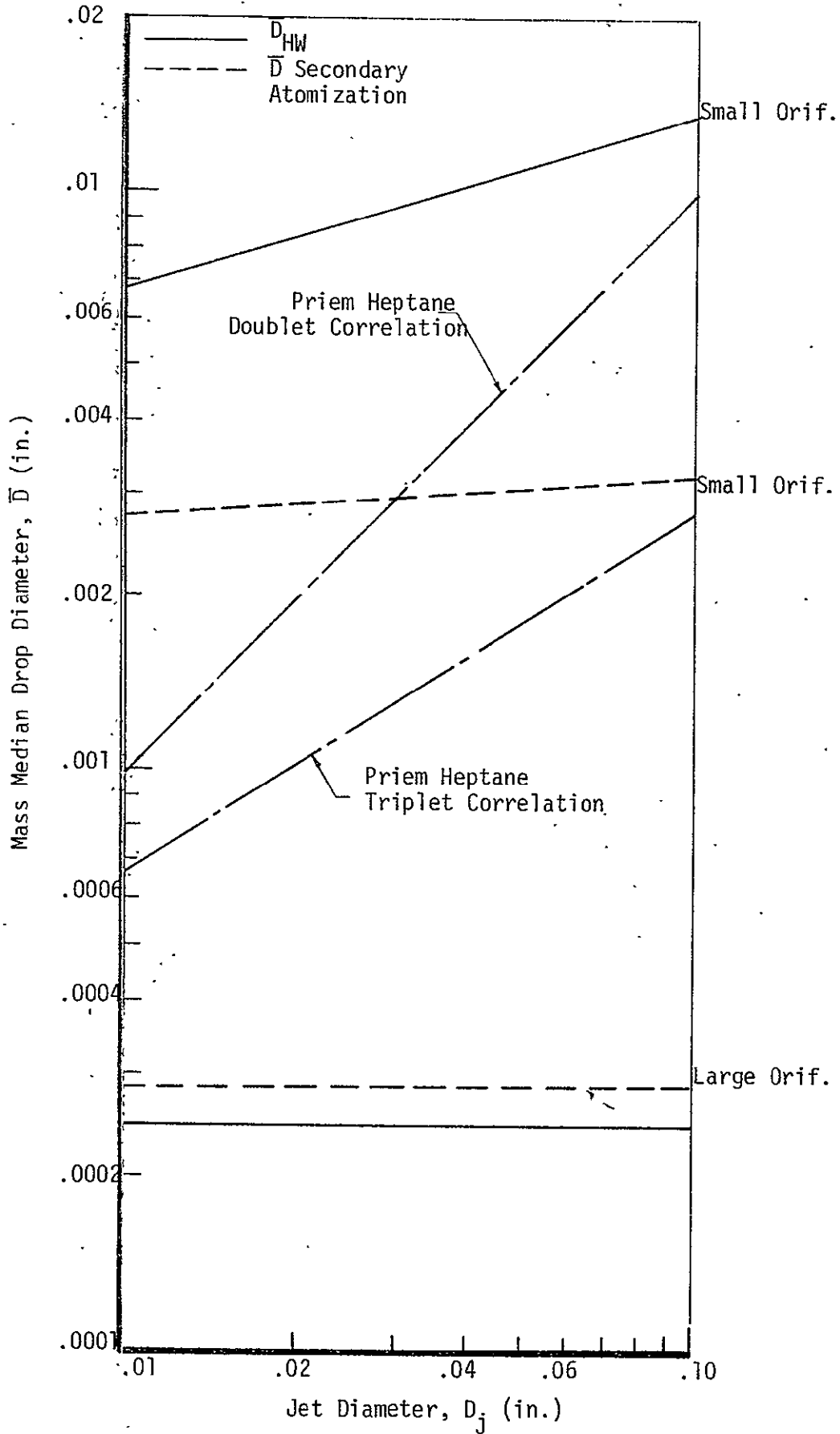
FIGURE A-1. UNLIKE DOUBLET DROP SIZES

A-7

third anomaly is that the large orifice equation correlated from the hot wax experiments shows that jet diameter has no influence on the mass median drop size. Included in the figure, for reference, are predicted drop size trends made with the Priem model for liquid heptane drops. The Priem data shows a significant effect of jet diameter on drop size. Last, the unlike doublet equations do not allow for propellant property effects on the predicted drop size. Priem's model results in drop size being proportional to the propellant properties grouping shown.

$$\overline{D} \sim \left(\frac{\sigma_L \quad \mu_L}{\rho_L} \right)^{1/4} \tag{A-4}$$

Typical atomization models found in the literature, such as those of Weiss and Worsham (Ref. 26), Ingebo and Foster (Ref. 27), and Nukiyama and Tanasawa (Ref. 28) also allow for the influence of liquid properties on the atomized drop diameter.

b.   Triplet and Pentad Drop Size Equations

The drop size equations for triplets and pentads, taken from Ref. 23, are shown below.

Triplet and 4-on-1 (Center Orifice) (Ref. 23)

$$\overline{D}_{HW} = 0.85 \frac{D^{.1} D_{opp}^{.12}}{U_D^{.74} U_{D,opp}^{.33}} \tag{A-5}$$

Triplet and 4-on-1 (Outer Impinging Streams)

$$\overline{D}_{HW} = 3.82 \frac{D^{.68}}{D_{opp}^{.35} U_D^{.56} U_{D,opp}^{.57}} \tag{A-6}$$

Examination of the DER code revealed a different equation for the center orifice.

A-8

$$\overline{D}_{HW} = 0.85 \ \frac{D^{.1} \ D_{opp}^{.12}}{U_D^{.086} \ U_{D,opp}^{.89}} \qquad (A-7)$$

For triplets and pentads DER uses J_A and B values of 0.03 and 310, respectively, in the secondary breakup equation (Eq. A-3). The variation in J_A and B constants for unlike doublets and triplets imply that equal drop sizes produced with different injector element types result in different secondary breakup characteristics. There would appear to be no physical basis for such an effect.

Predictions made with the DER triplet equations, for a range in orifice diameter from .01 to .1 inches, are shown in Figure A-2. The $\overline{D}_{HW}$ (hot wax) equations show realistic trends, but·these results are obliterated by the secondary breakup correction. As an example, the outer orifice $\overline{D}_{HW}$ predictions range from about .006 to .013 inches. When inserted in Eq. A-3 the predicted drop size range is from .00317 inches to .00320 inches. It is apparent from this result that the DER triplet equation is effectively a constant (1/310), since the first term in the Eq. A-3·denominator will always be small compared to the constant second term. Additionally, as was the case for the unlike doublet, the triplet equations do not allow for the effect of propellant properties on the predicted mass median drop size.

c.   Like Doublet (single or pair) Drop Size Equations

Ref. 2 shows the following equation to account for the combined effects of hydraulic and secondary breakup for like doublet elements.

$$\overline{D} = 1.524 \ \left\{ 2.64 \left(\frac{U_D}{D} \right)^{1/2} + \frac{0.0978}{C_{pr}} \ f(\epsilon_c) \left| \frac{480}{\epsilon_c} - U_D \right| \right\}^{-1} \qquad (A-8)$$

The formula for the contraction ratio function (ϵ_c) varies between Ref. 2 and the DER code.
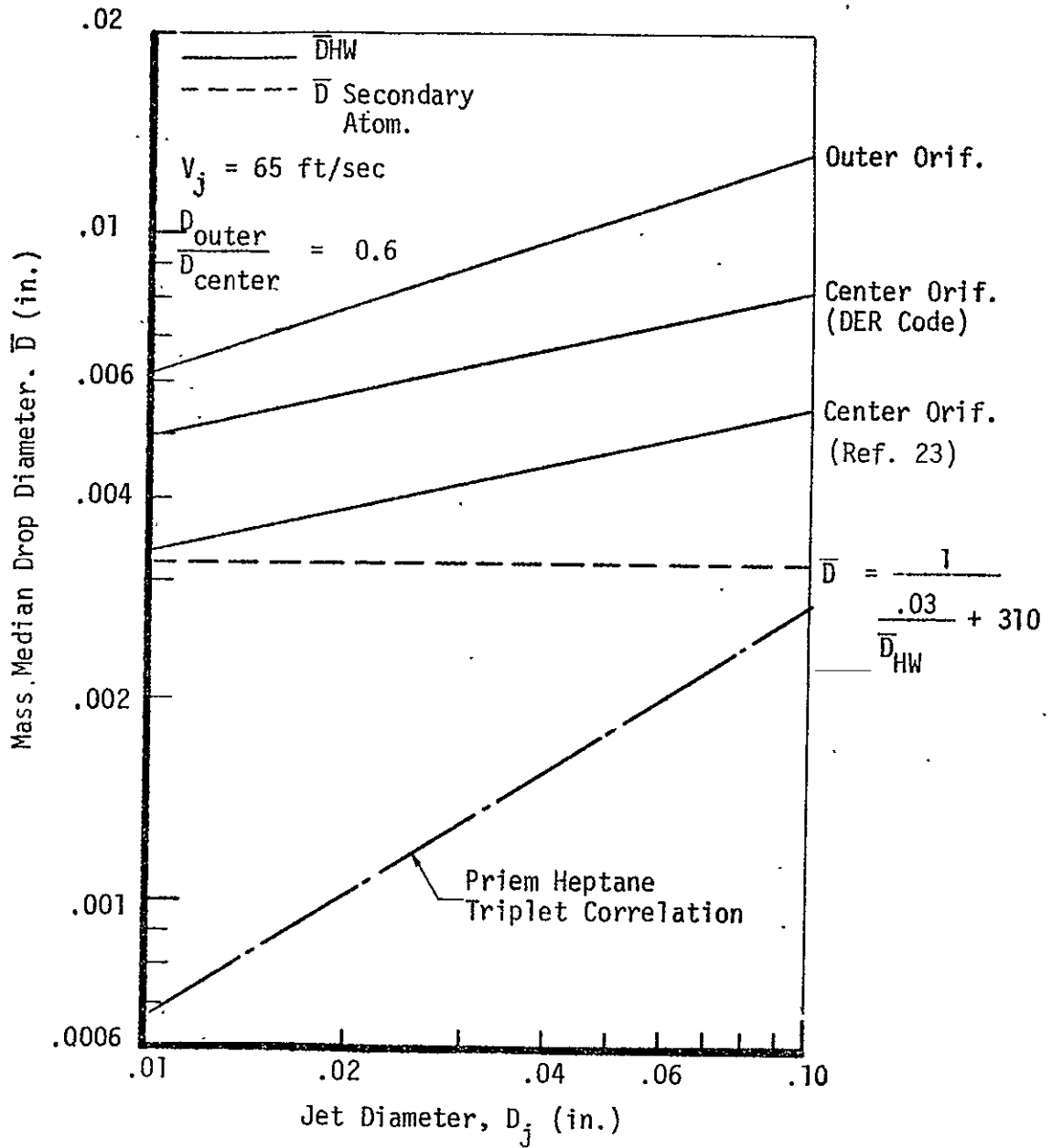
FIGURE A-2. TRIPLET AND PENTAD (4-on-1) DROP SIZES

$$f(\epsilon_c) = \frac{5(\epsilon_c - 1)}{\epsilon_c + 3} \qquad \text{(Ref. 2)} \qquad \text{(A-9)}$$

$$f(\epsilon_c) = \frac{(\epsilon_c - 1)}{\epsilon_c + 3} \qquad \text{(DER Code)} \qquad \text{(A-10)}$$

Predicted drop sizes for these equations are shown in Figure A-3. As shown, the Priem like doublet correlation shows considerably more sensitivity to jet orifice diameter than the DER correlations. The variable C_{pr} is a propellant properties term, that is only included for the secondary breakup part of the drop size equation.

2. ZOM Plane Selection

ZOM is the interface plane (measured from the injector face plane) between the LISP and STC subprograms that comprise DER. ZOM is the plane at which the LISP mass distribution is calculated. The mixing limited performance loss is directly dependent on the ZOM plane calculated mass distribution because STC does not account for turbulent mixing or combustion effects. Two analytical studies (Ref. 20 and 21) have determined that DER predictions are quite sensitive to selection of a value for ZOM. Ref. 2 provides only the following two guidelines to selection of ZOM: (1) the collection plane should be far enough downstream to account for substantial spray spreading and wall impingement, and (2) because LISP does not account for inter-element spray interaction, spray mixing and impingement effects can be over-predicted if ZOM is too far downstream. It is apparent that an a priori method for selection of ZOM does not currently exist.

LISP calculates the mass distribution from an injector element with the following general equation.

$$w_i(x,y,z) = \frac{w_{00i}}{z^2} \left\{ \left[1 + c_1\left(\frac{y}{z}\right) + c_2\left(\frac{y}{z}\right)^2 \right] + \left[c_3\left(\frac{x}{z}\right) \right. \right.$$
$$\left. \left. + c_4\left(\frac{x}{z}\right)^2 \right] \left[1 + c_5\left(\frac{y}{z}\right) + c_6\left(\frac{y}{z}\right)^2 \right] \right\} e^{-a\left(\frac{x}{z}\right)^2 - b\left(\frac{y}{z}\right)^2} \qquad \text{(A-11)}$$

Z is the distance from the element impingement point (H), thus ZOM is the sum
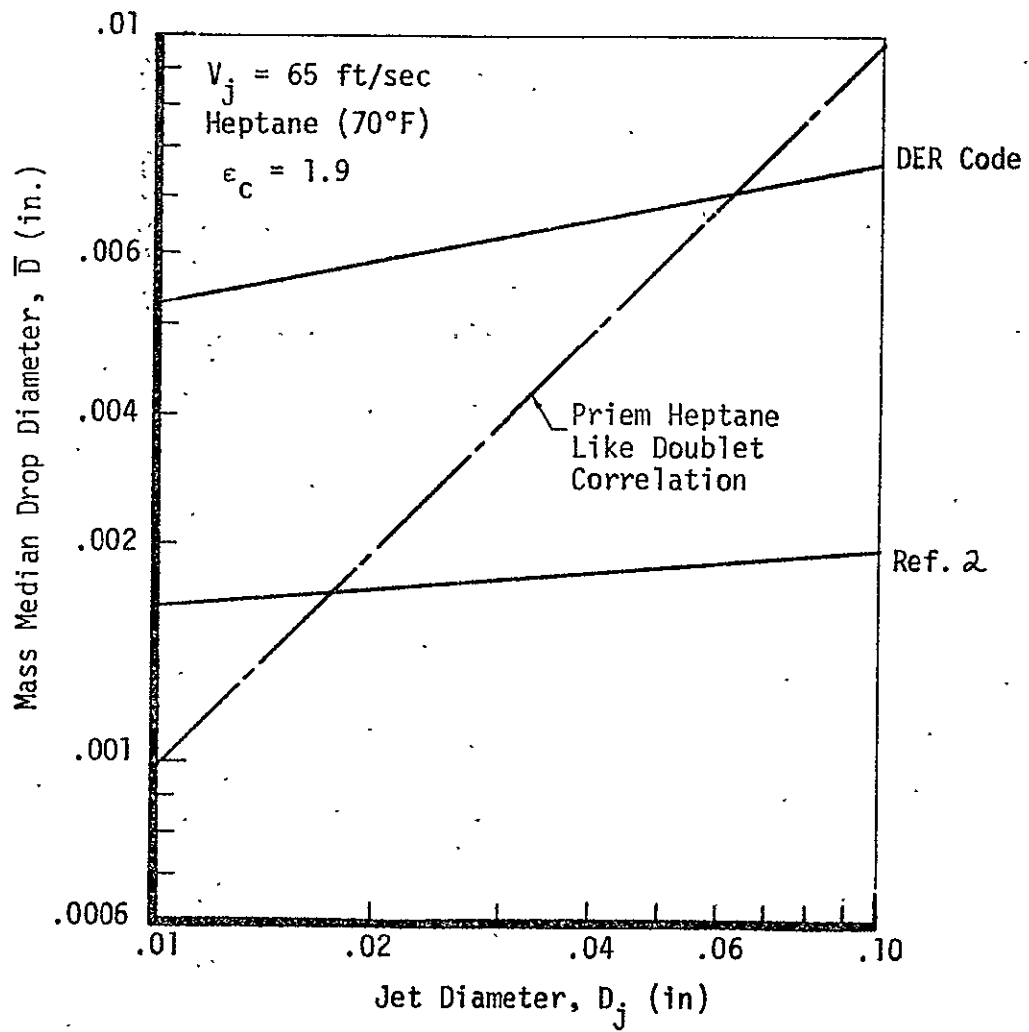
FIGURE A-3. LIKE DOUBLET DROP SIZES

of Z and H. The mass distribution coefficients (C_1, C_2, C_3, C_4, C_5, C_6, a,b) are evaluated empirically from single element cold flow data generated with propellant simulants. The equation assumes that the element spray can be characterized as point source flow and that the spray coefficients for the equation are constant, independent of the Z distance. This assumption has not been verified experimentally.

The LISP mass distribution equation results in a linear half angle spray fan spreading characterization as shown in Figure A-4. Inter-spray mixing increases as ZOM is increased because of spray fan overlap. LISP does not account for any spray fan interaction thus adjacent spray fan mass distributions are simply superimposed on one another. Since no consistently accurate a priori method for selection of the ZOM value exists, attainment of an accurate value usually depends on an iterative process utilizing available hot-fire performance data.

DER
COLD FLOW

HOT FIRE

ZOM

Z

ZOM

RSS EFFECTS'

SPRAY FAN RADIAL
FORCES INSIGNIFICANT
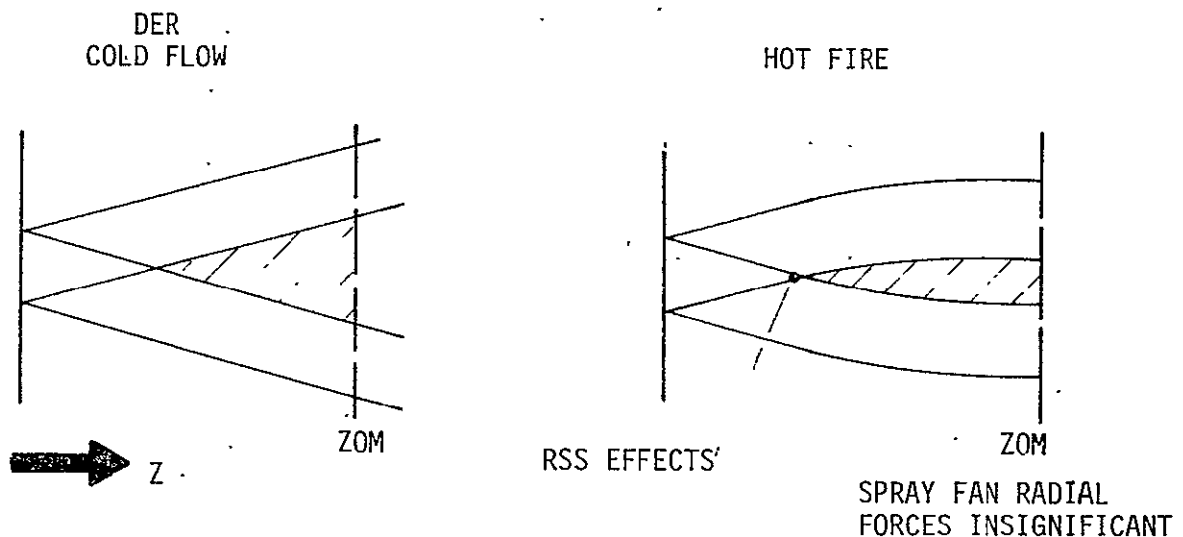
FIGURE A-4.   COMBUSTION EFFECTS ON COLD FLOW SPRAY FAN PROFILE

Finite mixing losses are experienced in hot firings because combustion gas acceleration and reactive stream separation (RSS) forces (if any) combine to impede inter spray fan mixing. It therefore seems reasonable that selection of the ZOM plane should account for the influence of combustion on the chamber spray fan mass distribution. As combustion gas is formed and accelerated significant axial droplet drag forces are generated. These forces result in an effective bending of the cold flow spray fan, as shown in Figure A-4. Eventually, the axial spray fan drag forces dominate any radial droplet velocity forces and inter spray fan mixing stops. During Task II of the IP program a methodology for accounting for combustion effects and for a priori selection of the ZOM plane location was developed. The current status of this model is detailed in Section V of this report.

Recent work (Ref. 18) indicates that, in addition to normal combustion gas acceleration effects, Reactive Stream Separation (RSS or "blow-apart") can also significantly affect chamber mixing performance. RSS has been successfully correlated as a function of the injector element design and operating point. Section B.5 of this appendix expands the RSS topic and suggests ways of incorporating RSS modeling in the LISP mass distribution formulation. A proposed overall development plan for general improvement and update of the LISP ZOM plane mixing technique is included in Section C.7 of this appendix.

A final limitation of the ZOM plane methodology is the relatively narrow parametric range over which spray distribution coefficients have been catelogued in LISP. Currently, if the design point to be analyzed is not within the spray coefficient range for the element type in question the spray coefficients for the nearest available design point are selected. No technique currently exists for extrapolation of the spray coefficients. The current parametric range for the LISP coefficients for the five primary liquid/liquid element types is shown below in Table A-I. Expansion of the spray coefficient matrix is required if the ZOM technique is retained in DER.

TABLE A-I

LISP SPRAY COEFFICIENTS PARAMETRIC RANGE

	Element	Orif. Dia. (in.)	Imping. Angle (deg)	Momentum Ratio (f/o)
(1)	Unlike Doublet	0.020-0.079	45-70	9.42-1.0
(2)	Like Doublet	0.020-0.079	45-70	1.0
(3)	Like Doublet Pair	0.020-0.028	60 Like, 40 Unlike	Not Correlated
(4)	Triplet	0.085-0.067 Outer 0.043-0.067 Inner	70	0.3-8.0
(5)	4-on-1 (Pentad)	0.21-0.47 Inner 0.1-0.22 Outer	60	0.2-1.25

3.   DER Vaporization Sensitivity Study

        The previous subsections have detailed the three most
critical DER analysis input parameters; the mass median drop diaemter, the LISP
spray distribution coefficients, and the LISP/STC interface plane, ZOM. The
specification of these LISP inputs controls, in large part, the accuracy of
the DER calculation. The most important function of the Streamtube Combustion
(STC) subprogram is to compute propellant vaporization to the chamber throat
plane, after correct input is established and STC has segregated the LISP
calculated mass distribution into a finite number of axisymmetric streamtubes.
The third subtask of the DER review was a vaporization sensitivity study
conducted to determine the influence of engine design and operating variables
on the DER vaporization calculation. DER predictions were compared to similar
calculations made with the simplified Priem L-General model (Ref. 17) for
reference. The Priem L-General model is an empirical correlation of an analy-
tical vaporization model that accounts for droplet heating. The L-General
model accounts for the effect of chamber length, contraction ratio, chamber
pressure, injection velocity, drop size, initial propellant temperature and
propellant properties on vaporization rate.

The vaporization sensitivity study was conducted by running single stream calculations with STC. The NTO/MMH propellant combination was selected because of experience obtained during the Space Shuttle OMS Engine program. Oxidizer and fuel mass median drop diameter, initial velocity, and total flowrates were input to STC. A log normal drop size distribution (σ = 2.3), with five size groups for each propellant, was used throughout the study, except during the phase of the study which evaluated the effect of the specified drop distribution on the vaporization efficiency prediction. The independent design and program input variables evaluated during the study included chamber length, mass median drop diameter, chamber pressure, droplet initial (injection) velocity, chamber contraction ratio, propellant inlet temperature, and the propellant drop size distribution. The study nominal calculation point and the parametric range of the independent variables is detailed in Table A-II.

TABLE A-II

DER VAPORIZATION SENSITIVITY STUDY
VARIABLE RANGES

Variable	Nominal Value	Range
Chanber Length, L' (in)	6	6-14
Mass Median Drop Diameter, $\overline{D}$ (in)	.002	.001-.004
Chamber Pressure, Pc (psia)	120	60-240
Injection Velocity, V_j (ft/sec)	65	65-200
Contraction Ratio, ε_c	1.9	1.9-5
Propellant Temp., T_p (°F)	70	40-130

In addition to the DER vaporization sensitivity study, the recent comprehensive combustion model evaluation conducted by Bracco (Ref. 7) was reviewed. This study resulted in three conclusions that are relevant to the DER review. First, the Priem vaporization model, used as the reference technique in the sensitivity study, was judged to be capable of accurate correlation of empirical ethanol mass vaporization profiles. Secondly, the Priem

C-2

technique was most accurate if the droplet drag coefficient was assigned a low but finite value ($0 < C_D < 24/Re$). A major conclusion by Bracco was that low drag coefficients give better results than higher drag equations, such as the Rabin equations (See Section C.3.d. of this appendix) used in DER. In support of lower drag coefficients he cites Eisenklam's suggestion (Ref. 29) that burning droplets actually have lower drag coefficients than solid spheres. The final significant conclusion of Braccos work is that a drop size distribution function is not necessary to accurately reproduce the steady combustion profile, although it does tend to improve the results.

The results of the vaporization study are presented below for each design variable shown in Table A-II.

- a.   Chamber Length

Propellant vaporization was calculated at three chamber lengths (6, 10, and 14 inches) with DER and the Priem L-General model. Figure A-5 shows that both models predict similar trends of propellant vaporization versus chamber length. The calculated absolute levels differ somewhat for the MMH vaporization characteristic. This difference is believed to be related to the fact that DER does not allow for the finite time required to heat the liquid propellant to the chamber "wet bulb" condition. This omission is described more fully in the section dealing with propellant inlet temperature considerations. The trend agreement versus chamber length for the Priem and DER models suggests that both model the gas dynamic, droplet ballistic, and steady state heat and mass transfer processes similarly. This result is clouded somewhat by the chamber pressure sensitivity result presented in the next paragraph.

b.   Chamber Pressure

Propellant vaporization was calculated for chamber pressures ranging from approximately 60 to 240 psia. The results of this phase of the sensitivity study are shown in Figure A-6. The figure indicates a significant difference exists between the predicted effect of chamber pressure on propellant vaporization for the DER and Priem models. The DER model indi-
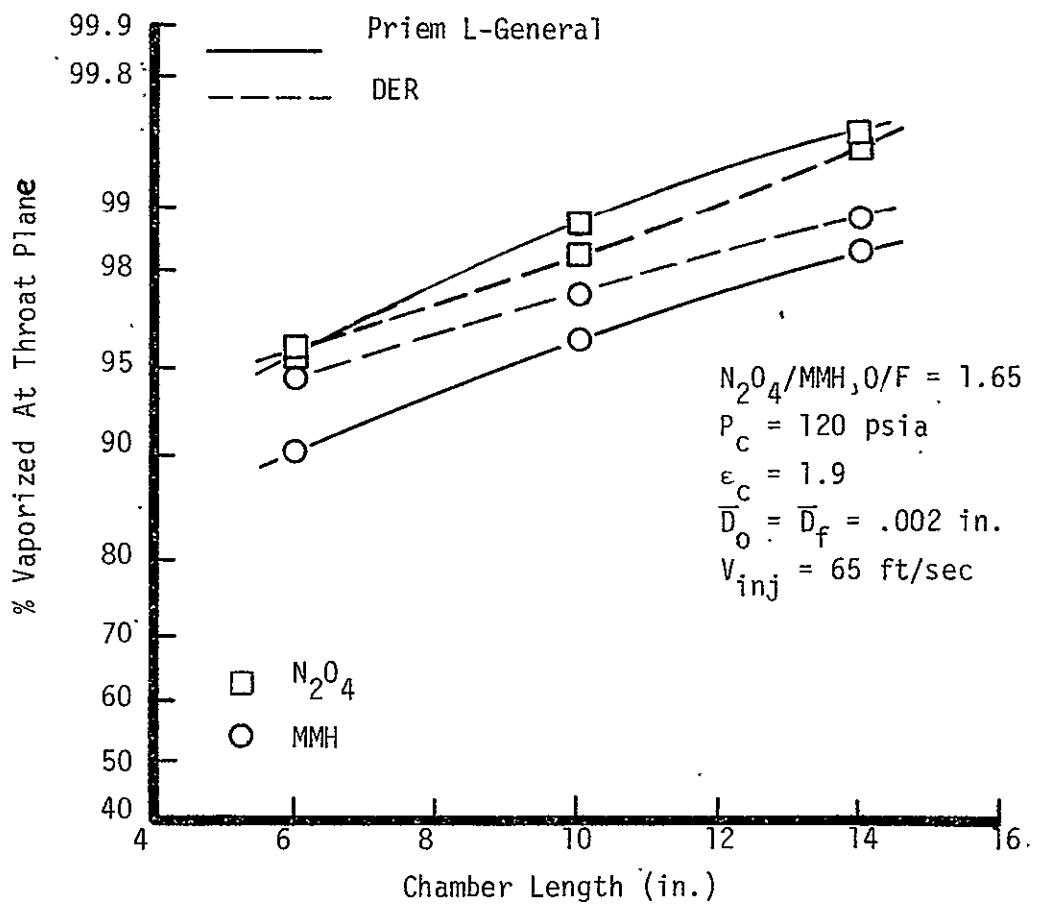
FIGURE A-5. CHAMBER LENGTH EFFECT ON VAPORIZATION
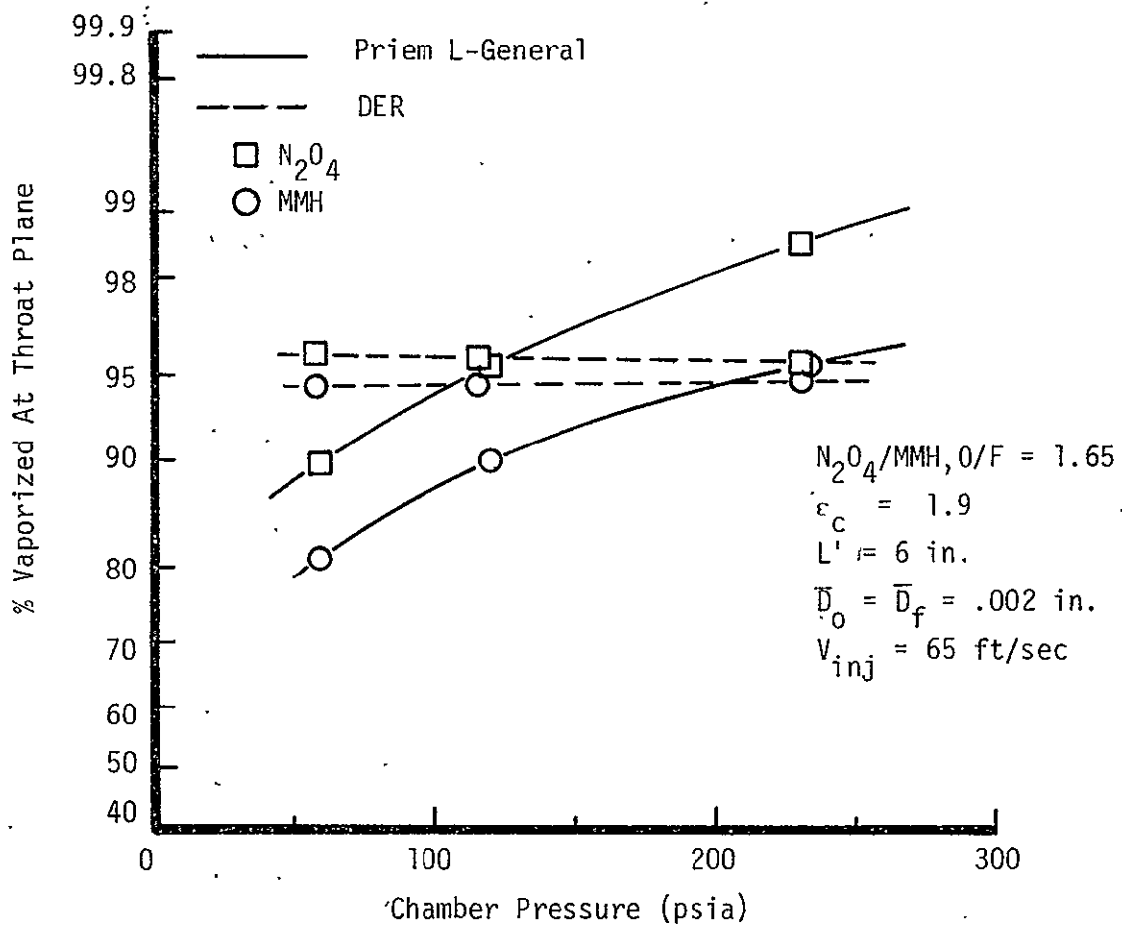
FIGURE A-6. CHAMBER PRESSURE EFFECT ON VAPORIZATION

cates no sensitivity to chamber pressure, while the Preim model shows a significant influence*. The DER and Priem vaporization formulations were briefly investigated to determine the reason for the chamber pressure influence difference. The DER K-Prime model is based on the early work of El Wakil and others (Ref. 30). An admitted weakness of this model was the need for a correction factor accounting for unidirectional, as opposed to equimolal, droplet vapor diffusion in the mass transfer equations. The Priem model accomplishes the transformation through the following equation.

$$(j_{a,s})_{unidirectional} = (j_{a,s})_{equimolal} \quad x \quad (\alpha)$$

where: $\quad \alpha = \dfrac{p_s}{p_{a,s}} \quad \ln \left[\dfrac{p_s}{p_s - p_{a,s}} \right]$ (A-12)

The mass transfer rate equation without the unidirectional diffusion correction is written as:

$$W = A_s K \, p_{a,s}$$ (A-13)

Including the α term yields the following, which results in a term showing a directly proportional relationship between the mass transfer rate and the local static pressure.

$$W = A_s K \, p_s \quad \ln \left[\dfrac{p_s}{p_s - p_{a,s}} \right]$$ (A-14)

It is suggested that possibly the DER K-Prime model does not accurately account for the effect of chamber pressure on the vaporization rate because of this omission. Complete resolution of this question was beyond the scope of the current work.

---

*Priem correlated an effective chamber length (L_{gen}) as being proportional to $p_c^{0.66}$.

c.   Mass Median Droplet Diameter

Propellant vaporization was calculated for mass
median driplet diameters of .001, .002, .003, and .004 inches. Relatively
small droplets were selected because state-of-the-art injector designs are
attaining performance consistent with such drop sizes. The results of the
drop diameter study are plotted in Figure A-7. The trends for the DER and
Priem models are nearly identical. The figure indicates that both formula-
tions account for the influence of drop diameter on mass transfer, heat
transfer, and droplet ballistics.

d.   Droplet Initial (Injection) Velocity

Propellant vaporization was calculated for droplet
initial velocities of 65, 100, and 200 ft/sec. The results are shown in
Figure A-8. The Priem model indicates a much greater sensitivity to initial
velocity than does DER. Two differences in the droplet ballistic equations
of the two models have been discovered.

First, the DER integration technique (a simple
step-by-step Euler approach) often predicts a droplet downstream station velo-
city greater than the downstream gas velocity. When this occurs DER sets the
downstream station droplet velocity equal to the upstream station droplet
velocity, resulting in an unrealistically long droplet chamber residence time
and increased propellant vaporization. This result is indicated in Figure
A-8 by the high DER vaporization efficiencies predicted for high droplet
initial velocities.

The second droplet ballistics difference between
the two models is in the formulation of the droplet drag coefficient. The
Priem model employs the empirical correlation developed by Ingebo (Ref. 16).

$$C_d = 27 \ Re_D^{-0.84} \qquad\qquad (A-15)$$

DER uses a variation of the Ingebo result, developed by Rabin (Ref. 31) above
Reynolds numbers of 80.
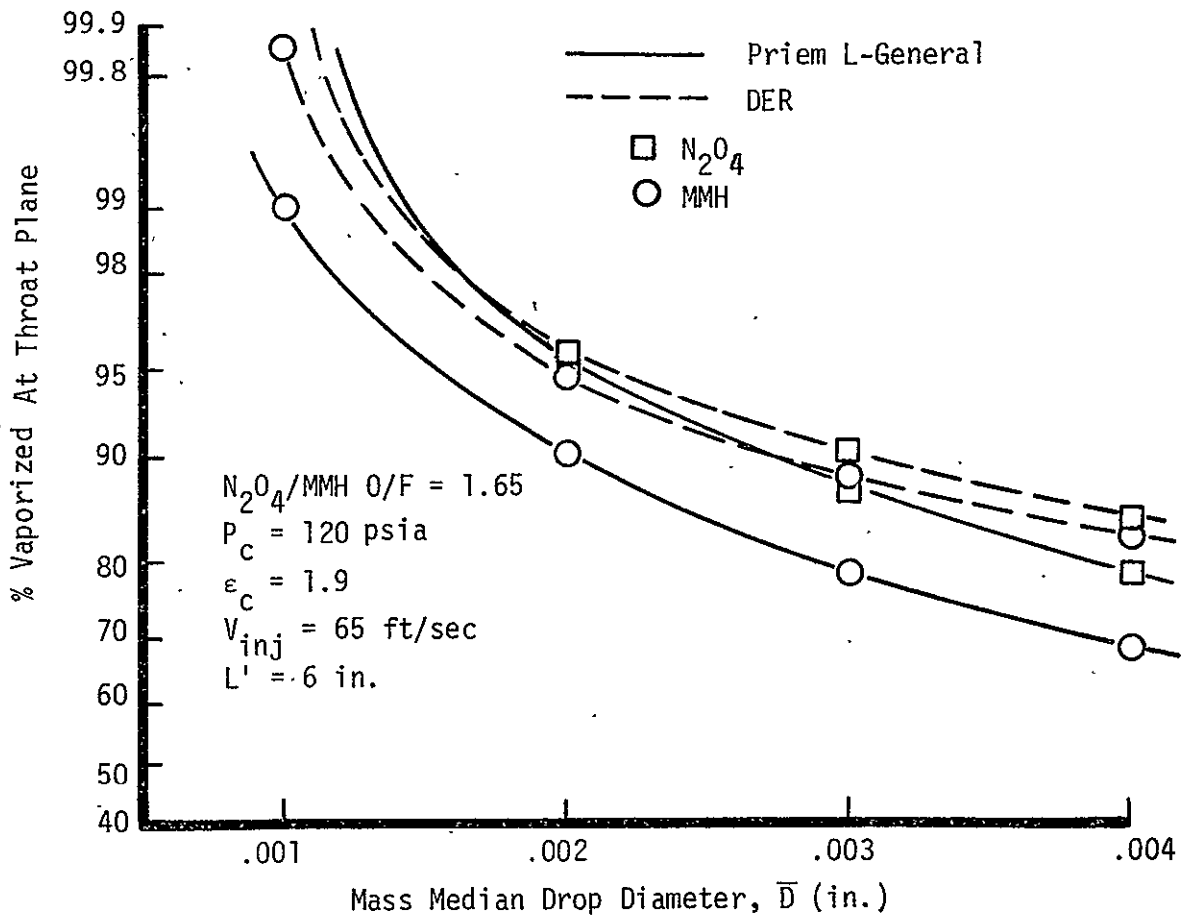
FIGURE A-7.MASS MEDIAN DROP DIAMETER EFFECT ON VAPORIZATION
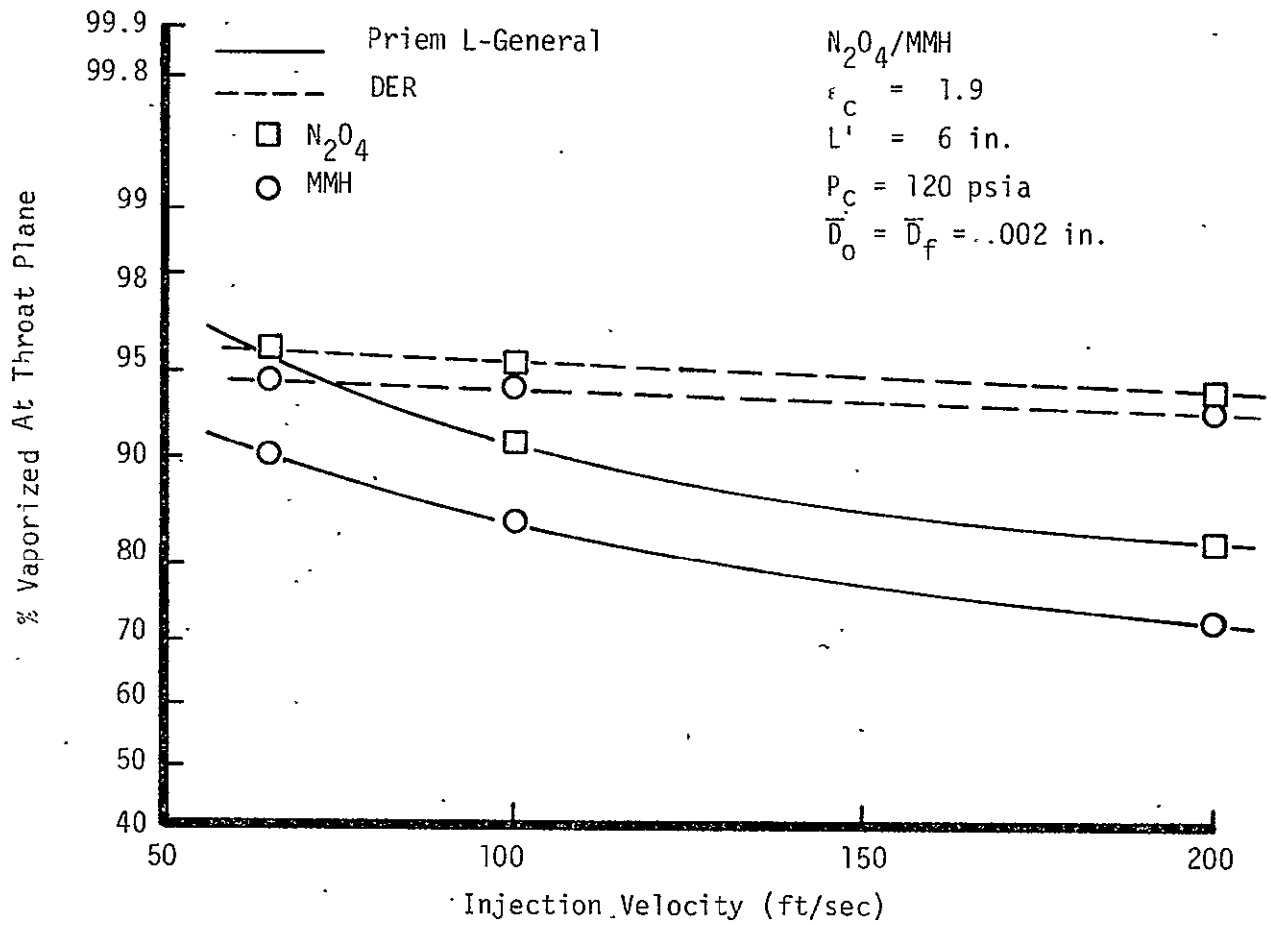
FIGURE A-8. INJECTION VELOCITY EFFECT ON VAPORIZATION

$$C_d = 27 \ Re_D^{-0.84} \qquad Re_D < 80 \qquad\qquad (A-16)$$

$$C_d = 0.271 \ Re_D^{.217} \qquad 80 \le Re_D \le 10^4 \quad (A-17)$$

$$C_d = 2 \qquad\qquad Re_D > 10^4 \qquad\qquad (A-18)$$

Considerable discussion occurs in the literature over the validity of the
two models. As introduced previously, Bracco (Ref. 7) has concluded that
high C_D's (such as the Rabin equations) give erroneous mass vaporization
profile results. Also, an excellent synopsis of relatively current thought
is contained in Ref. 32.

The effect of substituting the Ingebo correlation
for the Rabin correlation on DER vaporization predictions is shown in Figures
A-9 and A-10. In Figure A-9 the predicted vaporization efficiencies are
plotted versus injection velocity for both drag coefficient correlations. The
Ingebo equation increases the absolute vaporization efficiency level and results
in a slope more nearer the Priem model result. In Figure A-10 DER predictions
for both models are plotted versus chamber length. The slope of the predictions
are nearly equivalent, while the Ingebo equation results in a significantly
higher rate of propellant vaporization.

e.   Chamber Contraction Ratio

Propellant vaporization was calculated for chamber
contraction ratios of 1.9, 3, and 5:1 for a constant chamber length of 10
inches. The results are shown in Figure A-11. The differences in the slope
of the predicted DER and Priem model results are likely to be attributable
to the two droplet ballistic model inconsistencies commented on in the previous
paragraphs.

f.   Propellant Temperature

The DER K-Prime model does not allow for the finite
time required for a droplet to heat from its injection temperature to the "wet
bulb" state. DER has no prescribed method for accounting for the effect of the
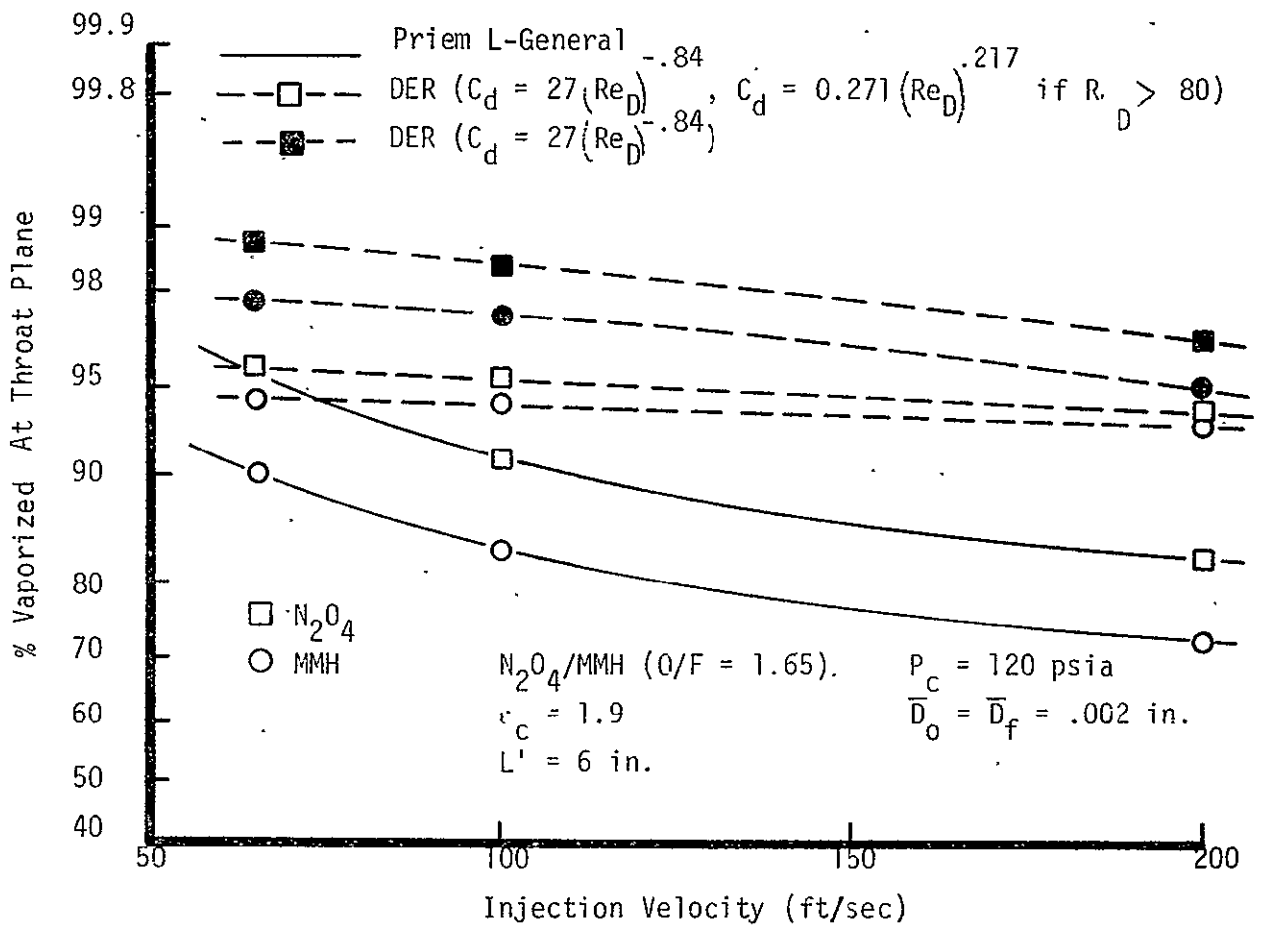
FIGURE A-9. INJECTION VELOCITY EFFECT ON VAPORIZATION FOR DIFFERENT DROPLET DRAG COEFFICIENTS
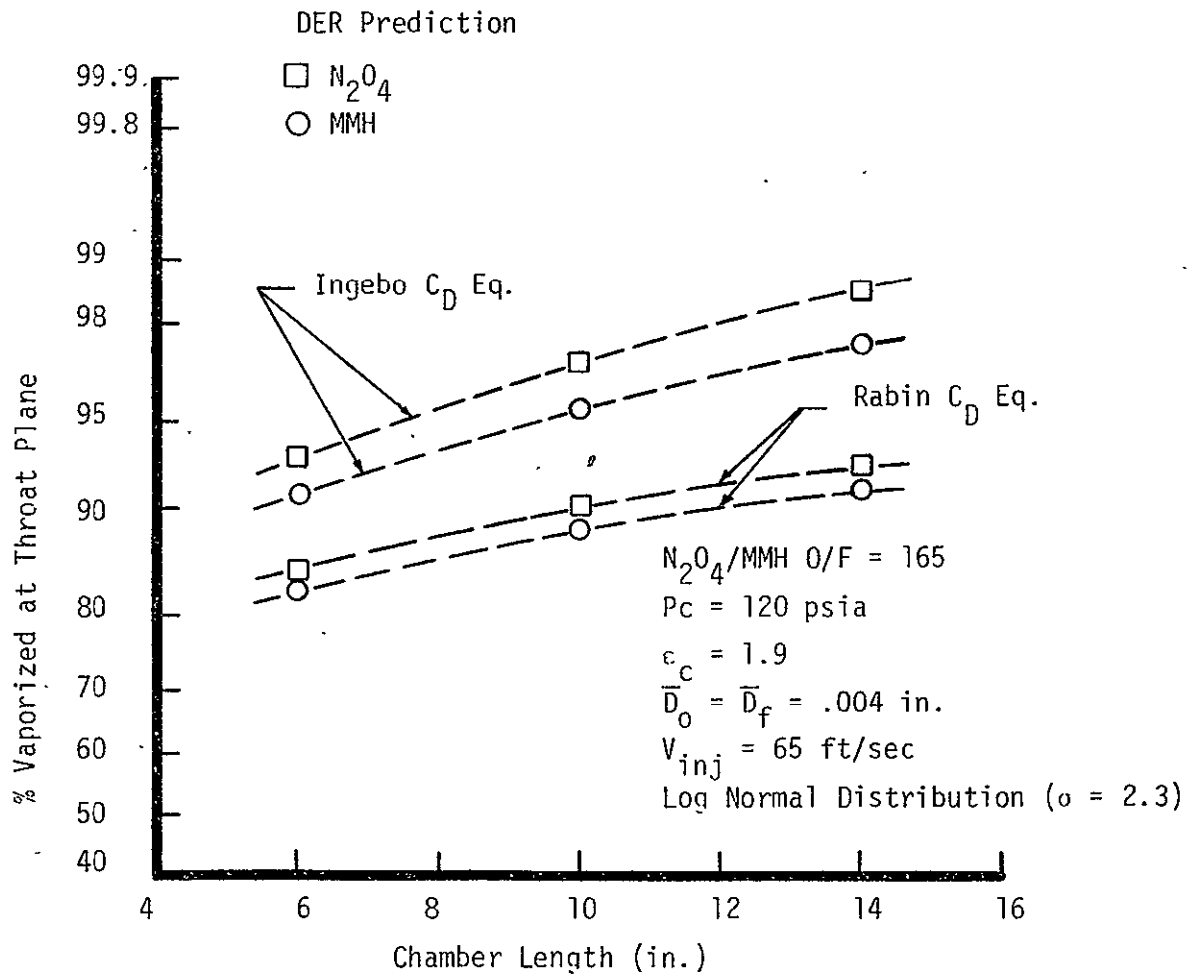
FIGURE A-10. CHAMBER LENGTH EFFECT ON VAPORIZATION FOR DIFFERENT
DROPLET DRAG COEFFICIENTS

A-26
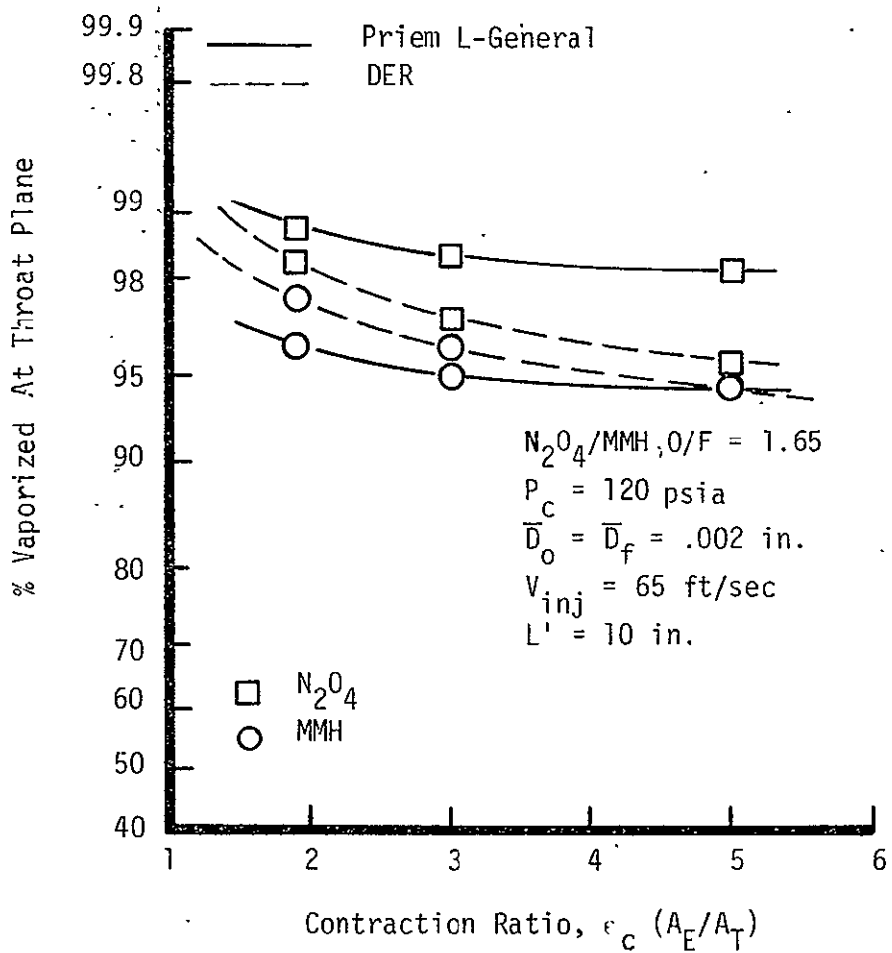
FIGURE A-11. CONTRACTION RATIO EFFECT ON VAPORIZATION

propellant inlet temperature on vaporization efficiency because of this model
simplification. Priem used his time based mass and heat transfer equations
to compare the time to reach the "wet bulb" condition to the time to vaporize
99 percent of the mass for several different propellants. The results are shown
below.

TABLE A-III

PROPELLANT HEAT-UP TIME CHARACTERISTICS

Propellant	$\dfrac{\text{Length to Wet Bulb}}{\text{Length to Vaporize}}$ (Pc = 300 psia)
Heptane	1/5
Hydrazine	1/12
Ammonia	1/16
Oxygen	1/10
Fluorine	1/10

It is apparent that this initial unsteady state can be significant when
accounting for a complete droplet time history. The time to reach the "wet
bulb" condition is primarily dependent on the droplet diameter and the initial
propellant temperature.

Figure A-12 shows the Priem model predicted effect
of propellant temperature on vaporization for the study baseline calculation
point. An attempt to allow for this effect with DER was made by adjusting the
MMH input latent heat of vaporization. This result, shown in the figure, is
considered to be unsatisfactory. The most physically correct way to solve
this shortcoming of DER would be to adopt a time dependent vaporization model.

g. Drop Size Distribution

The importance of the droplet size distribution
on propellant vaporization has long been recognized. The DER user should
realize that the DER builtin drop size distribution may not be physically
accurate for his particular injector design*. Figure A-13 shows various drop
size distributions found in the literature. The builtin DER drop size dis-

---

*The DER user can override the builtin distribution through input.
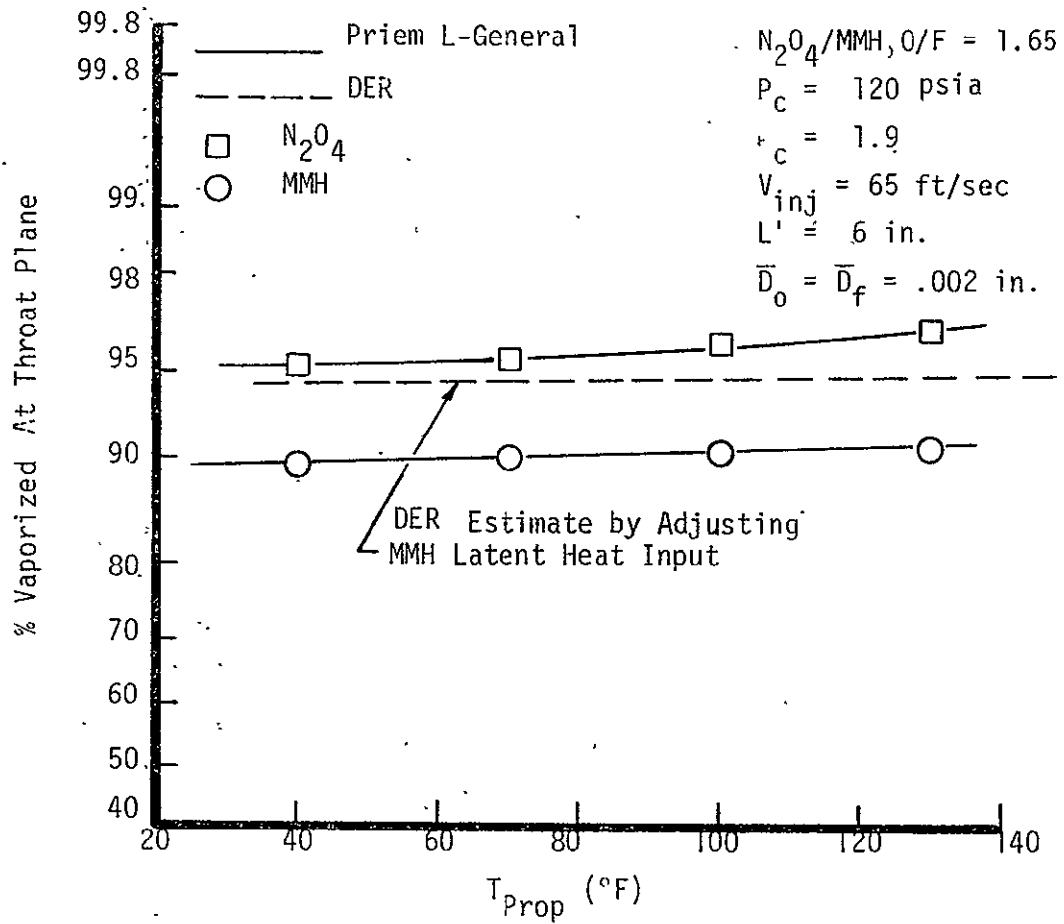
FIGURE A-12. PROPELLANT TEMPERATURE EFFECT ON VAPORIZATION
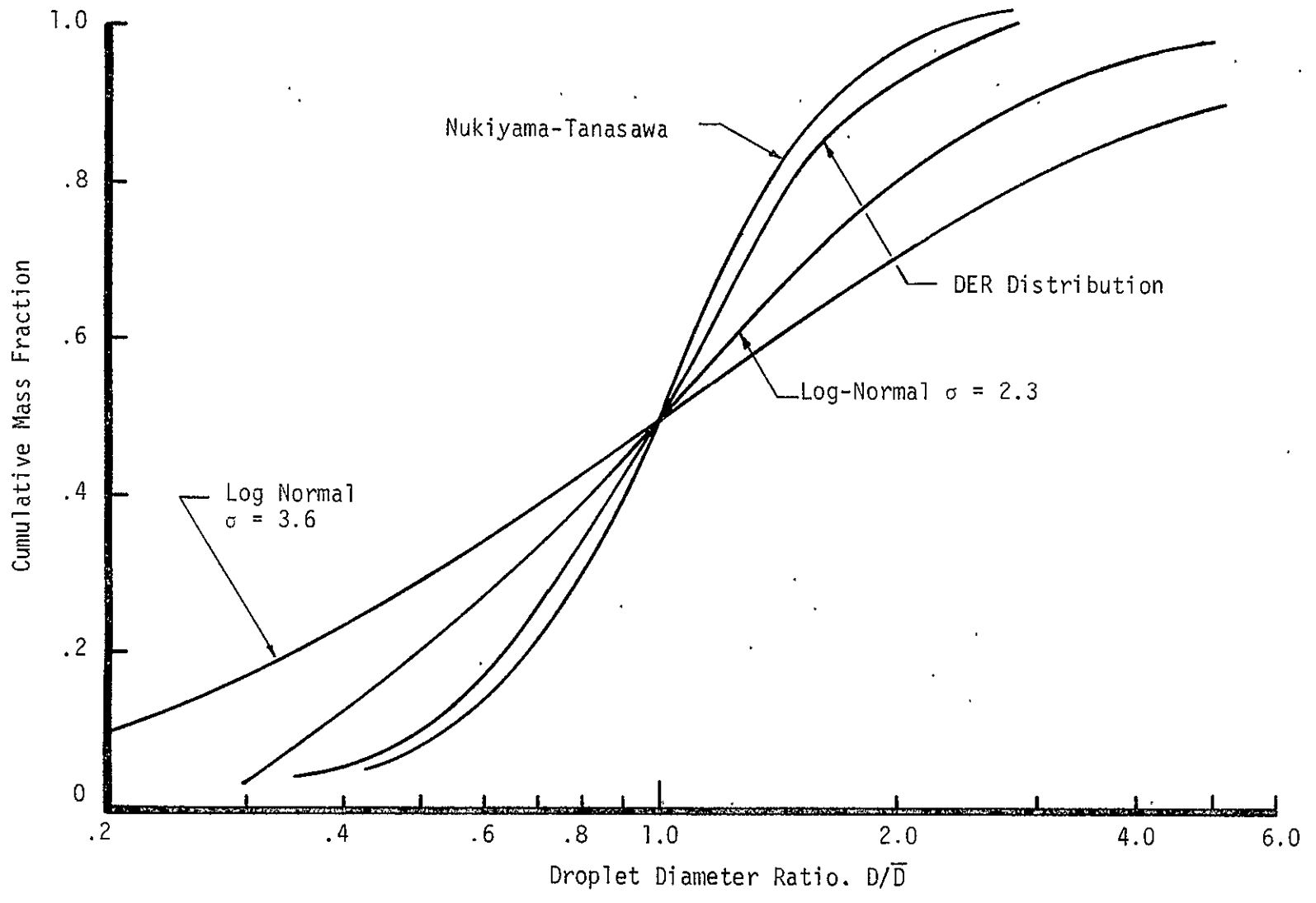
FIGURE A-13.DROPLET SIZE DISTRIBUTIONS

tribution is based on the Rocketdyne molten wax experimental results (Ref. 24). It is quite similar to the well-known Nukiyama-Tanasawa empirically determined cold flow distribution which is also shown in the figure. Priem correlated his hot fire data with log-normal distribution equations.

$$\frac{dR}{dD} = \frac{e^{-1/2 \left[\frac{Ln\ D/\overline{D}}{Ln\ \sigma}\right]^2}}{2\pi\ D\ ln\ \sigma} \qquad (A\text{-}19)$$

Priem determined that doublets and triplet hot test sprays were best described with standard deviations of 2.3 and 3.6, respectively. These two distributions are also shown in Figure A-13. The effect of the drop size distribution on propellant vaporization is shown in Figure A-14. The significance of the distribution on the predicted level of vaporization is evident. The DER and Nukiyama-Tanasawa distributions are cold flow (i.e., gas static) distributions. The implication of the Priem correlations is that a dynamic (i.e., accelerating) gas environment affects the atomization process thus resulting in a different hot test distribution.

4.   Near-Zone Combustion and Monopropellant Flame Considerations

Monopropellant decomposition burning for hydrazine based fuels has been verified by several investigators. Decomposition burning results in higher energy release than the bipropellant reaction in the injector face near zone. A recommendation has been made recently (Ref. 33) not to include a decomposition flame model in the "standardized" DER program. Two reasons for this recommendation were cited: (1) "Two Flame" effects are only important close to the injector face and do not significantly affect the vaporized propellant mass fraction at the chamber throat plane, and (2) the combustion chamber near-zone flow field can not be well defined analytically.

Monopropellant burning does not significantly affect performance for most thrust chamber designs. However, a valid DER performance model would extend itself naturally to combustion stability and chamber compatibility analytical modeling. Accurate stability and compatibility predictions hinge on a realistic representation of the near zone flow field, where monopropellant effects are significant. Also, the new ZOM mass distribution model described in Section V of this report depends on an accurate vaporization rate calculation near the injector face.

A-31
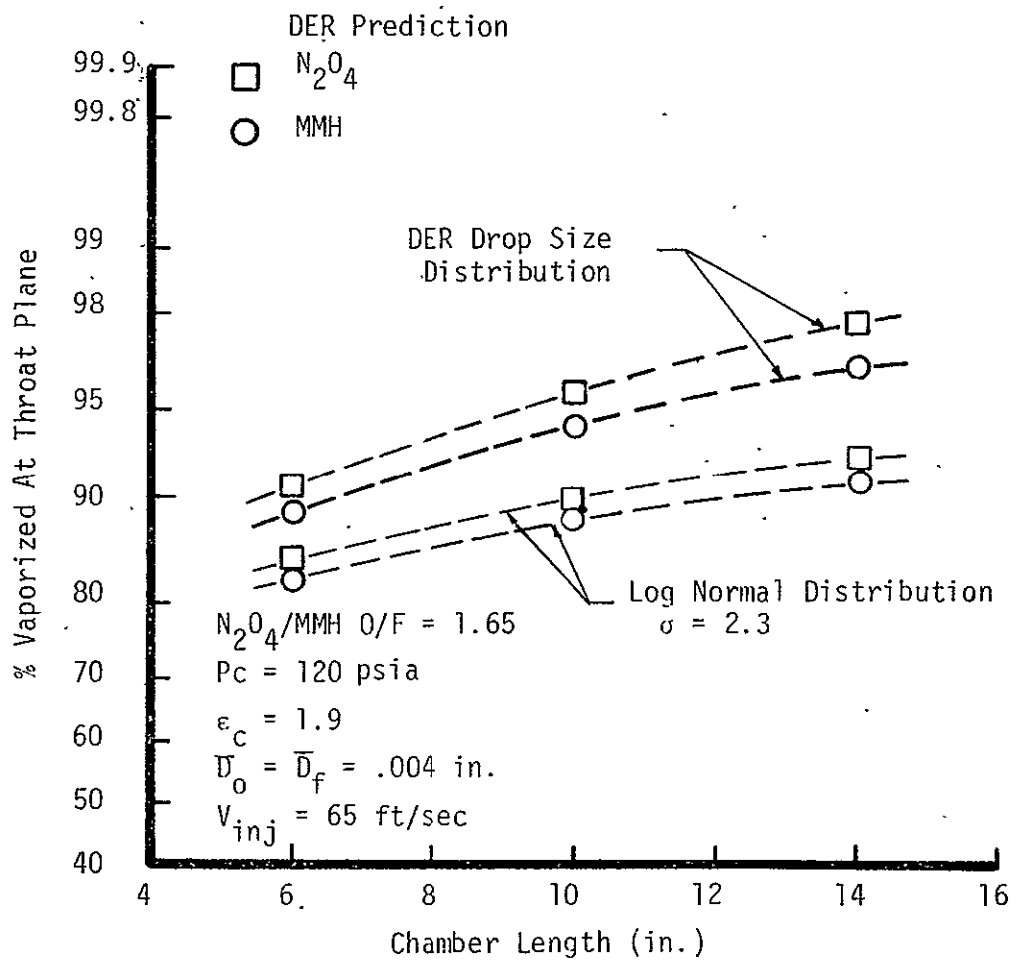
FIGURE A-14. CHAMBER LENGTH EFFECT ON VAPORIZATION
FOR DIFFERENT DROP DISTRIBUTIONS

Recent work on the Space Shuttle OMS engine program (Ref. 14) indicates that the near combustion zone can be well modeled. This conclusion was reached through correlation of analytical predictions made with the Priem model with empirically measured energy release rate data. Figure A-15 shows actual and predicted energy release data for a subscale platelet V-doublet injector. The analytical prediction was made with a "two flame" transformation to the simplified Priem L-general model. The OMS engine utilizes the Nitrogen Tetroxide (N_2O_4)/Monomethyl Hydrazine (MMH) propellant combination, thus justifying a two flame correction to the MMH vaporization calculation. Excellent agreement between prediction and test was obtained for the injector near zone, from 0-2 inches from the injector face, as shown in the plot. The correlation continued to be valid to the throat plane, 8 inches from the injector face plane (not shown). The predicted vaporized propellant (gas) mixture ratio profile for the two flame model prediction is also shown in the figure, along with the mixture ratio profile made with the Priem model without the "two flame" correction. The difference is quite significant, indicating the near zone is not modeled correctly unless decomposition burning is accounted for. The local gas composition is directly related to the local gas mixture ratio, indicating the importance of the "two flame" correction to chamber stability and compatibility modeling.

The semi-empirical technique developed to convert measured chamber axial static pressure profiles to injector energy release rate profiles is graphically illustrated in Figure A-16. The measured static pressure at any chamber axial location is used to calculate the local gas velocity and flowrate through isentropic relationships. The cumulative energy release to the same plane is calculated knowing the percentage of the total propellant burned. The energy release rate is predicted by taking the first derivative of the cumulative energy release profile. It has been determined that the resulting injector energy release rate characteristic can be directly related to the injector combustion stability characteristic. Additionally, data obtained in this manner for OMS multi-element subscale like-doublet pair injectors are being used to develop and verify the new ZOM mass distribution model described in Section V of this report.

Subscale V-Doublet Injector
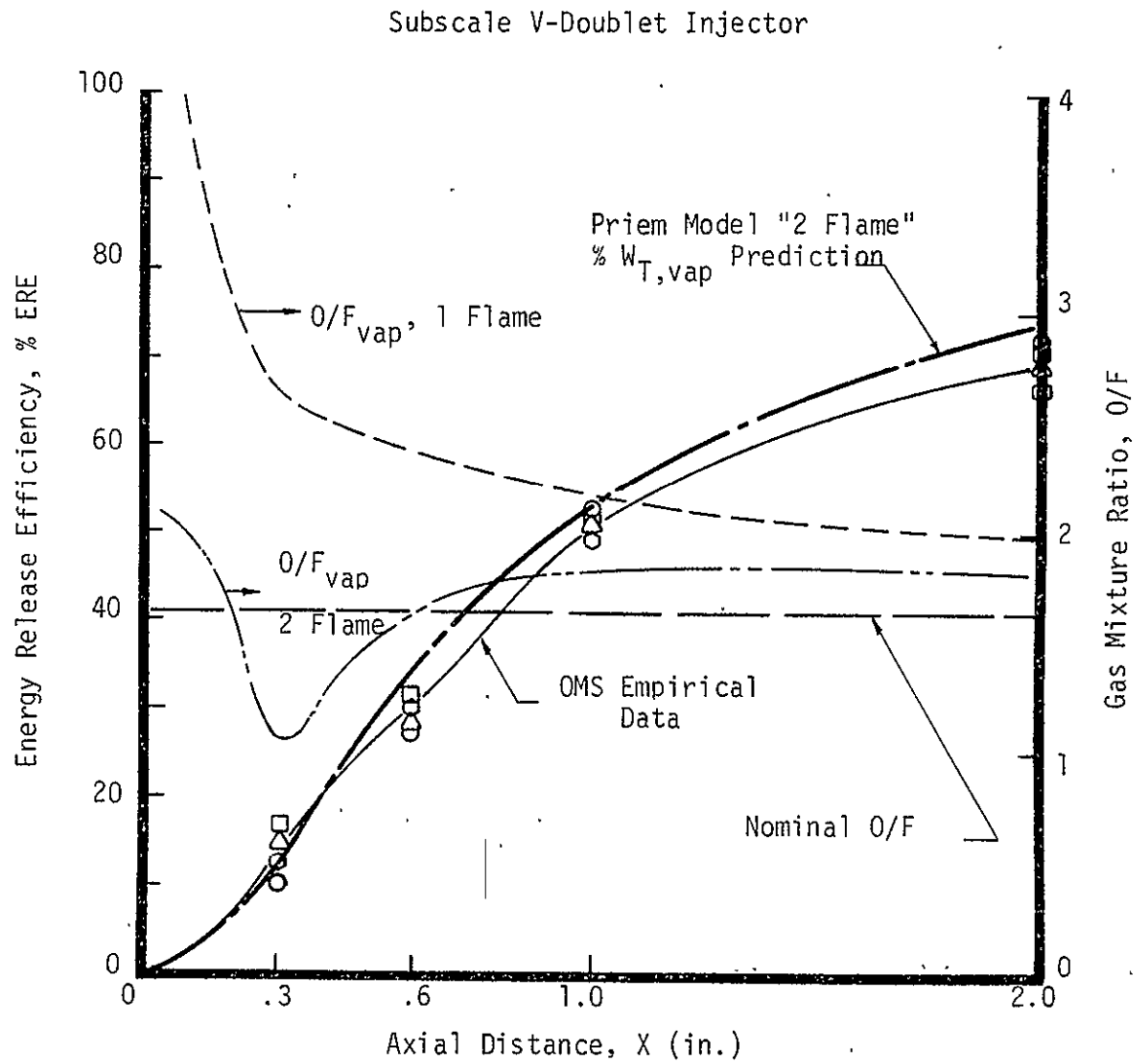
FIGURE A-15. CORRELATION OF PRIEM AND OMS SEMI-EMPIRICAL NEAR ZONE MODEL RESULTS
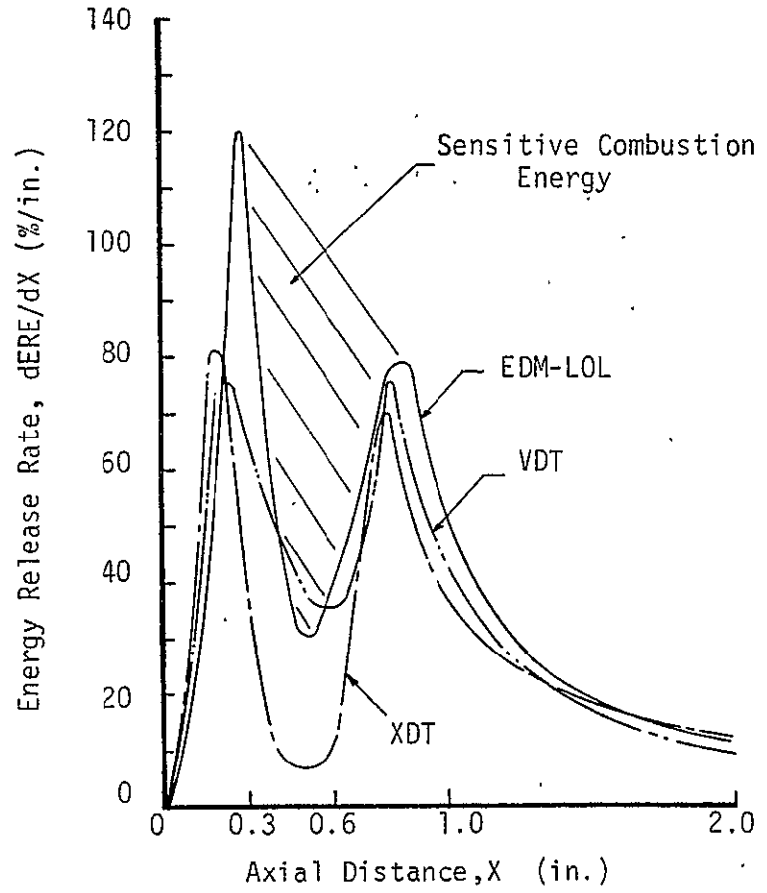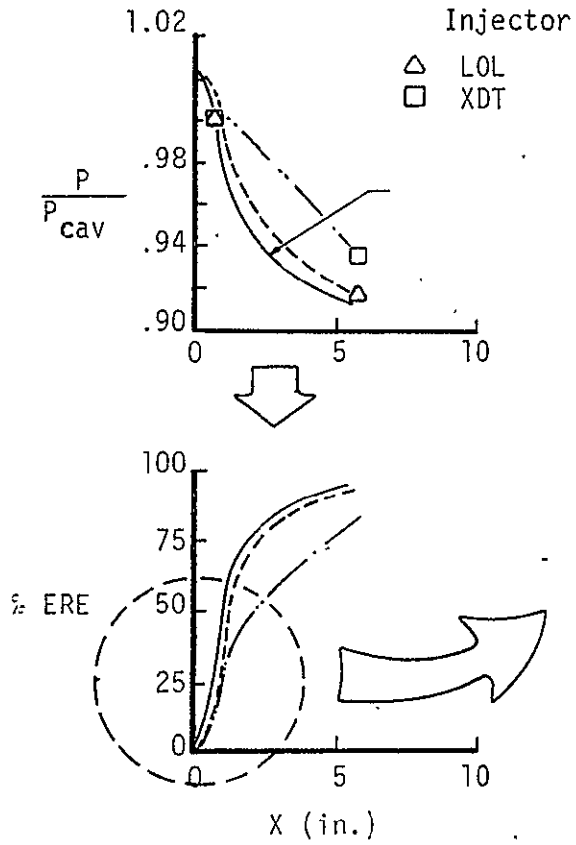
FIGURE A-16. SEMI-EMPIRICAL NEAR ZONE COMBUSTION MODEL

The OMS test results indicate a "two flame" model is required to accurately model the injector near zone for injectors employing hydrazine based fuels. Examples of available models are Refs. 34 through 37.

5. Combustion Gas Acceration and Reactive Stream Separation Effects on Cold Flow Mass Distribution

The LISP mass distribution calculation technique does not allow for the influence of combustion on the elemental cold flow mixing characteristics. The formation and acceleration of combustion gas affects spray distribution for all liquid propellant injectors. Additionally, dependent· on the injector operating point, the phenomenon termed Reactive Stream Separation (RSS or "blowapart") can also alter the hot fire case mass distribution from one measured under cold flow conditions.

A·model has been proposed to account for the influence of combustion gas acceleration on the calculated chamber mass distribution. Also, inherent in the proposed model is a technique for a priori estimation·of the ZOM plane location for mass distribution characterization. The model is des- . cribed, along with a report on the current status of a model.verification effort, in Section V of this report.

The effect of RSS on injector performance can be significant. Figure A-17 indicates the influence of RSS on the energy release efficiency (ERE) for platelet "splash plate" injectors as a function of engine chamber pressure. For one particular injector tested RSS decreased injector ERE approximately 10 percent for a chamber pressure range of from 50 to 110 psia.

A recently completed investigation (Ref. 18) indicates that RSS phenomenon can be accurately modeled and predicted in terms of injector/ chamber design and operating variables. Single element unlike doublet, F-O-F triplet, and platelet injectors were tested. The mode of operation of a parti- cular test (i.e., mixed, mixed-separated, or separated) was determined through filming of the combustion with a high speed motion picture camera. Results were correlated with the test design and operating point to result in a mechan- istic RSS model.
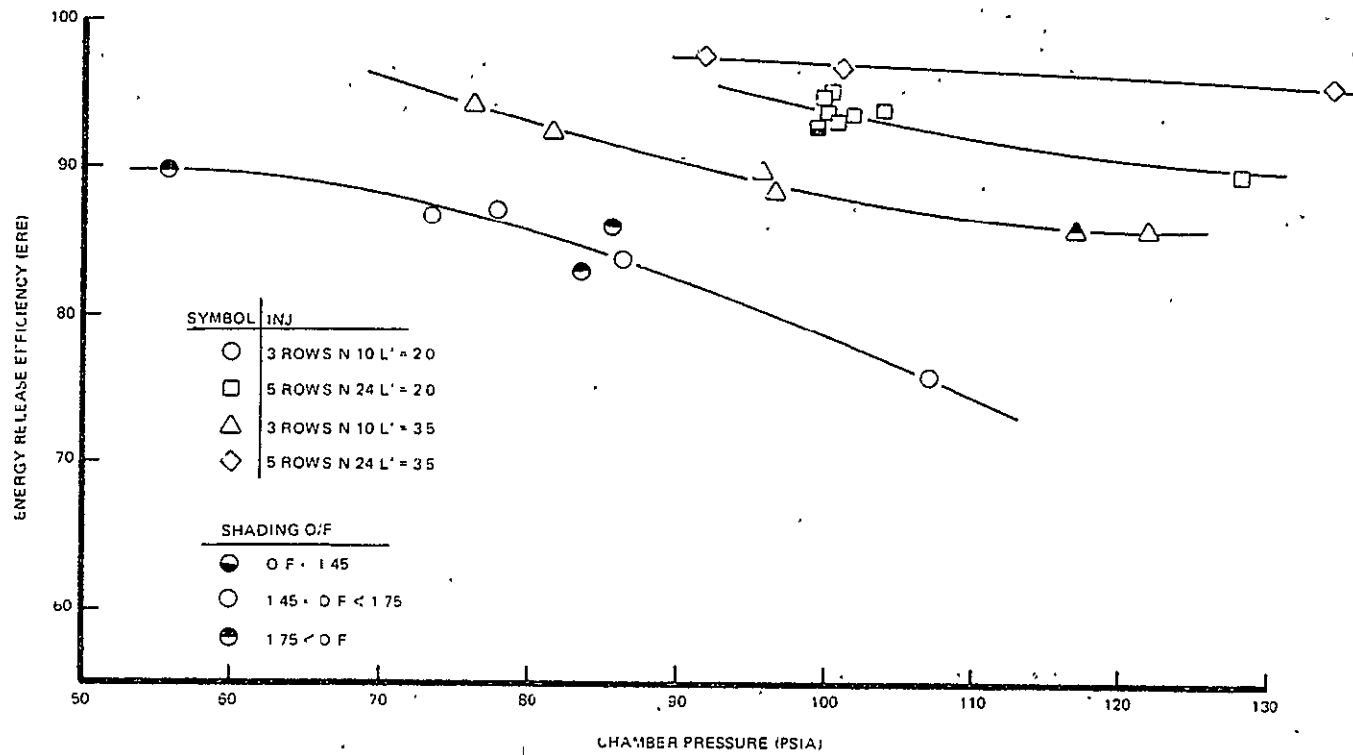
Figure A-17.RSS Effect on Injector Performance

An example RSS correlation is shown in Figure A-18. The occurrence of RSS is plotted for a single unlike doublet element as a function of chamber pressure and a parameter containing Weber Number, Reynolds Number, and a propellant temperature influence term. The Weber number relates the jet aerodynamic drag force to the liquid surface tension force. The results indicate that the occurrence of RSS can be accurately predicted if the injector operating point is well characterized.

Inclusion of RSS results, such as shown in Figure A-18, in LISP could provide a significant improvement in the DER performance prediction capabilities under conditions where RSS occurs. There appears to be two types of RSS models that could be incorporated into LISP. (1) A simple "warning" model that could tell the user that the occurrence of RSS is predicted for his input injector design and operating point, and (2) a model that would predict the occurrence of RSS and would adjust the LISP ZOM plane mass distribution based on actual hot test mass distribution results.

The first model would serve only to provide the designer with more information. It would not provide a quantitative estimate of the effect of RSS on injector performance.

The second model approach represents the most quantitatively accurate approach to RSS performance modeling. Testing would have to be performed that would result in measured hot fire mixed and separated mass distributions. LISP mass distribution coefficients would be developed to account for the influence of RSS. Such measurements have been performed for a gas/gas swirl coaxial element at ambient chamber pressure (Ref. 38). A double-walled, hot hydrogen cooled probe was used to withdraw the gas sample. The gas sample mass composition was measured by a mass spectrometer. Measured mixed and separated mass distribution coefficients could be correlated as a function of the injector design and operating point, to result in an experimentally verified model to be readily inserted into DER.

An additional RSS model approach exists that is adaptable to the JANNAF simplified performance prediction methodology, but not necessarily compatible with the DER program computational techniques. This model would

Injector: Unlike Doublet

$D_F = 0.020$

N_2O_4/MMH

Separated

Mixed

$$W_e = \frac{\rho_q \cdot V_\ell^2 \cdot d}{\sigma_\ell \cdot q_c}$$

$$P_{V_N} = \frac{P_{V_o} \times P_{V_f}}{P_c^2}$$

$$R_e = \frac{\rho_\ell \cdot V_\ell \cdot d}{\mu_\ell}$$

☐ Mix

△ Sep

○ Mix/Sep

Chamber Pressure, psia

$W_e \cdot R_e^{1/2} \cdot P_{VN}$
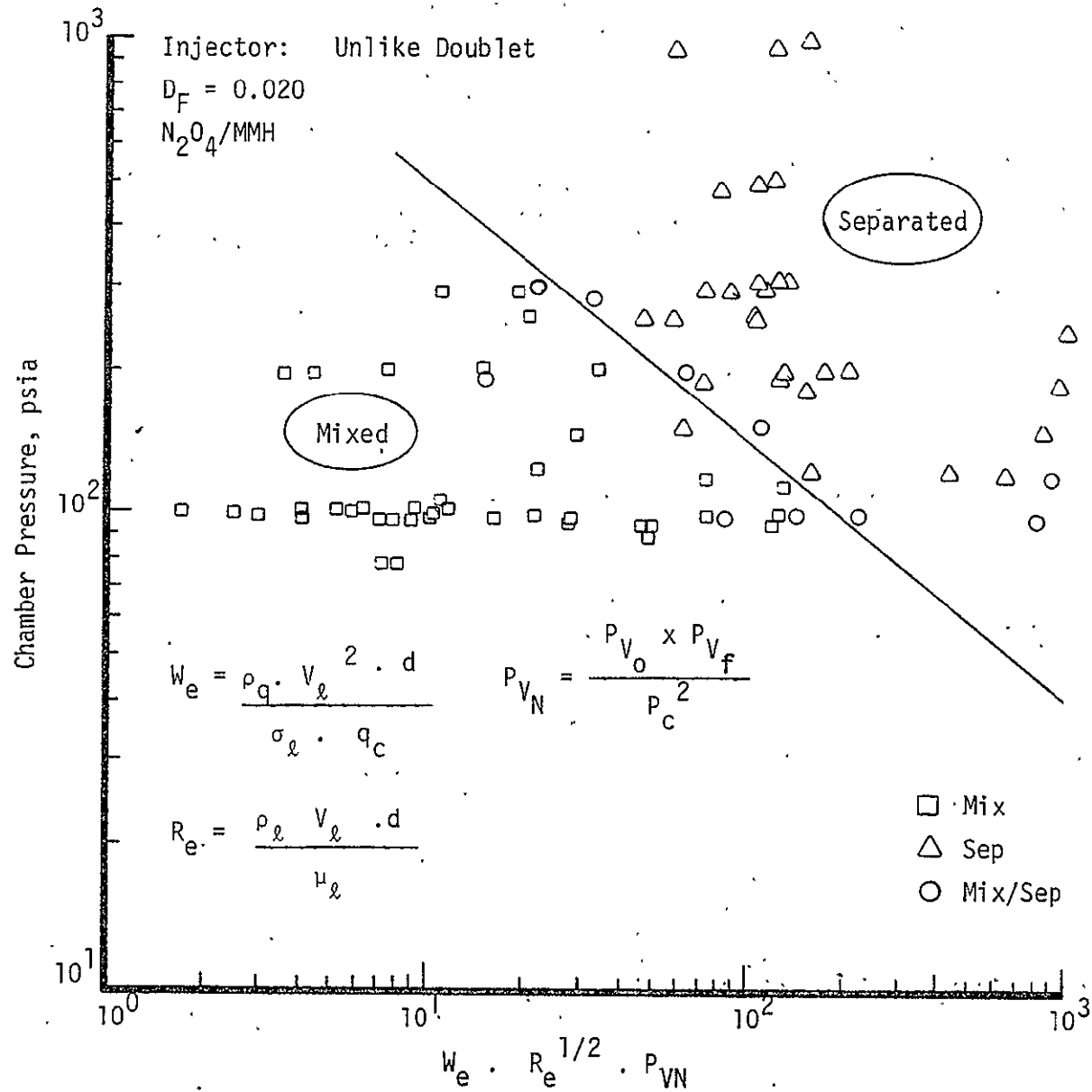
Figure A-18. Correlation of RSS Test Data

predict the occurrence of RSS and adjust the performance prediction through an empirically based performance correlation technique. The model would require development of a correlation between a RSS prediction parameter (such as the abscissa of Figure A-18) and actual injector performance. A possible technique would be to relate mixed and separated mass and mixture ratio distributions through stream tube performance relationships.

6. Turbulent Mixing Model

The LISP cold flow mass distribution calculated at the ZOM plane should account for the influences of combustion gas acceleration and RSS, as previously suggested. Another significant omission in DER mass distribution modeling is the characterization of turbulent mixing effects on performance and chamber compatibility (remembering that DER is the computational base for the Injector/Chamber Compatibility (ICC) model). Turbulent mixing effects downstream of ZOM could range from minimal (for uniform patterns with a large number of injector elements) to substantial (coarse patterns or film cooled chambers). The DER streamtube modeling does not calculate any inter-streamtube mass exchange downstream of the ZOM plane. The characterization of turbulent mixing effects would provide a large step in the direction toward providing DER with the desired a priori prediction capability. The effect of streamtube mixture ratio changes due to turbulent mixing on propellant vaporization efficiency can be shown to be a second order influence for most chamber designs. Therefore, the turbulent mixing and vaporization calculations could be separated, resulting in a relatively simplified computational approach. Conversely, a simultaneous mixing with vaporization model would result in a more accurate solution with an inherent increase in programming complexity and computer run time.

Two test programs have been conducted that resulted in the development of semi-empirical models for the prediction of mixing limited injector performance. The programs investigated gas/gas intraelement (Ref. 11) and film cooling/injector core mixing (Ref. 38). The physically mechanistic analytical modeling developed on both programs is naturally extendible to the DER program.

O'Hara, et. al., (Ref. 39) have recently completed work that resulted in a quantification of the intensity of turbulence and Lagrangian correlation for turbulent mixing in rocket combustion chambers. The analysis was based on gas sample measurements taken from a oxygen/heptane 300 psia chamber pressure small rocket engine. It is concluded that the Lagrangian correlation could be used in rocket engine diffusion calculations. Another significant discovery of the work was that turbulence intensity was very high near the injector face due to the rapid rate of combustion and presence of liquid spray in this area.

7.   Development of an A Priori DER Mixing Model

Two primary weaknesses in the DER ZOM plane mixing technique were determined during the DER review. (1) No methodology exists for calculating the correct ZOM plane value on an a priori basis, and (2) RSS and turbulent mixing effects can significantly alter the correct mass distribution for chamber throat plane mixing loss calculations.

Recent research indicates that RSS is a near-zone phenomenon. That is, combustion gas mass distribution is affected by RSS within an inch or two of the injector face plane. Combustion gas acceleration effects on spray distribution are also predominant in the near zone. (See Section V of this report). Conversely, turbulent mixing effects can extend to the chamber throat plane. For these reasons modeling of gas acceleration effects, RSS, and turbulent mixing can be easily adapted to the current DER computational methodology, as graphically suggested in Figure A-19.

New DER mixing methodology could be executed in the following three steps.

(1)   ZOM is calculated with the gas acceleration effects model presented in Section V of this report. The ZOM mass distribution would be calculated based on empirical cold flow spray coefficients (identically to the current model).

ZOM A PRIORI

PREDICTION
GAS ACCELERATION EFFECTS
MODEL

ZOM COLD FLOW
MASS DISTRIBUTION

- SPRAY COEFFS.

ZOM LOCATION AND
MASS DISTRIBUTION

RSS MODEL
ADJUST ZOM COLD
FLOW DISTRIBUTION

ZOM

RSS
EFFECTS

TURBULENT MIXING
MODEL
ZOM TO THROAT
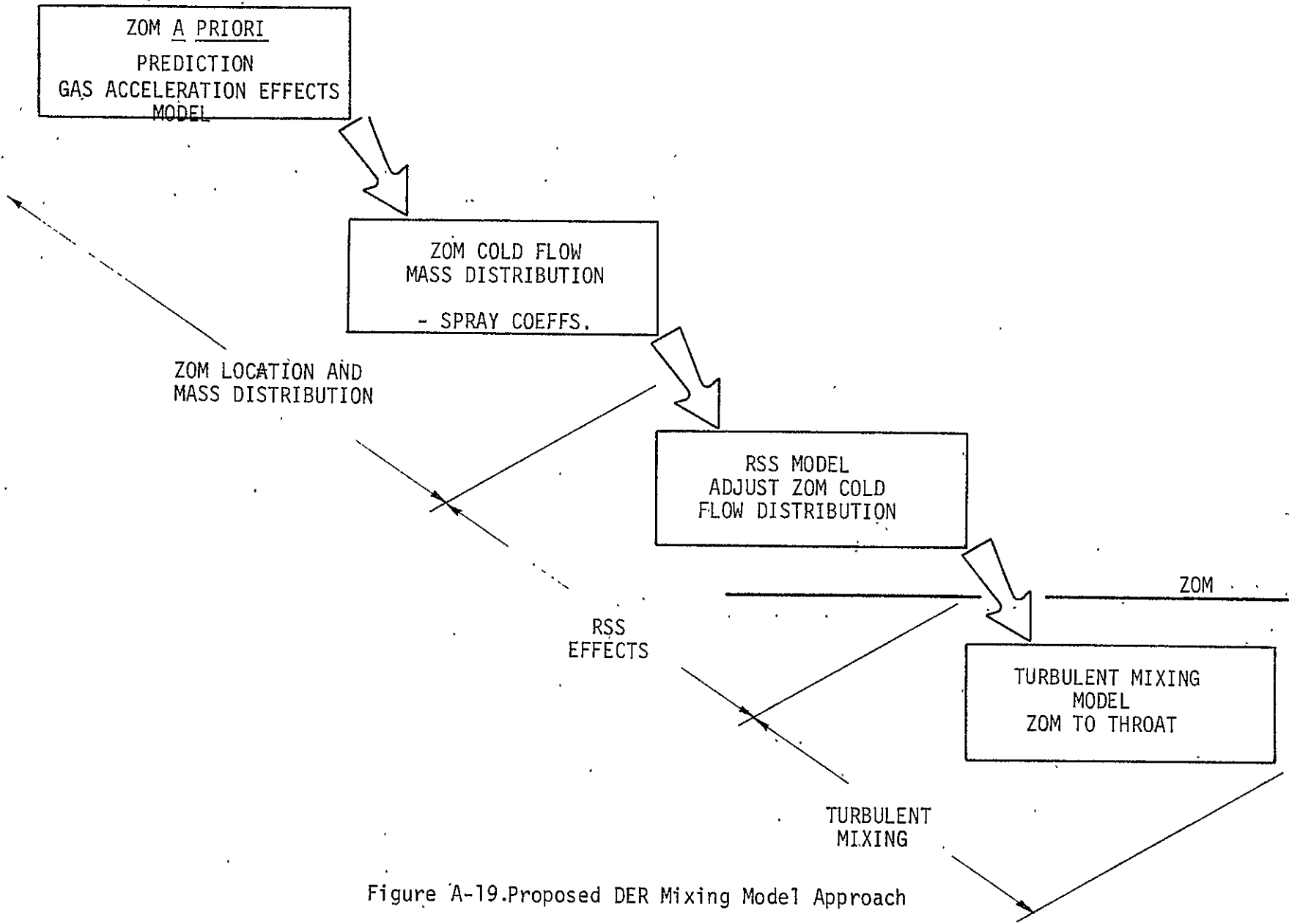
TURBULENT
MIXING

Figure A-19.Proposed DER Mixing Model Approach

(2)   The ZOM cold flow distribution would be adjusted for RSS effects.

(3)   The turbulent mixing model would adjust the new ZOM mass distribution in axial increments to the chamber throat plane.

D.   Inconsistencies Between JANNAF Procedures and DER Computer Program Operations

The JANNAF Performance Prediction Procedures described in CPIA 246 were reviewed with regard to use of the DER computer program. The primary functional purpose of DER in the rigorous JANNAF procedure is to provide STC output which can be directly input to the Two Dimensional Kinetic (TDK) Reference Program (Ref. 5). TDK analyzes the supersonic nozzle expansion process in the JANNAF methodology. During Task II of this program the STC/TDK interface problem was to be objectively evaluated. Rescoping of Task II eliminated STC and TDK analyses that would have determined if the interface is easily accomplished.

Review of CPIA 246 indicated several inconsistencies between the JANNAF methodology and the results of the DER review. Each point is elaborated on to the extent that task scope allowed. It is hoped that the significant questions will be resolved with future DER review and applications work.

1.   The DER Review results indicate that the intended predictive accuracy of the JANNAF rigorous procedure to within 1 percent for predicted specific impulse) is out of the question for a priori performance prediction. ZOM plane, mass median drop size, drop size distribution, droplet drag coefficient, and combustion effects on mixing considerations can each affect the prediction on the order of 1 percent.

2.   Section 2.8.1 of CPIA 246 suggests that the DER subcritical K-Prime vaporization model is valid for chamber pressures 20 percent below propellant critical pressures in which the droplet heating time to the "wet bulb" temperature is negligible and combustion gas solubility is low. For other cases the DER supercritical version is recommended for use. The problem is that the

A-43

JANNAF methodology includes no formulation for predicting the significance of the droplet unsteady temperature state or gas solubility effects.

3.   Section 2.8.3 of CPIA 246 recommends that the most physically realistic technique for selection of ZOM is to run LISP to a ZOM plane value at which the spray patterns from different elements start to overlap. It is almost impossible to recognize this point in a typical LISP output unless one possesses an intimate knowledge of the injector element spray characteristics. Also, this technique ignores interelement mixing effects on injector performance.

APPENDIX B

CICM COMPUTER MODEL REVIEW RESULTS

APPENDIX B

CICM COMPUTER MODEL REVIEW RESULTS

TABLE OF CONTENTS

This appendix details the results of the critical review of the JANNAF CICM computer model. Three subtasks were accomplished during the review. (1) Identification of Operational Problems Including a Code Review and Inclusion of Diagnostic Print-Out Statements, (2) Identification of Inadequate Formulations and Model Technical Shortcomings, (3) Review of the JANNAF Performance Prediction Procedure (CPIA 246) with Regard to the Use of CICM and Identification of Inconsistencies Between the Procedure and Program Operations. A complete summary of recommendations resulting from the CICM review is included in Section III.B. of this report.

A.   Coding Errors and Diagnostic Statements

The review of the CICM computer code consisted of verification of the key model equations. The equations checked in the code were: (1) jet stripping rate, (2) mass median drop size, (3) droplet drag coefficient, (4) droplet drag force and acceleration, (5) droplet heating, and (6) droplet vaporization. These formulations were all coded correctly.

One possible code (or formulation) error was discovered during the review. Examination of the documented sample case output revealed that periodically, in the chamber vaporization calculation, drop size groups that should not have been completely vaporized are dropped from the calculation. As an example, refer to pages 117-122 of the Appendix C sample case output in the user's manual (Ref. 4). At the 0.75 inch axial station there are 22 drop size groups. At the 1.00 inch axial station the number 2 drop size group is missing, though the smaller drops in group number 1 still remain. At the 0.75 inch station the group 1 $\overline{D}$ was 75 microns and the group 2 $\overline{D}$ was 88 microns. It is physically incorrect that the group 2 drops would vaporize more quickly than group 1 drops. This error occurs again at the 1.250 axial station when the number 3 drop size group vanishes, but the group 1 still exist. The source of this computation error was not discovered during the review. It should be added that, for the following reason, this possible error was not expected to affect the CICM analysis of the M-1 engine reported in report Section IV. The drop size groups in question were consistently vaporized completely long before the chamber throat plane calculation station was reached.

B.   Identification of Inadequate Formulations and Model Technical
      Shortcomings

          The purpose of this subtask of the CICM review was to identify
model technical problem areas and, if possible, to propose approaches for
improvement. Incorporation of the improvements was, for the most part,
beyond the scope of the program, but their identification provides a basis for
future CICM work. The CICM user's manual states that the model controlling
processes are: (1) the local stripping rate of the liquid jet, M_A, (2) the
local mean drop size produced when M_A is stripped from the jet, $\overline{D}$, (3) the
droplet heating and vaporization rates, (4) the assumed droplet drag coefficient
formulation, and (5) for the chamber flow, the rate of mixing of the external
"rigimesh" face flow. Careful review of the program input requirements and
model analytical assumptions indicated that two additional important controlling
CICM parameters should be defined, (6) the input specification of the intra-
element fuel and oxidizer mass and mixture ratio distribution, and (7) the
input specification of separate flow analysis zones to allow for manifold mass
and mixture ratio maldistribution. The CICM program does not calculate mixing
and requires that mass distribution input be user justified. Currently no
standard guidelines exist in the CICM user's manual or the JANNAF Performance
Prediction Manual (CPIA 246, Ref. 3) for measurement or input specification of
these propellant mass distributions. The results of the CICM formulations review
are presented below in seven sub-sections that deal with the model controlling
processes defined above.

      1. Jet Stripping Rate Correlation

          The circular stripping rate correlation used by CICM is
defined below.

$$M_A = C_A \left[\frac{\mu_j (\rho_g U_r^2)^2}{\sigma_j/\rho_j} \right]^{1/3} \pi D_j (\Delta z) \qquad (B-1)$$

The CICM and JANNAF open literature does not include a derivation of the
stripping rate correlation. A cursory examination of the literature on the
atomization of liquid jets injected concurrently into gas streams yielded no

directly applicable correlation for jet disintegration rate. The scope of the CICM review did not allow for a comprehensive literature review on liquid jet atomization. Qualitatively, the equation appears to be correctly formulated. As the jet to gas relative velocity increases the stripping rate increases due to aerodynamic drag. The stripping rate will also increase as the jet density, viscosity, and surface area (πD_j Δz) and the gas density increase. It is also correct that the stripping rate should decrease as the jet liquid surface tension increases. For the atomization constant (C_A) to be a universal constant the respective terms in the atomization equations must be raised to the correct power. Also, no physical variables that have a significant influence on the stripping rate can be omitted from the equation and still result in development of a universally applicable value of C_A. Variables that could possibly fall in this category are the absolute liquid jet velocity, the absolute gas stream velocity, and the gas stream viscosity.

The stripping rate equation calculates the time lag between jet initial contact with a concurrent gas stream and final jet disintegration. For a coaxial injector, the initial contact can occur in the recessed portion of the element cup or at the injector face plane. Typical gas/liquid coaxial injector designs require relatively long chamber lengths to reduce mixing and vaporization performance losses. Therefore, the atomization time lag is usually small compared to the total chamber residence time. As an example, the M-1 engine design analyzed during Task II has a conical chamber length (face plane to throat plane) of nearly 30 inches. Based on documented previous CICM runs it was expected that the element oxidizer jet would be completely atomized from 2 to 4 inches of the injector face. It was apparent that the drop sizes calculated to be shed from the oxidizer jet will have a far more significant effect on M-1 predicted engine performance than the rate of jet atomization.

2.   Mass Median Drop Size Correlation

The mass median drop size correlation used by CICM is defined below.

$$\overline{D}_j = B_A \left[\frac{\mu_j \, (\sigma_j/\rho_j)^{1/2}}{\rho_g \, U_r^{\,2}} \right]^{2/3} \tag{B-2}$$

Similarly to the jet stripping rate correlation described previously, the open literature does not include explanation of development of the CICM drop size correlation equution. However, a number of investigations are documented that concentrated on measurement of drop sizes generated from injection of liquid jets into non-accelerating concurrent gas streams. Table B-I summarizes the results of three of these investigations and compares their correlation results to the CICM equation. The table shows the power exponent correlated by each study for nine different independent variables. The Ingebo study (Ref. 13) developed the most mathematically stringent correlation by assuming that the measured maximum drop size was controlled by six non-dimensional parameters that characterized liquid hydraulics, gas dynamics, gas acceleration, and liquid hydrostatic and surface tension forces. The CICM correlation accounts for five of the nine variables modeled by Ingebo. The most significant CICM omission identified by Ingebo appears to be that the absolute gas velocity (not just the velocity differential) has a significant influence on the atomized drop size. Comparison of the exponents of the variables modeled by both Ingebo and CICM shows that the exponent sign agrees for all variables except the liquid jet viscosity. The Ingebo result is inconsistent with other atomization models that indicate drop size increases with increasing liquid viscosity. For example, Priem (Ref. 17) uses a propellant properties grouping that results in a liquid jet viscosity exponent of + 0.25. The other variable exponents shown agree in sign but consistently disagree on the absolute magnitude. It is apparent that the cited jet drop size equations differ because of the influence of measurement technique, measurement error, and the method of data correlation.

The CICM code was examined to determine the drop size distribution relationship used by CICM as an addition to the drop size equation review. During the DER review (Appendix A) it was shown that the assumed drop size distribution, about the mass median diameter, significantly influences the predicted total mass vaporization rate. Review of the CICM code indicated that subroutine ATOM calculates the portion of the liquid jet that is atomized over one axial computational increment. ATOM calculates a droplet spray group based on the total jet mass shed during the axial step. All the drops in the group are assigned an initial diameter equal to the mass median diameter calculated with the previously introduced drop size correlation equation. Thus,

B-5

TABLE B-I. COMPARISON OF LIQUID JET
BREAKUP CORRELATIONS IN NONACCELERATING GAS STREAMS

Investigator	Characteristic Drop Diameter	Exponent for -								
		Orifice Diameter, D_0	Differential Velocity, U_r	Liquid-Jet Velocity, V_j	Gas Stream Velocity, V_g	Gas Stream Density ρ_g	Liquid-Jet Density, ρ_j	Gas Stream Viscosity, μ_g	Liquid-Jet Viscosity, μ_j	Surface Tension, σ_j
Ingebo (Ref. 13)	Maximum	0.08	-1.6	0.1	-0.5	-0.3	-0.76	0.5	-0.1	0.66
Weiss & Worsham (Ref. 26)	Mass-Median	.16	-1.33	.08	---	---	-.84	.09	.34	.41
Nukiyama Tanasawa (Ref. 28)	Sauter	---	-1.0	---	---	---	-.5	---	---	.5
Sutton (CICM)	Mass-Median	---	-1.33	---	---	-.67	-.33	---	.67	.33

in reality, CICM does not calculate a real droplet size distribution. CICM assumes that all the mass shed during a finite time period, defined by the axial step distance, is shed with a constant diameter defined by the $\overline{D}$ equation. The influence of this calculational assumption on the total liquid vaporization rate can not be estimated simply. It is apparent, though, that the drop size distribution tabulated at the end of a CICM run is only the summation of several constant mass median diameter groups, each group being calculated over a particular axial step. This resultant distribution is quite different than a drop size group calculated with distributions typically used to model rocket combustor sprays.

3. Droplet Heating and Vaporization Rate Formulations

CICM contains an advanced droplet heat-up and vaporization model that is described in detail in the program user's manual. The CICM formulation is far superior to the DER K-Prime model in that the droplet temperature transient and continuous vaporization through subcritical and supercritical propellant states are allowed for. The CICM/STC interface procedure review reported in Section C.2 of this appendix resulted in a recommendation that, in the JANNAF performance prediction methodology, CICM should compute to the chamber plane at which all the calculated drop size groups have reached the chamber "wet bulb" temperature. For oxygen this temperature transient typically takes place over a time period equal to about 10 percent of the total time required to vaporize 99 percent of the propellant (Ref. 17). After CICM has calculated the transient the STC program calculates droplet steady state burning from the interface plane to the chamber throat plane. Therefore, STC is responsible for calculating droplet vaporization rates over approximately 90 percent of the total droplet chamber residence time.

The two most important functions of CICM in the JANNAF methodology, based on the information in the previous paragraph, are to; (1) calculate liquid drop sizes resulting from aerodynamic stripping of the liquid jet; the bulk of which will be vaporized in STC, and (2) calculate the droplet temperature time transients. The CICM drop size correlation was discussed in the previous sub-section. The CICM droplet heat-up formulations were checked by comparing, for reference, CICM calculated heating rates for oxygen to heat-up rates calculated in Ref. 17. The results of the comparison are shown in Figure B-1. Initially, heat-up rates were compared, as a function of
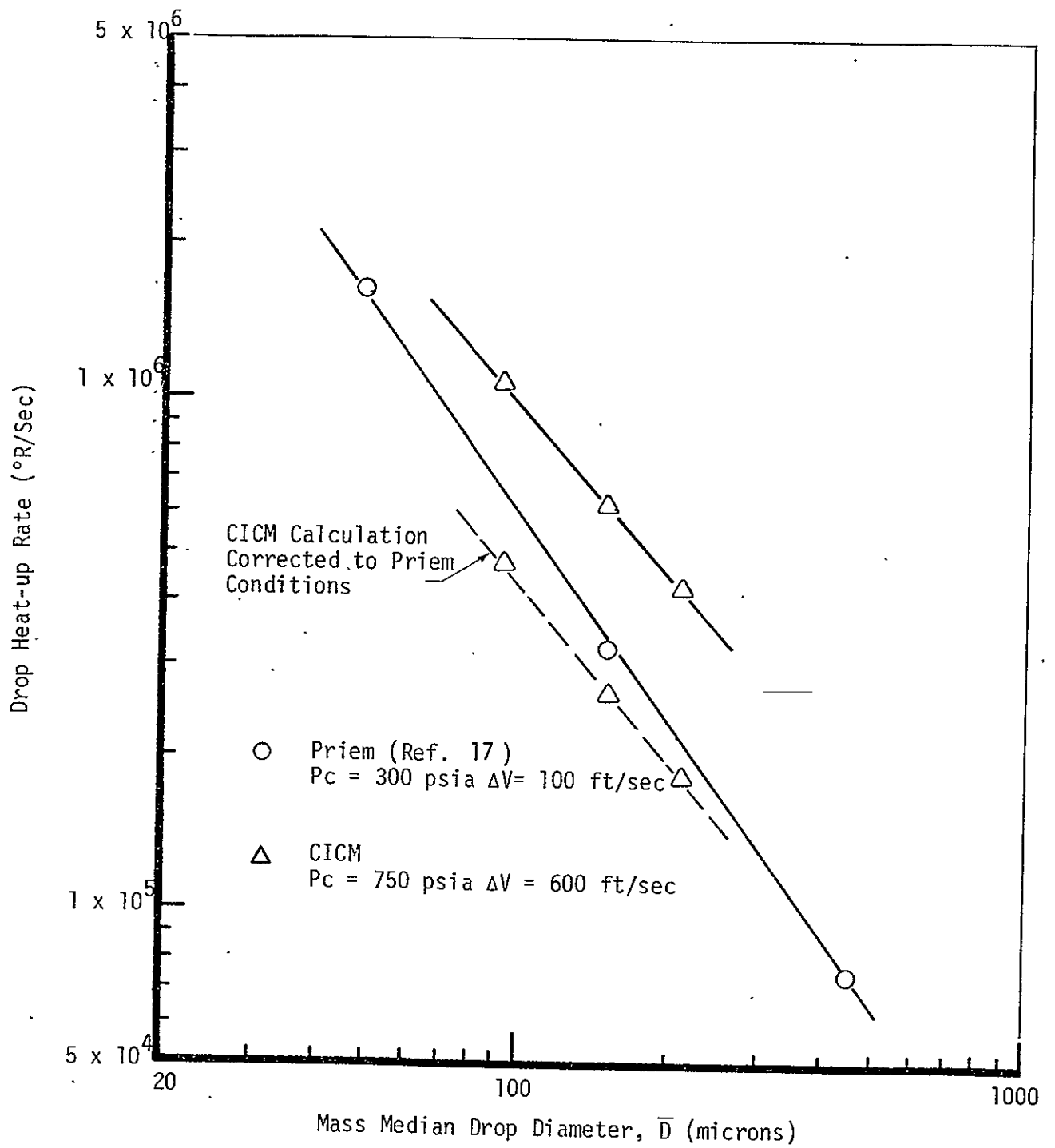
FIGURE B-1.   COMPARISON OF OXYGEN HEATING RATE CALCULATIONS

The figure is a log-log plot. The vertical axis is labeled "Drop Heat-up Rate (°R/Sec)" with gridline labels 5×10^6, 1×10^6, 1×10^5, and 5×10^4. The horizontal axis is labeled "Mass Median Drop Diameter, $\overline{D}$ (microns)" with labels 20, 100, and 1000.

CICM Calculation Corrected to Priem Conditions

O   Priem (Ref. 17)
      Pc = 300 psia ΔV= 100 ft/sec

△   CICM
      Pc = 750 psia ΔV = 600 ft/sec

mass median drop diameter, for the solid line conditions shown in the figure. The agreement between the two models improved when chamber pressure and velocity differential effects on the local drop heat transfer rate were accounted for in the CICM calculation. Since no attempt was made to ensure that both model predictions were made with exactly the same gas and liquid properties the agreement can be considered to be excellent. The results of the droplet heating rate comparison verify the CICM droplet heat-up model.

4.   Droplet Drag Coefficient Correlation

CICM employs the droplet drag correlation equations developed by Rabin (Ref. 31).

$$C_d = 27 \ Re_D^{-0.84} \qquad Re_D < 80 \qquad \text{(B-3)}$$

$$C_d = 0.271 \ Re_D^{.217} \qquad 80 \leq Re_D \leq 10^4 \qquad \text{(B-4)}$$

$$C_d = 2 \qquad Re_D > 10^4 \qquad \text{(B-5)}$$

The influence of the assumed droplet drag correlation on the vaporization rate was examined during the DER review. This investigation indicated that the droplet drag correlation significantly affects the final performance prediction made by STC. The review recommended that the Rabin drag coefficient correlation be reviewed and compared to other available correlations.

5.   Chamber Mixing of Face "Rigimesh" Flow

The CICM program calculates mixing of any face rigimesh flow by assuming the rate of mixing to be a linear function between the face and an input downstream distance. The mixed flow is spread uniformly over the cross-sectional area of the element flow field and becomes part of the propellant (usually fuel) to be reacted. The CICM user's manual states that calculations have been performed for rigimesh mixing that indicate that rapid

acceleration reduces the rigimesh flow area to only approximately 3 percent of its injection area. This rarefaction occurs on the order of only 2 inches from the injector face plane. The rigimesh area reduces to an annulus trapped between coaxial element flows; the average thickness of the annulus was calculated to typically be on the order of .01 inch. It is therefore argued that turbulence sweeps the flow into adjacent element flow fields. This calculational technique would seem to be satisfactory for ordinary amounts of rigimesh flow (on the order of five percent of the total fuel flow) because the axial variation of the expansion area of the combusting flow field of adjacent elements will not be affected significantly. As an example of a typical case in point, the M-1 injector design analyzed during Task II of the program has 3 percent of the total hydrogen fuel flowing through the rigimesh portion of the injector face.

6.   Intra-Element Mass Distribution Specification

CICM allows for the effect of intra-element mass and mixture ratio distribution through user input specification. For each zone (i.e., single element) analyzed by CICM, the user is instructed to input radial zonal oxidizer and fuel mass fractions based on single element cold flow data. An example of such input is shown in Figure B-2 , taken from the CICM J-2S sample case in CPIA 246. There are several problems associated with accounting for intra-element mass non-uniformities in this manner.

(1)   There is no available standard technique for measuring single element cold flow gas/liquid coaxial mass distribution.

(2)   The JANNAF methodology does not specify the axial plane (i.e., collection plane) at which the intra-element mass distribution should be specified. Face plane measurements are most easily accomplished but will be significantly altered by the high ΔV shear mixing inherent to coaxial element designs.

(3)   The test cases used to back out the recommended atomization and drop size input constants to CICM assumed that the thrust chamber in question had uniform throat plane mixtue ratio distributions. For

Y-axis: Normalized Mass Flux, $(\dot{M}/A)_{local}/\dot{M}_{total}$

Y-axis values: 1.2, 1.0, 0.8, 0.6, 0.4, 0.2, 0.0

X-axis values: 1.5, 0.5, 0.5, 1.5

X-axis: Inches from Element
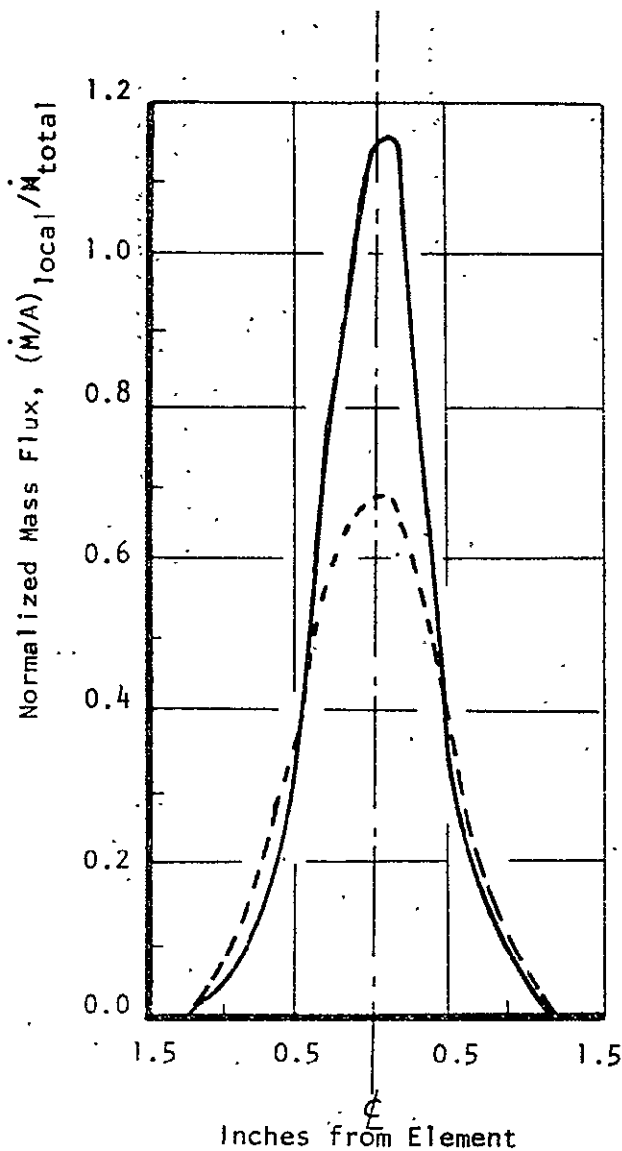
Legend:
——— $\left((\dot{M}/A)_{local}/\dot{M}_{total}\right)$ OXIDIZER
----- $\left((\dot{M}/A)_{local}/\dot{M}_{total}\right)$ FUEL

○ For input to CICM, the
normalized oxidizer and
fuel mass fluxes in any
given zone between an R_1
and an R_2 are integrated
over the area of the zone
to obtain the flowrate
and the mixture ratio.
The process is carried out
from the centerline to the
edge of the spray, break-
ing up the flow into con-
centric mixture ratio and
corresponding flowrate
zones.

FIGURE B-2.   COAXIAL ELEMENT COLD-FLOW SPRAY MASS FLUX DISTRIBUTION

most real coaxial injectors there will be a finite mixing loss because the coaxial element is a relatively slow mixing element. It is apparent that the correct values for the C_A and B_A coefficients will be directly dependent on the assumed single element mixture ratio distribution. Unless a standard method for measuring or calculating single element mixture ratio distributions is developed it is extremely doubtful that universal values for the C_A and B_A constants can be verified.

(4)   Similarly to the DER program for liquid/liquid injectors, CICM does not allow for the influence of combustion on the single element mass and mixture ratio distribution.

Currently, it appears that, without a standard coaxial element mixing model or approach, standardization of the parameters that influence the propellant vaporization rate will be difficult. That is, two processes affect coaxial injector performance (mixing and vaporization) and each process must be physically modeled to a comparable degree to result in a model that can calculate an accurate superimposed solution. At this stage CICM has been verified for engines that apparently have only one effective performance loss mechanism, i.e., incomplete propellant mass vaporization.

7.   Manifold Mass Distribution Zone Specification

The CICM user's manual recommends that measured or calculated manifold mass maldistributions should be accounted for by modeling separate chamber flow field zones when executing the program. Since the manifold distribution is usually calculated at the injector face plane, this technique assumes that the mass maldistribution will persist to the chamber throat plane. The manifold mass maldistribution performance loss is inevitably overpredicted with this technique, since turbulent mixing is ignored. Also, there is no recommended methodology for dividing the measured distribution into analysis zones. Therefore, the method of zone mass fraction assignment also becomes an user controlled input that affects the final performance prediction.

The solution of this problem is more complicated than the intra-element mixing problem discussed in the previous sub-section. It would be difficult to generalize a chamber zonal mixing model. Measurement of performance for thrust chamber assemblies having negligible vaporization and intra-element mixing losses would seem to provide a reasonable approach for solution of this problem. That is, if the engine vaporization and single element mixing losses are small (or can be accurately calculated) the manifold induced maldistribution loss can be backed out from the performance data.

C. Inconsistencies Between JANNAF Procedures and Program Operations

1. Background

CICM was developed as a rigorous analytical model that describes the atomization, vaporization and combustion of gas/liquid coaxial jets in a rocket engine environment. In the context of the JANNAF series of performance prediction models, CICM is intended to replace the LISP subprogram of DER for gas/liquid coaxial elements.

CICM is a highly specialized program intended to be used for one specific injector design concept. Additionally, the model has only been applied, to this date, to coaxial injectors using a central liquid O_2 circular core surrounded by a gaseous H_2 or H_2/O_2 combustion gas mixture annulus. The program input requires an extensive group of propellant property cards (644 cards for the CICM user's manual sample case) that will have to be generated for each propellant combination analyzed in the future. Another factor that currently limits the generality of CICM in the JANNAF methodology is that key empirical atomization rate and drop size constants, that control program performance predictions, have only been determined from test data for the LO_2/GH_2 propellant combination. Detailed discussion on these program inputs is included in Section B of this appendix. The CICM analysis documented in Section IV of this report was also restricted to a LO_2/GH_2 injector. Therefore, there are no current plans for testing the ability of CICM to model gas/liquid coaxial designs using other propellant combinations.

During this phase of the review task CICM was critiqued for its ability to function as documented in the JANNAF rigorous performance prediction procedure described in CPIA 246. The evaluation emphasized two areas; (1) test and evaluation of the CICM/STC interface procedure by running the CICM sample case and subsequently using the CICM input to generate an input deck for STC, and (2) development of a criteria for specifying the chamber axial location of the CICM/STC interface plane.

2.   Evaluation of the CICM/STC Interface Procedure

The CICM/STC interface procedure was examined carefully to ensure that the JANNAF performance prediction methodology accuracy and utilization time is not being compromised by the currently recommended interface technique. It was determined that the CICM interface routine DERINI was incomplete and punched improperly formated cards for input to the STC subcritical K-Prime version. The CICM user's manual states that DERINI punches input for the supercritical version of the DER program. No check was made to see if the punched output was compatible with the input requirements of that DER version. The next section of this appendix completely details the interface evaluation and development of a new interface procedure. This new DERINI version was successfully utilized during the program Task II CICM analysis effort.

3.   Description of Improved CICM/STC Interface Procedure

The JANNAF Performance Prediction Manual (CPIA 246) specifies that CICM will replace the LISP model for the analysis of gas/liquid coaxial elements. In this function, CICM must be capable of calculating spray formation, vaporization,and gaseous combustion and of generating output which is consistent with STC input and operational requirements.

The CICM/STC interface procedure was critically evaluated during the CICM review task of the Injection Processes Program. The CICM sample case documented in the user's manual was executed to determine if an interface with the STC program could be easily accomplished. The documented CICM sample case considers two injector zones (elements) which are each

divided into two intra-element mixture ratio zones through input mass fraction distributions. This input specification results in four separate sets (2 interelement zones x 2 intraelement zones) of streamtube input for the STC subprogram of DER. The DER user's manual was then used to determine that this four streamtube case required an input deck consisting of eight-six separate cards. The CICM interface subroutine (DERINI) was designed to punch only the streamtube flowrate and drop size input cards required by STC (cards 6720, 7010-7016, 7020-7026, 7030-7036, and 7040-7046 for this case). These cards comprised twenty-nine of the eighty-six cards required to correctly interface the CICM output and the DER input. Also, the cards punched to designate the streamtube and drop size group droplet flowrates (GWSPR (I, J)), velocities (VELD1 (I, J)), and diameters (GDIAD1 (I, J)) were improperly formated to be input to STC. The format error occurred because the interface subroutine DERINI also punched droplet temperatures for each streamtube and drop size group, while STC (in the subcritical DER K' version) does not require or allow for this input.

This attempt to join the CICM sample case output with the subcritical STC program indicated that the interface procedure required improvement. The six improvements that were grouped to result in the new interface procedure are detailed below.

(1)   The streamtube and droplet size group input cards were properly formated and labeled with their correct sequence numbers, as indicated in the DER user's manual.

(2)   A number of STC inputs that have constant values when LISP execution does not precede STC execution (e.g., when CICM interfaces with STC) were assigned values in the CICM interface routine DERINI and included in the STC input cards to be punched.

(3)   All STC inputs that are also input or internally calculated in CICM (e.g., combustion gas transport properties as a function of mixture ratio) were included in the DERINI output deck for input to STC.

(4)   STC inputs that could not be specified as constants and are not set by CICM input or calculation were grouped into a new namelist input set for DERINI.

(5)   Coding was included in DERINI to result in each STC input card having its correct sequence number, as specified in the DER user's manual, punched in columns 73-80.

(6)   An option was included in the new DERINI namelist input group to allow for writing the DERINI formulated STC input deck on a computer system drum file (or stratch tape) without having to punch an actual card deck.

The listed improvements resulted in an interface technique, completely internal to CICM, that allows generation of all required STC input. The new CICM/STC interface procedure is detailed in the following three paragraphs that include in turn; (1) a listing of the new CICM interface routine DERIN and specification of required line changes and additions to generate the new routine from the old verison, (2) a description of the required namelist input for DERINI, and (3) a description of the STC input deck generated with the new procedure for the CICM sample case documented in the program user's manual.

A compilation of the new version of the CICM subroutine DERINI, designed to provide punched card or mass storage file input to the DER subprogram STC, is shown in Table B-II. The line modifications that were applied to the original version of DERINI are detailed in Table V-III. No other changes are required to any CICM routine to develop the new interface procedure.

The required namelist input variables for DERINI are defined in Table B-IV. The DERINI namelist variable inputs must be preceded by a $STC specification and followed by a $END specification (or the system equivalent to these Univac 1108 Exec-8 designations). The first three variables listed in the table designate forms by which the STC input data may be output from DERINI. Any combination of these three output forms may be specified. The remaining input variables listed are identical to descriptions given in the DER user's manual. The oxidizer latent heat input, DHVO, should be consistent with the droplet "wet bulb" temperature calculated by CICM at the interface plane axial chamber location. Any STC variables not listed are either input to, internally set within, or calculated by CICM. Liquid fuel properties are not

included in the namelist because CICM requires that one propellant be gaseous and one liquid. The namelist input set used to check the new interface technique for the CICM sample case is shown in Table B-V.

The STC input generated by DERINI for the CICM sample case is listed in Table B-VI. The STC program was successfully executed with the data set shown.

aFOR,S DERINI
FORTRAN Vi. ISD VERSION a.68=02/26/76=08152:12 (6,)

SUBROUTINE DERINI   ENTRY POINT 002334

STORAGE USED: CODE(1) 002370; DATA(0) 006755; BLANK COMMON(2) 000000

COMMON BLOCKS:

```
0003   TCPLF   001514
0004   PROPI.  000013
0005   CGTABC  000135
0006   CHCOM   000072
```

EXTERNAL REFERENCES (BLOCK, NAME)

```
0007   LOCFAC
0010   XVDHV
0011   EQSTAT
0012   CGPROP
0013   RHOGF
0014   NRDUS
0015   NIOIS
0016   NIO2S
0017   SQRT
0020   NRNLS
0021   XPRR
0022   NRDUS
0023   NERR3S
```

STORAGE ASSIGNMENT   (BLOCK, TYPE, RELATIVE LOCATION, NAME)

```
0000    006503 1F      0001   000003 10L     0001   002224 1057G    0001    002244 1071G    0000    006545 11F
0001    002273 1100G    0001   001330 12L     0001   000270 120L    0001    001334 13L     0001    001340 14L
0001    000307 140L     0001   000027 145G    0001   001343 15L     0001    000042 154G    0001    001316 16L
0001    000312 160L     0001   000066 166G    0000   006550 17F     0000    006551 18F     0000    006506 2F
0001    000466 200L.    0001   000523 210L    0001   000160 217G    0001    000170 224G    0001    000227 241G
0001    000246 247G     0001   000272 261G    0001   000327 276G    0000    006511 3F      0001    000647 300L
0001    000346 307G     0001   000537 340G    0001   000653 355G    0001    000674 362G    0000    006514 4F
0001    001054 414G     0001   001100 426G    0001.  001273 472G    0000    006516 5F      0001    001404 556G
0001    001441 563G     0001   001461 576G    0000   006520 6F      0001    001067 610L    0001    001512 620G
0001    001073 620L     0001   001257 640L    0001   001574 660G    0001    001624 670G    0001    001650 677G
0000    006522 7F       0001   001267 700L    0001   001712 715G    0001    001721 720G    0001    001751 727G
0001    002004 741G     0001   002013 744G    0001   002043 753G    0000    006532 8F      0000    006534 9F
0000    006651 9000F    0001   002310 9999L   0006 R 000046 ACHAMC  0006    000014 ACSC    0000 R 004110 AGO
0005    000002 AMRT     0000 R 004350 AREA1   0000 R 006424 AHK     0000 R 006353 ARTOLD   0000 R 006425 BRK
0006    000012 BSPRC    0000 R 006442 C       0006    000017 CCANGC  0006    000015 CLNTC   0006    000016 CONRAC
0000 R 006255 CPVO      0000 R 006352 CRTOL   0006    000013 CSPRC   0000 R 006203 CSTR    0004    000011 CXOV
0006    000011 DELTXC    0000 R 006423 DHV    0000 R 006470 DHVF     0000 R 006357 DHVO    0000 R 005107 DOD
0000 R 006430 DRLDT     0000 R 006431 DWS     0000 R 006372 EMRCG    0006    000004 EMRGJC  0000 R 006432 EMRI
0000 R 004160 EMR      0000 R 006377 EMRCG    0006    000006 EMRGJC  0004 R 000000 EMRL    0004    000012 EMRPR
0004 R 000006 EMRV      0000 R 006443 FA      0000 R 006400 FCHA     0000 R 006362 FCHAM   0000 R 004610 FFMIX
0000 R 006417 FN        0000 R 004660 FUMIX   0000 R 004730 FSDER    0000 R 006406 F1      0000 R 003770 GAM
```

```
 0006     000007 GAMGJC    0000 R 000000 GASFL    0000 R 001060 GDIAD1    0000 R 005607 GMR      0000 R 006413 GSWB
 0008 R 005763 GTK       0000 R 002020 GTDD1    0000 R 002760 GVELD1    0000 R 000120 GWSPR    0000 R 006421 HD
 0000 I 006365 I         0000 I 006440 IC      0000 I 006472 ICARD     0000 I 006347 ICRC     0000 I 006355 IDRUM
 0000 I 006450 IFILE     0000 I 006410 II      0000 I 006420 IJ        0000 I 006451 ILISP    0000   006715 INJPS
 0000 I 006351 IPRMST    0000 I 006350 IPRSST   0000 I 006356 IPUNCH    0000 I 006467 IPUN3D   0000 I 006455 IST
 0000 I 006452 ISTC      0000 I 006454 ITDK    0000 I 006453 ITRANS    0000 I 006354 IWRITE   0000 I 006405 I1
 0000 I 006360 J         0000 I 006407 JJ      0000 I 006412 JJJ       0000 I 006335 JK1      0000 I 006336 JSPC
 0000 I 006411 K         0000 I 006500 L       0000 I 006475 M         0006   000001 M2C      0000 I 006476 N
 0000 I 006447 NASEG     0000 I 006474 NC      0006 I 000000 NCHAMC    0006   000002 NCON4C   0000 I 006361 NDER
 0000 I 006366 NDSC      0000 I 006367 NELEM   0000 I 006446 NGF       0000 I 006364 NGO      0000 I 006444 NGT
 0000 I 006363 NMIXZ     0000 I 006346 NMSTI   0000 I 006464 NOZUN     0000 I 006344 NP       0003 I 001512 NPCP
 0000 I 006345 NSSTI     0000 I 006445 NST     0000 I 006465 NSTPZ     0005 I 000000 NTAB     0003 I 001510 NTCP
 0000 I 006337 NTK       0000 I 006466 NUG     0000 R 003720 P        0000 R 006370 PC       0000 R 006441 PCI
 0004   000000 PCRIT     0000 R 006436 PHIGH   0000 R 006437 PLOW     0000 R 004230 PUS      0006   000020 RCBCC
 0006   000021 RCTC      0000 R 006427 RG      0000 R 006426 RHOD     0000 R 004540 RHOG     0013 R 000000 RHOGF
 0000 R 006461 RHOLF     0000 R 006343 RHOLO   0000 R 006460 RHONBF   0000 R 006342 RHONBO   0000 R 000050 SMRG
 0000   006553 STC       0006   000005 STGJC    0004   000010 STOCMR   0005   000001 STT      0000 R 006414 SUM1
 0000 R 006415 SUM2      0000 R 006416 SUM3    0000 R 006373 SWSPR    0000 R 006456 TBF      0000 R 006341 TBO
 0000 R 006305 TCONVO    0003   000050 TCP     0004 R 000002 TCRIT    0005 R 000003 TGAM     0000 R 004470 TGAS
 0000 R 005563 THL       0003 R 000670 THOL    0000 R 006376 TLI      0005 R 000003 TMR      0005 R 000071 TMW
 0000 R 006457 TNBF      0000 R 006340 TNBO     0000 R 004040 TO       0000 R 005253 TOD      0003 R 000024 TPCPL
 0003 R 000000 TTCPL     0005 R 000025 TTO     0005 R 000113 TVIS     0000 R 006225 TVO      0000 R 006374 VCG
 0000 R 004420 VGAS      0000 R 006433 VISC    0000 R 006375 VLJI     0000 R 005417 VOD      0000 R 004300 VUS
 0000 R 006371 WCG       0000 R 006403 WFE      0006   000003 WGJC     0000 R 006402 WOXE     0000 R 006404 WSPE
 0000 R 004743 WSPR      0000 R 006435 WT       0000 R 006401 WTE      0000 R 006462 WTMLLF   0000 R 006463 WTMLVF
 0006 R 000022 XCHAMC    0006   000010 XLMC    0000 R 006473 XNAP     0000 R 006502 XNGT     0000 R 006477 XNMR
 0000 R 006501 XNTK      0000 R 006434 XOV     0000 R 006422 XV       0000 R 006471 ZSTART
```

```
 00101    1*            SUBROUTINE  DERINI(IDER,ACHAM,XMINDE,IRDER)              00000010
 00103    2*            DIMENSION  GASFL(40), SMRG(40), GWSPR(12,40), GDIAD1(12,40),   00000020
 00103    3*           1    GTDD1(12,40), GVELD1(12,40), P(40), GAM(40), TO(40),       00000030
 00103    4*           2    AGO(40), EMW(40), PUS(40), VUS(40), AREA1(40), VGAS(40),   00000040
 00103    5*           3    TGAS(40), RHOG(40)                                         00000050
 00104    6*            DIMENSION  FFMIX(40), FOMIX(40), FSDER(11)                      00000060
 00105    7*            DIMENSION  WSPR(100), DOD(100), TOD(100), VOD(100), THL(20)     00000070
 00106    8*            DIMENSION GMR(6,18),GTK(6,24),CSTR(18),TVO(24),CPVO(24),TCONVO(24)
 00107    9*            COMMON  /TCPLF/  TTCPL(20,1), TPCPL(20,1), TCP(20,20,1),        00000080
 00107   10*           1    THOL(20,20,1), NTCP(2), NPCP(2)                            00000090
 00110   11*            COMMON  /PROP1/  PCRIT(2), TCRIT(2), EMWL(2), EMWV(2),          00000100
 00110   12*           1    STOCMR, CXOV, EMWPR                                        00000110
 00111   13*            COMMON/CGTABC/NTAB,STT,AMRT,TMR(18),TTO(18),TGAM(18),TMW(18),
 00111   14*           *    TVIS(18)
 00112   15*            COMMON/CHCOM/NCHAMC,M2C,NCON4C,WGJC,EMRGJC,STGJC,EMWGJC,GAMGJC,
 00112   16*           *         XLMC,DELTXC,BSPRC,CSPRC,ACSC,CLNTC,CONRAC,CCANGC,
 00112   17*           *         RCBCC,RCTC,XCHAMC(20),ACHAMC(20)
 00113   18*
 00113   19*            DATA  JK1,JSPC/0,1/                                             00000120
 00116   20*          1 FORMAT(4I12,24X,I8)
 00117   21*          2 FORMAT(3E12,6,36X,I8)
 00120   22*          3 FORMAT(4E12,6,24X,I8)
 00121   23*          4 FORMAT(12I6,I8)
 00122   24*          5 FORMAT(6E12,6,I8)
 00123   25*          6 FORMAT(6I12,I8)
 00124   26*          7 FORMAT(6X,'STC INPUT FROM CICM PROGRAM CASE',T73,I8)
```

```
00125    27*          8 FORMAT(72X,I8)
00126    28*          9 FORMAT(6X,'O2/H2 GAS PROPERTIES FROM CICM INPUT',T7:,I*)
00127    29*         11 FORMAT(2E12.6,48X,I8)
00130    30*         17 FORMAT(12I6)
00131    31*         18 FORMAT(6E12.6)
00132    32*            NAMELIST/STC/TVO,TCONVO,NTK,TN8O,T8O,RHONBO,RHOLO,NP,NSST:I,NMST:,
00132    33*          *          ICRC,IPRSST,IPRMST,CRTOL,ARTOLD,IWRITE,IDRUM,IPUNCH,
00132    34*          *          CPVO,DHVO
00133    35*            CSTAR(XMW,TO,GAM)=SQRT(49677.*GAM*TO/XMW/((2./(GAM+1.))**((GAM+1.)
00133    36*          */(GAM-1.))))/GAM
00134    37*            J = 0                                               0000C100
00135    38*            NDER = 0                                           00000200
00136    39*            FCHAM = 0.0                                        00000220     ......
00137    40*         10 READ(IRDER,17) NMIXZ,NGO                                         000003
00143    41*            READ(IRDER,18) (FFMIX(I),FOMIX(I),I=1,NMIXZ)                      000014
00152    42*            READ(IRDER,18) (FSDER(I),I=1,NGO)                                 000033
00160    43*            READ(IRDER,17) NDSC,NELEM                                         000045
00164    44*            READ(IRDER,18) (WSPR(I),DOD(I),TOD(I),VOD(I),I=1,100)             000054
00175    45*            READ(IRDER,18) PC,WCG,EMRCG,SWSPR,VCG,VLJI,TLI,EMWCG,FCHA         000074
00210    46*            WTE = (SWSPR+WCG)*NELEM                            00000310       000112
00211    47*            WOXE = (SWSPR+WCG*EMRCG/(1.+EMRCG))*NELEM          00000320       000116
00212    48*            WFE = WTE-WOXE                                     00000330       000126
00213    49*            WSPE = SWSPR*NELEM                                 00000340       000130
00214    50*            CALL LOCFAC(JK1,PC,TPCPL,NPCP(1),I1,F1)            00000350       000133
00215    51*            NP = NTCP(1)                                      00000360       000143
00216    52*            DO 20 I=1,NP                                      00000370       000151
00221    53*         20 THL(I) = THOL(I1,I,1)+F1*(THOL(I1+1,I,1)-THOL(I1,I,1))  00000380  000160
00223    54*            DO 100 JJ=1,NMIXZ                                  00000390       000170
00226    55*            I = J+JJ                                          00000400       000174
00227    56*            GASFL(I) = FFMIX(JJ)*WFE+FOMIX(JJ)*(WOXE-WSPE)     00000410       000177
00230    57*            SMRG(I) = FOMIX(JJ)*(WOXE-WSPE)/(FFMIX(JJ)*WFE)    00000420       000203
00231    58*            GWSPR(1,I) = 0.0                                  00000430       000205
00232    59*            GDIAD1(1,I) = 0.0                                 00000440       000210
00233    60*            GTUD1(1,I) = 100.0                                00000450       000211
00234    61*        100 GVELD1(1,I) = 100.0                                             000213
00236    62*            IF(NGO.LT.NDSC) GO TO 160                         00000490       000216
00240    63*            DO 140 II=1,NGO                                   00000500       000222
00243    64*            I = II+1                                         00000510       000234
00244    65*            IF(II.GT.NDSC) GO TO 120                          00000520       000237
00246    66*            DO 110 K=1,NMIXZ                                  00000530       000246
00251    67*            JJ = J+K                                         00000540       000246
00252    68*            GWSPR(I,JJ) = WSPR(II)*NELEM*FOMIX(K)             00000550       000251
00253    69*            GDIAD1(I,JJ) = DOD(II)                            00000560       000256
00254    70*            GTOD1(I,JJ) = TUD(II)                             00000570       000260
00255    71*        110 GVELD1(I,JJ) = VOD(II)                                           000262
00257    72*            GO TO 140                                         00000600       000266
00260    73*        120 DO 130 K = 1,NMIXZ                                               000272
00263    74*            JJ = J+K                                         00000630       000272
00264    75*            GWSPR(I,JJ) = 0.0                                 00000640       000277
00265    76*            GDIAD1(I,JJ) = 0.0                                00000650       000300
00266    77*            GTUD1(I,JJ) = 100.0                               00000660       000301
00267    78*        130 GVELD1(I,JJ) = 100.0                                             000303
00271    79*        140 CONTINUE                                          00000690       000310
00273    80*            GO TO 300                                         00000700       000310
00274    81*        160 JJJ = 1                                          00000720       000312
00275    82*            DO 230 II=1,NGO                                  00000730       000313
00300    83*            I = II+1                                         08000740       000332
```

R-20

```
00301    84*        GSWS = 0.0                                                    00000750    000335
00302    85*        SUM1 = 0.0                                                    00000760    000336
00303    86*        SUM2 = 0.0                                                    00000770    000337
00304    87*        SUM3 = 0.0                                                    00000780    000340
00305    88*        FN = FSDER(II)                                               00000790    000341
00306    89*        DO 170 IJ=JJJ,NDSC                                           00000800    000346
00311    90*        JJ = IJ                                                       00000810    000346
00312    91*        CALL LUCFAC(JK1,TOD(IJ),TTCPL,NTCP(1),I1,F1)                 00000820    000350
00313    92*        HD = THL(I1)+F1*(THL(I1+1)-THL(I1))                          00000830    000362
00314    93*        CALL XVDHV(XV,DHV,ARK,BRK,PC,TOD(IJ),JSPC)                   00000840    000370
00315    94*        CALL EQSTAT(RHOD,RG,DRLDT,PC,TOD(IJ),XV,EMHL(JSPC),EMWCG,    00000850    000403
00315    95*       1    ARK,BRK,JSPC)                                            00000860    000403
00316    96*        IF(WSPR(IJ).GT.FN*SWSPR) GO TO 200                           00000870    000425
00320    97*        GSWS = GSWS+WSPR(IJ)                                         00000880    000432
00321    98*        SUM1 = SUM1 + WSPR(IJ)*VOD(IJ)                               00000890    000435
00322    99*        SUM2 = SUM2 + WSPR(IJ)*HD                                    00000900    000441
00323   100*        SUM3 = SUM3 + WSPR(IJ)/(VOD(IJ)**2*RHOD*DOD(IJ)**2)          00000910    000445
00324   101*   170  FN = FSDER(II) - GSWS/SWSPR                                              000457
00326   102*        GO TO 210                                                    00000940    000464
00327   103*   200  DWS = FN*SWSPR                                               00000950    000466
00330   104*        GSWS = GSWS+DWS                                              00000960    000470
00331   105*        JJJ = JJ                                                     00000970    000472
00332   106*        WSPR(JJ) = WSPR(JJ)+DWS                                      00000980    000474
00333   107*        SUM1 = SUM1 + DWS*VOD(JJ)                                    00000990    000500
00334   108*        SUM2 = SUM2 + DWS*HD                                         00001000    000504
00335   109*        SUM3 = SUM3 + DWS/(VOD(JJ)**2*RHOD*DOD(JJ)**2)               00001010    000510
00336   110*   210  SUM2 = SUM2/GSWS                                                         000523
00337   111*        DO 230 K = 1,NMIXZ                                                       000525
00342   112*        JJ = J+K                                                     00001050    000537
00343   113*        GWSPR(I,JJ) = SWSPR*FSDER(II)*NELEM*FOMIX(K)                 00001060    000542
00344   114*        GVELD1(I,JJ) = SUM1/GSWS                                     00001070    000547
00345   115*        CALL LUCFAC(JK1,SUM2,THL,NTCP(1),I1,F1)                      00001080    000551
00346   116*        GTOD1(I,JJ) = TTCPL(I1,1)+F1*(TTCPL(I1+1,1)-TTCPL(I1,1))     00001090    000563
00347   117*        CALL XVDHV(XV,DHV,ARK,BRK,PC,GTOD1(I,JJ),JSPC)              00001100    000571
00350   118*        CALL EQSTAT(RHOD,RG,DRLDT,PC,GTOD1(I,JJ),XV,EMHL(JSPC),     00001110    000604
00350   119*       1    EMWCG,ARK,BRK,JSPC)                                      00001120    000604
00351   120*   230  GDIAD1(I,JJ) = SQRT(GSWS/(GVELD1(I,JJ)**2*RHOD*SUM3))                    000626
00354   121*   300  DO 500 K = 1,NMIXZ                                                       000647
00357   122*        JJ = J+K                                                     00001200    000656
00360   123*        GSWS = 0.0                                                   00001210    000666
00361   124*        DO 400 I=1,NGO                                               00001220    000674
00364   125*   400  GSWS = GSWS+GWSPR(I,JJ)                                      00001230    000674
00366   126*        P(JJ) = PC                                                   00001240    000677
00367   127*        EMRI = SMRG(JJ)                                             00001242    000701
00370   128*        CALL CGPROP(SMRG(JJ),TO(JJ),EMW(JJ),GAM(JJ),VISC,GASFL(JJ), 00001250    000703
00370   129*       1    0.0,0,XOV,EMRI,PC,NGO,VLJI,GTOD1(1,JJ),GVELD1(1,JJ),     00001260    000703
00370   130*       2    GWSPR(1,JJ),GSWS,TLI)                                    00001270    000703
00371   131*        AREA1(JJ) = FCHA*(FFMIX(K)*WFE+FOMIX(K)*WOXE)/WTE*ACHAM      00001280    000750
00372   132*        PUS(JJ) = PC                                                 00001290    000761
00373   133*        VUS(JJ) = VCG                                                00001300    000763
00374   134*        VGAS(JJ) = VCG                                               00001310    000765
00375   135*        AGO(JJ) = SQRT(32.2*GAM(JJ)*1545.*TO(JJ)/EMW(JJ))           00001320    000766
00376   136*        TGAS(JJ) = TO(JJ)*(1.-(GAM(JJ)-1.)*0.5*(VGAS(JJ)/AGO(JJ))**2) 00001330  001000
00377   137*   500  RHOG(JJ) = RHOGF (TGAS(JJ),PC,EMW(JJ),2)                                 001012
00401   138*        FCHAM = FCHAM+FCHA                                           00001360    001027
00402   139*        J = J+NMIXZ                                                  00001370    001032
00403   140*        NDER = NDER+1                                               00001380    001035
```

B-21

R-22

```
00404    141*        IF(NDER.LT.IDER) GO TO 10                                    00001390   001040
00406    142*        SUM1 = 0.0                                                   00001410   001043
00407    143*        HT = 0.0                                                     00001420   001044
00410    144*        PHIGH = 0.0                                                  00001430   001045
00411    145*        PLOW = 0.0                                                   00001440   001046
00412    146*        IC = 0                                                       00001450   001047
00413    147*        DO 600 I=1,J                                                 00001460   001054
00416    148*        SUM1 = SUM1+GASFL(I)*P(I)                                    00001470   001054
00417    149*   600  HT = HT + GASFL(I)                                                      001057
00421    150*        PCI = SUM1/HT                                               00001500   001063
00422    151*        GO TO 620                                                   00001510   001065
00423    152*   610  PCI = (PLOW+PHIGH)/2.0                                      00001530   001067
00424    153*   620  SUM1 = 0.0                                                             001073
00425    154*        DO 630 I=1,J                                                           001073
00430    155*        C = -144.*(PUS(I)-PCI)*32.2/RHOG(I)                         00001570   001100
00431    156*        IF(VUS(I)*VUS(I).LT.4.*C) GO TO 640                         00001580   001106
00433    157*        VGAS(I) = (VUS(I)+SQRT(VUS(I)*VUS(I)-4.*C))/2.0             00001590   001114
00434    158*        TGAS(I) = TO(I)*(1.-(GAM(I)-1.)*0.5*(VGAS(I)/AGO(I))**2)    00001600   001130
00435    159*        RHOG(I) = RHOGF(TGAS(I),PCI,EMW(I),2)                       00001610   001141
00436    160*        AREA1(I) = 144.*GASFL(I)/(VGAS(I)*RHOG(I))                  00001620   001154
00437    161*   630  SUM1 = SUM1 + AREA1(I)                                      00001630   001161
00441    162*        FA = SUM1/(FCHAM*ACHAM)                                                001161
00442    163*        IF(ABS(FA-1.).LE.0.001) GO TO 700                           00001670   001165
00444    164*        IF(FA.LT.1.0) PLOW = PCI                                    00001680   001171
00446    165*        IF(FA.GE.1.0) PHIGH = PCI                                   00001690   001176
00450    166*        IC = IC+1                                                   00001700   001204
00451    167*        IF(IC.GT.60) GO TO 700                                      00001710   001212
00453    168*        IF(IC.GE.2) GO TO 610                                       00   172    001215
00455    169*        IF(PHIGH.LE.0.0.OR.PLOW.LE.0.0) IC = 0                      00001730   001220
00457    170*        IF(PLOW.LE.0.0) PCI = PCI-1.0                               00001740   001224
00461    171*        IF(PHIGH.LE.0.0) PCI = PCI+1.0                              00001750   001241
00463    172*        GO TO 620                                                   00001760   001247
00464    173*   640  PHIGH = PCI                                                 00001770   001255
00465    174*        IF(PLOW.GT.0.0) GO TO 610                                   00001780   001257
00467    175*        PCI = PCI-1.0                                              00001790   001260
00470    176*        GO TO 620                                                   00001800   001263
00471    177*.  700  DO 710 I=1,J                                               00001810   001265
00474    178*   710  AREA1(I) = AREA1(I)/FA                                      00001830   001267
00476    179*        NGT = NGO+1                                                            001273
00477    180*        NST = J                                                     00001870   001276
00500    181*        NGF = 1                                                     00001880   001301
00501    182*        NASEG = 1                                                   00001890   001303
00502    183*        IWRITE=1                                                    00001900   001305
00503    184*        IDRUM=0                                                                001306
00504    185*        IPUNCH=0                                                               001307
00504    186*   C    INPUT TO CICM THROUGH $STC                                            001310
00505    187*        READ(5,STC)                                                           001310
00510    188*    16  CONTINUE                                                              001311
00511    189*        IF(IWRITE.EQ.1) GO TO 12                                              001316
00513    190*        IF(IDRUM.EQ.1) GO TO 13                                               001316
00515    191*        IF(IPUNCH.EQ.1) GO TO 14                                              001320
00517    192*        GO TO 9999                                                            001323
00520    193*    12  CONTINUE                                                              001326
00521    194*        IFILE=6                                                               001330
00522    195*        IWRITE=0                                                              001330
00523    196*        GO TO 15                                                              001331
```

```
00525   198*      5         IFILE=11                                                                    001334
00526   199*                IDRUM=0                                                                     001335
00527   200*                GO TO 15                                                                    001336
00530   201*            14 CONTINUE                                                                     001340
00531   202*                IFILE=7                                                                     001340
00532   203*                IPUNCH=0                                                                    001341
00533   204*            15 CONTINUE                                                                     001343
00534   205*                ILISP=0                                                                     001343
00535   206*                ISTC=1                                                                      001343
00536   207*                ITRANS=0                                                                    001345
00537   208*                ITDK=0                                                                      001346
00540   209*                IST=1                                                                       001347
00541   210*                TBF=0.0                                                                     001350
00542   211*                TNBF=0.0                                                                    001351
00543   212*                RHONBF=0.0                                                                  001352
00544   213*                RHULF=0.0                                                                   001353
00545   214*                WTMLLF=0.0                                                                  001354
00546   215*                WTMLVF=0.0                                                                  001355
00547   216*                NOZON=0                                                                     001356
00550   217*                NSTPZ=0                                                                     001357
00551   218*                NUG=0                                                                       001360
00552   219*                IPUN3D=0                                                                    001361
00553   220*                DHVF=0.0                                                                    001362
00554   221*                ZSTART=XHINDE                                                               001363
00555   222*                DO 31 I=1,NTAB                                                              001404
00560   223*            31 CSTR(I)=CSTAR(TMW(I),TTO(I),TGAM(I))                                         001405
00562   224*                DO 715 J=1,NTAB                                                             001441
00565   225*                GMR(1,J)=TMR(J)                                                             001441
00566   226*                GMR(2,J)=TTO(J)                                                             001442
00567   227*                GMR(3,J)=TVIS(J)                                                            001444
00570   228*                GMR(4,J)=TGAM(J)                                                            001446
00571   229*                GMR(5,J)=TMW(J)                                                             001450
00572   230*                GMR(6,J)=CSTR(J)                                                            001452
00573   231*           715 CONTINUE                                                                     001461
00575   232*                DO 716 J=1,NTK                                                              001461
00600   233*                GTK(1,J)=0.0                                                                001461
00601   234*                GTK(2,J)=0.0                                                                001461
00602   235*                GTK(3,J)=0.0                                                                001462
00603   236*                GTK(4,J)=TVO(J)                                                             001463
00604   237*                GTK(5,J)=CPVO(J)                                                            001465
00605   238*                GTK(6,J)=TCONVO(J)                                                          001467
00606   239*           716 CONTINUE                                                                     001472
00610   240*          9000 FORMAT(1H1,///,23X,'CICM GENERATED INPUT DATA FOR DER SUBPROGRAM 8          001472
00610   241*               *TC'///)                                                                     001472
00611   242*                WRITE(6,9000)                                                               001472
00613   243*                ICARD=10                                                                    001477
00614   244*                WRITE(IFILE,7) ICARD                                                        001501
00617   245*                DO 720 I=2,4                                                                001512
00622   246*                ICARD=I*10                                                                  001512
00623   247*           720 WRITE(IFILE,8) ICARD                                                         001515
00627   248*                ICARD=50                                                                    001525
00630   249*                WRITE(IFILE,1) ILISP,ISTC,ITRANS,ITDK,ICARD                                 001527
00637   250*                ICARD=5010                                                                  001541
00640   251*                WRITE(IFILE,1) NOZON,NSTPZ,NUG,IPUN3D,ICARD                                 001543
00647   252*                ICARD=5020                                                                  001555
00650   253*                WRITE(IFILE,1) NP,NCHAMC,NTAB,NTK,ICARD                                     001557
00657   254*                DO 725 I=1,NCHAMC                                                           001574
```

```
00662   255*          ACHAMC(I)=SQRT(4./3.14157*/CHAMC(I))                     001574
00663   256*      725 CONTINUE                                                 001603
00665   257*          XNAP=NCHAMC                                              001603
00666   258*          NC=XNAP/3.+.9                                            001606
00667   259*          DU 730 I=1,NC                                            001620
00672   260*          ICARD=5020+I*10                                          001624
00673   261*          M=I*3-2                                                  001630
00674   262*          N=M+2                                                    001634
00675   263*      730 WRITE(IFILE,5) (XCHAMC(J),ACHAMC(J),J=M,N),ICARD        001636
00706   264*          ICARD=5100                                              001660
00707   265*          WRITE(IFILE,9) ICARD                                    001662
00712   266*          XNMR=NTAR                                               001670
00713   267*          NC=XNMR/6.+.9                                            001673
00714   268*          DU 740 I=1,6                                            001705
00717   269*          DU 740 J=1,NC                                            001721
00722   270*          ICARD=5000+I*100+J*10                                   001721
00723   271*          M=J*6-5                                                  001725
00724   272*          N=M+5                                                    001731
00725   273*      740 WRITE(IFILE,5) (GMR(I,L),L=M,N),ICARD                   001736
00736   274*          XNTK=NTK                                                001762
00737   275*          NC=XNTK/6.+.9                                            001765
00740   276*          DU 750 I=1,6                                            001777
00743   277*          DU 750 J=1,NC                                            002013
00746   278*          ICARD=5600+I*100+J*10                                   002013
00747   279*          M=J*6-5                                                  002017
00750   280*          N=M+5                                                    002023
00751   281*      750 WRITE(IFILE,5) (GTK(I,L),L=M,N),ICARD                   002030
00762   282*          ICARD=6510                                              002054
00763   283*          WRITE(IFILE,5) TNBF,TBF,RHONBF,RHOLF,EMWL(2),EMWV(2),ICARD   002056
00774   284*          ICARD=6520                                              002072
00775   285*          WRITE(IFILE,5) TNBU,TBU,RHONBU,RHOLU,EMWL(1),EMWV(1),ICARD   002074
01006   286*          ICARD=6530                                              002110
01007   287*          WRITE(IFILE,3) TCRIT(2),TCRIT(1),DHVF,DHVU,ICARD        002112
01016   288*          ICARD=6540                                              002124
01017   289*          WRITE(IFILE,6) IST,NSSTI,NMSTI,ICRC,IPRSST,IPRMST,ICARD 002126
01030   290*          ICARD=6550                                              002142
01031   291*          WRITE(IFILE,11) CRTOL,ARTOLD,ICARD                      002144
01036   292*          ICARD=6710                                              002154
01037   293*          WRITE(IFILE,11) PCI,ZSTART,ICARD                        002156
01044   294*          ICARD=6720                                              002166
01045   295*          WRITE(IFILE,1) NGT,NGF,NST,NASEG,ICARD                  002170
01054   296*          XNGT=NGT                                                002202
01055   297*          NC=XNGT/2.+.9                                           002205
01056   298*          DU 800 J=1,NST                                          002217
01061   299*          ICARD=7000+J*10                                         002224
01062   300*          WRITE(IFILE,2) AREAI(J),GASFL(J),SMRG(J),ICARD          002230
01070   301*          DU 800 I=1,NC                                           002244
01073   302*          ICARD=ICARD+1                                          002244
01074   303*          M=I*2-1                                                 002247
01075   304*          N=M+1                                                   002253
01076   305*      800 WRITE(IFILE,5) (GWSPR(L,J),GVELDI(L,J),GDIADI(L,J),L=M,N),ICARD   002260
01111   306*          GO TO 16                                                002306
01112   307*     9999 CONTINUE                                                002310
01113   308*          RETURN                                       00002170   002310
01114   309*          END                                          00002180   002367
```

```
∂FOR,URS DERINI
-7
      DIMENSION GMR(6,18),GTK(6,20),CSTR(18),TVO(24),CPVO(24),TCONVO(24)
-11
      COMMON/CGTABC/NTAB,STT,AMRT,TMR(18),TTO(18),TGAM(18),TMW(18),
     *                TVIS(18)
      COMMON/CHCOM/NCHAMC,M2C,NCON4C,WGJC,EMRGJC,STGJC,EMWGJC,GAMGJC,
     *             XLMC,DELTXC,BSPRC,CSPRC,ACSC,CLNTC,CONRAC,CCANGC,
     *             RCBCC,RCTC,XCHAMC(20),ACHAMC(20)
-13,17
    1 FORMAT(4I12,24X,I8)
    2 FORMAT(3E12.6,36X,I8)
    3 FORMAT(4E12.6,24X,I8)
    4 FORMAT(12I6,I8)
    5 FORMAT(6E12.6,I8)
    6 FORMAT(6I12,I8)
    7 FORMAT(6X,'STC INPUT FROM CICM PROGRAM CASE',T73,I8)
    8 FORMAT(72X,I8)
    9 FORMAT(6X,'O2/H2 GAS PROPERTIES FROM CICM INPUT',T73,I8)
   11 FORMAT(2E12.6,48X,I8)
   17 FORMAT(12I6)
   18 FORMAT(6E12.6)
      NAMELIST/STC/TVO,TCONVO,NTK,TNBO,TBO,RHONBO,RHOLO,NP,NSSTI,NMSTI,
     *             ICRC,IPRSST,IPRMST,CRTOL,ARTOLD,IWRITE,IDRUM,IPUNCH,
     *             CPVO,DHVO
      CSTAR(XMW,TO,GAM)=SQRT(49677.*GAM*TO/XMW/((2./(GAM+1.))**((GAM+1.)
     */(GAM-1.))))/GAM
-20,20
-22,27
   10 READ(IRDER,17) NMIXZ,NGO
      READ(IRDER,18) (FFMIX(I),FOMIX(I),I=1,NMIXZ)
      READ(IRDER,18) (FSDER(I),I=1,NGO)
      READ(IRDER,17) NDSC,NELEM
      READ(IRDER,18) (WSPR(I),DOD(I),TOD(I),VOD(I),I=1,100)
      READ(IRDER,18) PC,WCG,EMRCG,SWSPR,VCG,VLJI,TLI,EMWCG,FCHA
-165,187
      IWRITE=1
      IDRUM=0
      IPUNCH=0
C     INPUT TO CICM THROUGH $STC
      READ(5,STC)
   16 CONTINUE
      IF(IWRITE.EQ.1) GO TO 12
      IF(IDRUM.EQ.1) GO TO 13
      IF(IPUNCH.EQ.1) GO TO 14
      GO TO 9999
   12 CONTINUE
      IFILE=6
      IWRITE=0
      GO TO 15
   13 CONTINUE
      IFILE=11
      IDRUM=0
      GO TO 15
   14 CONTINUE
```

```
      IFILE=7
      IPUNCH=0
   15 CONTINUE
      ILISP=0
      ISTC=1
      ITRANS=0
      ITDK=0
      IST=1
      TBF=0.0
      TNBF=0.0
      RHONBF=0.0
      RHOLF=0.0
      WTMLLF=0.0
      WTMLVF=0.0
      NOZON=0
      NSTPZ=0
      NUG=0
      IPUN3D=0
      DHVF=0.0
      ZSTART=XMINDE
      DO 31 I=1,NTAB
   31 CSTR(I)=CSTAR(TMW(I),TTO(I),TGAM(I))
      DO 715 J=1,NTAB
      GMR(1,J)=TMR(J)
      GMR(2,J)=TTO(J)
      GMR(3,J)=TVIS(J)
      GMR(4,J)=TGAM(J)
      GMR(5,J)=TMW(J)
      GMR(6,J)=CSTR(J)
  715 CONTINUE
      DO 716 J=1,NTK
      GTK(1,J)=0.0
      GTK(2,J)=0.0
      GTK(3,J)=0.0
      GTK(4,J)=TVO(J)
      GTK(5,J)=CPVO(J)
      GTK(6,J)=TCONVO(J)
  716 CONTINUE
 9000 FORMAT(1H1,///,23X,'CICM GENERATED INPUT DATA FOR DER SUBPROGRAM S
     *TC'///)
      WRITE(6,9000)
      ICARD=10
      WRITE(IFILE,7) ICARD
      DO 720 I=2,4
      ICARD=I*10
  720 WRITE(IFILE,8) ICARD
      ICARD=50
      WRITE(IFILE,1) ILISP,ISTC,ITRANS,ITDK,ICARD
      ICARD=5010
      WRITE(IFILE,1) NOZON,NSTPZ,NUG,IPUN3D,ICARD
      ICARD=5020
      WRITE(IFILE,1) NP,NCHAMC,NTAB,NTK,ICARD
      DO 725 I=1,NCHAMC
      ACHAMC(I)=SQRT(4./3.14159*ACHAMC(I))
  725 CONTINUE
      XNAP=NCHAMC
      NC=XNAP/3.+.9
```

```
      DO 730 I=1,NC
      ICARD=5020+I*10
      M=I*3-2
      N=M+2
730   WRITE(IFILE,5) (XCHAMC(J),ACHAMC(J),J=M,N),ICARD
      ICARD=5100
      WRITE(IFILE,9) ICARD
      XNMR=NTAB
      NC=XNMR/6.+.9
      DO 740 I=1,6
      DO 740 J=1,NC
      ICARD=5000+I*100+J*10
      M=J*6-5
      N=M+5
740   WRITE(IFILE,5) (GMR(I,L),L=M,N),ICARD
      XNTK=NTK
      NC=XNTK/6.+.9
      DO 750 I=1,6
      DO 750 J=1,NC
      ICARD=5600+I*100+J*10
      M=J*6-5
      N=M+5
750   WRITE(IFILE,5) (GTK(I,L),L=M,N),ICARD
      ICARD=6510
      WRITE(IFILE,5) TNBF,TBF,RHONBF,RHOLF,EMWL(2),EMWV(2),ICARD
      ICARD=6520
      WRITE(IFILE,5) TNBO,TBO,RHONBO,RHOLO,EMWL(1),EMWV(1),ICARD
      ICARD=6530
      WRITE(IFILE,3) TCRIT(2),TCRIT(1),DHVF,DHVO,ICARD
      ICARD=6540
      WRITE(IFILE,6) IST,NSSTI,NMSTI,ICRC,IPRSST,IPRMST,ICARD
      ICARD=6550
      WRITE(IFILE,11) CRTOL,ARTOLD,ICARD
      ICARD=6710
      WRITE(IFILE,11) PCI,ZSTART,ICARD
      ICARD=6720
      WRITE(IFILE,1) NGT,NGF,NST,NASEG,ICARD
      XNGT=NGT
      NC=XNGT/2.+.9
      DO 800 J=1,NST
      ICARD=7000+J*10
      WRITE(IFILE,2) AREA1(J),GASFL(J),SMRG(J),ICARD
      DO 800 I=1,NC
      ICARD=ICARD+1
      M=I*2-1
      N=M+1
800   WRITE(IFILE,5) (GWSPR(L,J),GVELD1(L,J),GDIAD1(L,J),L=M,N),ICARD
      GO TO 16
9999  CONTINUE
```

TABLE B-IV
NAMELIST INPUT VARIABLES FOR
IMPROVED CICM/STC INTERFACE ROUTINE

VARIABLE NAME	DEFINITION	UNITS
IWRITE*	STC input data generated by CICM will be printed out when IWRITE = 1	-
IDRUM*	STC input data generated by CICM will be written on system drum file 11 when IDRUM = 1	-
IPUNCH*	STC input data generated by CICM will be punched on cards when IPUNCH = 1	-
NP	Total number of z-planes between z=ZSTART and nozzle throat	-
NSSTI	Maximum number of complete passes, marching from z = ZSTART to throat, in single tube analysis	-
NMSTI	Maximum number of passes in multiple stream tube analysis	-
ICRC	Number of corrector cycles calculated at each Δz interval	-
IPRSST	Number of Δz intervals between single stream tube printouts	-
IPRMST	Number of Δz intervals between multiple stream tube printouts	-
CRTOL	Decimal tolerance, deviation of computed single stream tube throat contraction ratio from unity	-
ARTOLD	Decimal tolerance, deviation of computed multiple stream tube throat contraction ratio from unity	-
NTK	Number of temperatures at which propellant vapor specific heats and film thermal conductivity are tabulated	-
TVO (20)	Temperatures at which oxidizer CPVO and TCONVO are tabulated	°R
CPVO (20)	Oxidizer vapor specific heat at constant pressure	Btu/lbm-°R
TCONVO (20)	Thermal conductivity of vapor/gas film surrounding oxidizer droplets	Btu/ft-sec-°R
DHVO	Oxidizer latent heat of vaporization at chamber "wet bulb" temperature calculated by CICM	Btu/lbm
TNBO	Oxiidzer normal boiling point	°R

VARIABLE NAME	DEFINITION	UNITS
TBO	Oxidizer droplet saturation temperature at Pc	°R
RHONBO	Oxidizer density at normal boiling point	lbm/in^3
RHOLO	Oxidizer density at saturation temperature corresponding to Pc	lbm/in^3

:

NOTE: All parameters except those asterisked are identical to descriptions given in the DER users manual (Ref. 2).

```
$STC
CRTOL=0.01, ARTOLD=0.01, IWRITE=1, IDRUM=0, IPUNCH=0,
NP=50, NSSTI=3, NMSTI=3, ICRC=1, IPRSST=25, IPRMST=25,
TNBO=162., TBO=265., RHONBO=.0413, RHOLO=.0271, DHVO=45.,
NTK=20,
TVO(1)=200.,265.,275.,285.,300.,340.,400.,600.,1200.,1800.,
        2400.,3000.,3400.,3800.,4200.,4600.,5000.,5600.,
        6000.,6400.,
CPVO(1)=.94,.94,.55,.43,.356,.286,.257,.226,.245,.260,.269,
        .276,.280,.284,.288,.292,.2955,.301,.304,.307,
TCONVO(1)=.00000917,.00000917,.0000108,.00001105,.00001130,
        .00001167,.00001389,.00001806,.00002778,.000035,
        .00004028,.00004444,.00004583,.00004681,.00004722,
        .00004639,.000045,.00003806,.00001917,.0,
SEND
```

TABLE B-VI   CICM SAMPLE CASE GENERATED INPUT ELEMENT FOR STC

@ELT,L STC
PROCESSED BY UNIVAC 1100 SERIES ELT PROCESSOR LEVEL H8 AT 8:52:18 AM ON THURSDAY, FEBRUARY 26, 1976 (CYCLE 2)

#							
1.	STC INPUT FROM CICM PROGRAM CASE						10
2.							20
3.							30
4.							40
5.	0	1	0	0			50
6.	0	0	0	0			5010
7.	50	2	16	20			5020
8.	.000000+00	.463300+01	.500000+01	.255300+01			5030
9.	O2/H2 GAS PROPERTIES FROM CICM INPUT						5100
10.	.000000	.100000+00	.500000+00	.100000+01	.150000+01	.200000+01	5110
11.	.250000+01	.300000+01	.350000+01	.400000+01	.450000+01	.500000+01	5120
12.	.550000+01	.600000+01	.700000+01	.800000+01	.000000	.000000	5130
13.	.540000+03	.723514+03	.143978+04	.226954+04	.300818+04	.366881+04	5210
14.	.425866+04	.477364+04	.520902+04	.556641+04	.585309+04	.607691+04	5220
15.	.624526+04	.636535+04	.648942+04	.650686+04	.000000	.000000	5230
16.	.599022-05	.751828-05	.133827-04	.209151-04	.281415-04	.349234-04	5310
17.	.411218-04	.466813-04	.514907-04	.555499-04	.589147-04	.616405-04	5320
18.	.638106-04	.654806-04	.675984-04	.686049-04	.000000	.000000	5330
19.	.140500+01	.139700+01	.138000+01	.133800+01	.130100+01	.127400+01	5410
20.	.125400+01	.124000+01	.122900+01	.122000+01	.121400+01	.120900+01	5420
21.	.120500+01	.120200+01	.119900+01	.119800+01	.000000	.000000	5430
22.	.201600+01	.221800+01	.302400+01	.403200+01	.504000+01	.604700+01	5510
23.	.705000+01	.804000+01	.900700+01	.994100+01	.108370+02	.116920+02	5520
24.	.125020+02	.132660+02	.146520+02	.158620+02	.000000	.000000	5530
25.	.532077+04	.588331+04	.713801+04	.784513+04	.815831+04	.828650+04	5610
26.	.831491+04	.827652+04	.819444+04	.808436+04	.795385+04	.781410+04	5620
27.	.766980+04	.752364+04	.723488+04	.696488+04	.000000	.000000	5630
28.	.000000	.000000	.000000	.000000	.000000	.000000	5710
29.	.000000	.000000	.000000	.000000	.000000	.000000	5720
30.	.000000	.000000	.000000	.000000	.000000	.000000	5730
31.	.000000	.000000	.000000	.000000	.000000	.000000	5740
32.	.000000	.000000	.000000	.000000	.000000	.000000	5810
33.	.000000	.000000	.000000	.000000	.000000	.000000	5820
34.	.000000	.000000	.000000	.000000	.000000	.000000	5850
35.	.000000	.000000	.000000	.000000	.000000	.000000	5840
36.	.000000	.000000	.000000	.000000	.000000	.000000	5910
37.	.000000	.000000	.000000	.000000	.000000	.000000	5920
38.	.000000	.000000	.000000	.000000	.000000	.000000	5930
39.	.000000	.000000	.000000	.000000	.000000	.000000	5940
40.	.200000+03	.265000+03	.275000+03	.285000+03	.300000+03	.340000+03	6010
41.	.400000+03	.600000+03	.120000+04	.180000+04	.240000+04	.300000+04	6020
42.	.340000+04	.380000+04	.420000+04	.460000+04	.500000+04	.560000+04	6030
43.	.600000+04	.640000+04					6040
44.	.940000+00	.940000+00	.550000+00	.430000+00	.356000+00	.286000+00	6110
45.	.257000+00	.226000+00	.245000+00	.260000+00	.269000+00	.276000+00	6120
46.	.280000+00	.284000+00	.288000+00	.292000+00	.295500+00	.301000+00	6130
47.	.304000+00	.307000+00					6140
48.	.917000-05	.917000-05	.108000-04	.110500-04	.113000-04	.116700-04	6210
49.	.138900-04	.180600-04	.277800-04	.350000-04	.402800-04	.444400-04	6220
50.	.458300-04	.468100-04	.472200+04	.463900-04	.450000-04	.380600-04	6230
51.	.191700-04	.000000					6240
52.	.000000	.000000	.000000	.000000	.201600+01	.201600+01	6510
53.	.162000+03	.265000+03	.413000-01	.271000-01	.320000+02	.320000+02	6520
54.	.590000+02	.278600+03	.000000	.450000+02			6530

B-31

55.	1	3	3	1	25	25	6540
56.	.100000-01	.100000-01					6550
57.	.741407+03	.150000+01					6710
58.	12	1	4	1			6720
59.	.289392+01	.184291+01	.235410+01				7010
60.	.000000	.100000+03	.000000	.167655+00	.369130+03	.553597-02	7011
61.	.167655+00	.338165+03	.797571-02	.167655+00	.317580+03	.921044-02	7012
62.	.167655+00	.295141+03	.108685-01	.167655+00	.271784+03	.128331-01	7013
63.	.167655+00	.250306+03	.148369-01	.167655+00	.227946+03	.171472-01	7014
64.	.167655+00	.205843+03	.195475-01	.167655+00	.189710+03	.193214-01	7015
65.	.838276-01	.184154+03	.153935-01	.838276-01	.162630+03	.126132-01	7016
66.	.330055+01	.213035+01	.287724+01				7020
67.	.000000	.100000+03	.000000	.204912+00	.369139+03	.553597-02	7021
68.	.204912+00	.338165+03	.797571-02	.204912+00	.317580+03	.921044-02	7022
69.	.204912+00	.295141+03	.108685-01	.204912+00	.271784+03	.128331-01	7023
70.	.204912+00	.250306+03	.148369-01	.204912+00	.227946+03	.171472-01	7024
71.	.204912+00	.205843+03	.195475-01	.204912+00	.189710+03	.193214-01	7025
72.	.102456+00	.184154+03	.153935-01	.102456+00	.162630+03	.126132-01	7026
73.	.332128+01	.220514+01	.318061+01				7030
74.	.000000	.100000+03	.000000	.228233+00	.367647+03	.518475-02	7031
75.	.228233+00	.334501+03	.797777-02	.228233+00	.314769+03	.911975-02	7032
76.	.228233+00	.291444+03	.108120-01	.228233+00	.268513+03	.126896-01	7033
77.	.228233+00	.246842+03	.146856-01	.228233+00	.223920+03	.170421-01	7034
78.	.228233+00	.201528+03	.194719-01	.228233+00	.183104+03	.197896-01	7035
79.	.114116+00	.175840+03	.158903-01	.114116+00	.152905+03	.126287-01	7036
80.	.382225+01	.246888+01	.212041+01				7040
81.	.000000	.100000+03	.000000	.228233+00	.367647+03	.518475-02	7041
82.	.228233+00	.334501+03	.797777-02	.228233+00	.314769+03	.911975-02	7042
83.	.228233+00	.291444+03	.108120-01	.228233+00	.268513+03	.126896-01	7043
84.	.228233+00	.246842+03	.146856-01	.228233+00	.223920+03	.170421-01	7044
85.	.228233+00	.201528+03	.194719-01	.228233+00	.183104+03	.197896-01	7045
86.	.114116+00	.175840+03	.158903-01	.114116+00	.152905+03	.126287-01	7046

END ELT. TIME: 0.3866 SECONDS.

ƏFIN

4.   Criteria for Specifying the CICM/STC Interface
      Plane Location

          In Section 2.1.2 of CPIA 246 it is recommended that for
CICM/STC analyses the CICM program should be executed to the axial plane at
which the liquid jet has disappeared for all flow zones. At this point CICM
output is transferred into STC input. There are two problems with specifying
the interface plane in this manner.

          (1)   The CICM program contains an advanced droplet heat-
up and vaporization model. The subcritical K-Prime STC version assumes a
constant "wet bulb" propellant temperature. If CICM execution is limited to
the point of liquid jet dissipation a significant percentage of the liquid
droplets will not have yet heated to the "wet bulb" temperature. It is phy-
sically incorrect to ignore this effect and to characterize all the liquid
droplets with a constant temperature and latent heat of vaporization in the
STC input.

          (2)   CICM performance predictions are controlled, in
large part, by two empirically correlated input constants, C_A and B_A. C_A is
an atomization (jet stripping) rate constant and B_A is a drop size constant.
The recommended input values for these coefficients were backed out from CICM
by correlating hot test data. In these instances, CICM was allowed to compute
to the chamber throat plane. Thus, the technique used to derive the constant
input values is inconsistent with the recommended procedure of joining the CICM
and STC analyses at an intermediate chamber axial plane.

          CICM improves the JANNAF methodology for subcritical
propellants because it allows for the droplet temperature transient. However,
it is economically unrealistic to use CICM to the chamber throat plane
because of the high computation time this technique requires. Also, using CICM
to the throat plane would cause the coaxial injector analysis technique to be
inconsistent with the JANNAF conventional liquid/liquid injector methodology,
which utilizes STC. The most physically realistic technique is to have CICM
execute until all the calculated oxidizer drop size groups have been heated
to the chamber "wet bulb" temperature. As previously cited, for oxygen the
unsteady state typically comprises only approximately 10 percent of the total

time required to vaporize 99 percent of the propellant. Thus, STC would still be responsible for calculating the majority of the liquid mass transfer to the gaseous phase. Importantly, the STC assumption of constant liquid drop temperature is verified when CICM calculates the complete unsteady state time period.

5. Specification of Intra-Element and Manifold Zone Mass Distributions

There is one additional technical problem in interfacing the CICM and STC programs. CICM does not contain formulations for calculating intra or inter-element mixing. The subjects were previously discussed in Sections B.6-7 of this appendix. CPIA 246 and the CICM user's manual recommend the following two solutions.

(1) Manifold mass maldistributions should be accounted for by modeling separate chamber flow field zones.

(2) Intra-element mass maldistributions are modeled by using empirical single element cold flow data to input distinct radial mass distribution sub-zones to CICM for each chamber flow field zone designated as described in (1) above.

There are at least the following four limitations to these suggested solution techniques.

(1) The JANNAF programs can not allow for the dissipation, due to diffusion mixing, of the face plane measured manifold distributions.

(2) The JANNAF methodology does not recommend where the single element mass and mixture ratio distribution should be specified. If the distribution is measured at the face plane the solution will be in error because coaxial elements rely on shear (gas/liquid ΔV) mixing to produce nearly uniform mass distribution at the chamber throat plane.

(3) The CICM and DER literature list only one example of application of the recommended coaxial mass distribution specification technique (the J-2S sample case that is included in CPIA 246). The method that was used to specify the given flow distribution is not described. However, it was stated

that the given distribution was known to result in low performance predictions. This would be expected if the given distribution did not account for shear mixing to the chamber throat plane.

(4)   As previously cited in Section B.6 of this appendix, the test cases used to back out the recommended atomization and drop size inputs to DER assumed that the thrust chambers in question had uniform throat plane mixture ratio distributions. For most real coaxial injectors there will be a finite mixing loss because the coaxial element is a relatively slow mixing element. It is apparent that the correct values for the C_A and B_A coefficients will be directly dependent on the assumed single element mixture ratio distribution. Unless a standard method for measuring or calculating single element and chamber mixture ratio distributions is developed it is extremely doubtful that universal values for the C_A and B_A constants can be verified.

APPENDIX C

JANNAF SIMPLIFIED PREDICTION PROCEDURE FOR CICM ANALYSIS

The M-1 sea-level, pressure fed facility for ablative chamber testing is shown in Figure C-1. The corresponding instrumentation code sheet follows Figure 1. Figure C-2 specifies chamber pressure tap axial and circumferential locations.

The M-1 injector design layout is shown in Figure C-3. The injector contained 3248 coaxial elements with gaseous hydrogen being injected annularly around the oxidizer. A row of orifices, drilled through the porous face, was located around the injector periphery and provided the chamber wall film cooling. Approximately 3.7% of the total fuel flow rate was used for chamber wall film cooling. Total fuel element flow rate was 89.8% of the thrust chamber fuel flow rate with a baffle fuel film cooling flow rate of 3.9%. The remaining 2.6% of the fuel flowed through the rigimesh injector face. The element consisted of two basic components which were threaded together. An oxidizer tube was recessed within the fuel sleeve producing a fuel annulus between the two parts. The fuel annulus was fed by four holes having an area four times that of fuel annulus. The oxidizer tube was flared at a fifteen degree included angle and was recessed 0.231 inches from the injector face. Elements were arrayed in 33 concentric rows.

The low area ratio combustion chamber used for testing with the M-1 injector is comprised of an outer steel shell and an inner ablative liner. The assembled combustion chamber (Figure C-4) consists of an upper fuel torous and a lower conical combustion chamber. The thrust chamber design parameters, as related to the ODK input parameters, are identified in Figure C-5.

The test 009 nominal computer input decks for the JANNAF programs utilized during the M-1 analysis are shown in Figures C-6 through C-9.

Fluorine Ignition System

LN$_2$

GF$_2$

GF$_2$ TANK

LF$_2$

TCFV

FBV

GJ$_2$V

GH$_e$ Purge
Start & Shutdown

Feed System
Control Surface

F2   F4   F5

FSV

F8

Thrust Chamber
Control Surface

GH$_2$

FT

H2 Mix

F3

F6   F7

F9

F10

GH$_2$

RESERVOIR
SYSTEM

O9

O10

11

OSV   O3 O4

TCOV   O8

GN$_2$ Purge
Start & Shutdown

GN$_2$

OT

O2

O6   O7

TCOV-BP

OBV   ODV

Oxidizer
Dump System

Overboard
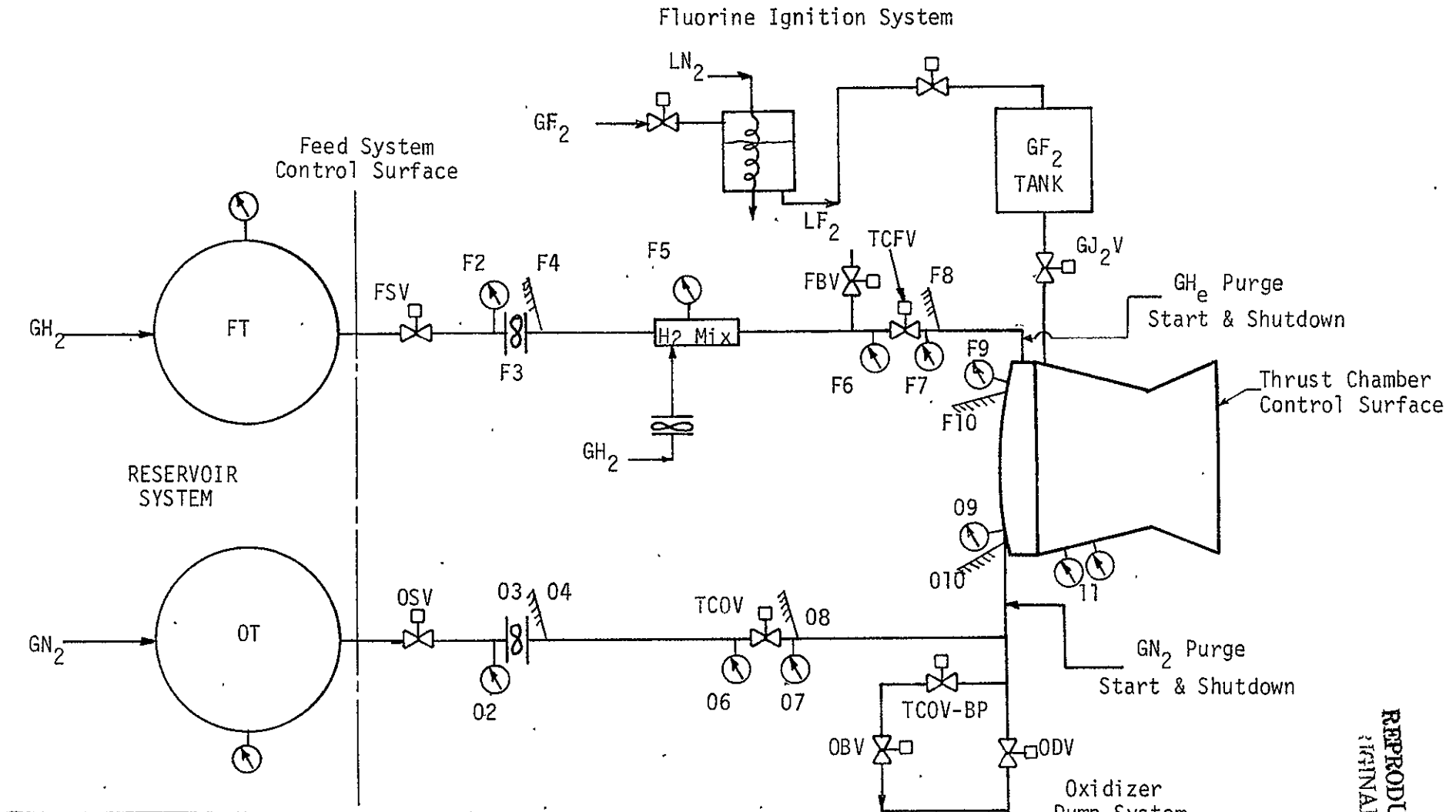
Symbol	Hardware Description
OT	Oxidizer Tank
FT	Fuel Tank
OSV	Oxidizer Safety Valve
FSV	Fuel Safety Valve
OBV	Oxidizer Bypass Valve
FBV	Fuel Bypass Valve
TCOV	Thrust Chamber Oxidizer Valve
TCFV	Thrust Chamber Fuel Valve

Pressure Gage

Flowmeter

Valve

Temperature Gage

C-2

FIGURE C-1. M-1 TEST FACILITY SCHEMATIC

M-1 INSTRUMENTATION TAP LOCATIONS

Measurement	Oxid. Tap Loc.	Fuel Tap Loc.
Tank Pressure (POT, PFT)	01	F1
Flow Meter Pressure (POFM, PFFM)	02	F2
Flow Meter Temperature (TOFM, TFFM)	04	F4
GH$_2$ Mixer Pressure (PFMIX-2)		F5
Thrust Chamber Pressure-1 (POTCV-1, PFTCV-1)	06	F6
Thrust Chamber Pressure-2 (POTCV-2, POTCV-2)	07	F7
Thrust Chamber Temperature (TOTCV-2, TFTCV-2)	08	F8
Thrust Chamber Injector Pressure (POJ, PFJ)	09	F9
Thrust Chamber Injector Temperature (TOJ, TFJ)	010	F10
Thrust Chamber Pressure (Pc4B-1 & 2)	11	11

FIGURE C-1.(cont.)   INSTRUMENTATION CODE

Location	Dist. Face (in.)	D (in.)	Cham. Area (in.^{2})	ε_c
Face	0.00	40.62	1296.	1.833
Pc_5	1.43	40.05	1260.	1.782
Pc_4	11.67	35.96	1016.	1.437
Pc_3	18.64	33.18	864.6	1.223
Pc_2	21.23	32.15	811.6	1.148
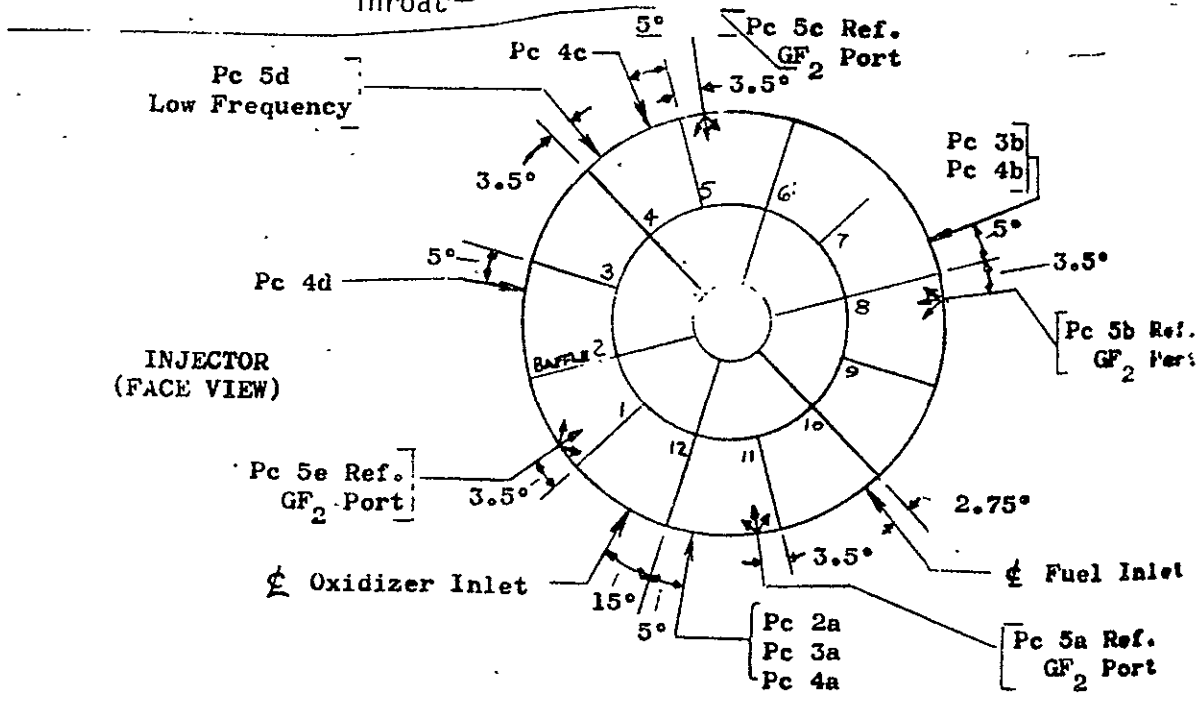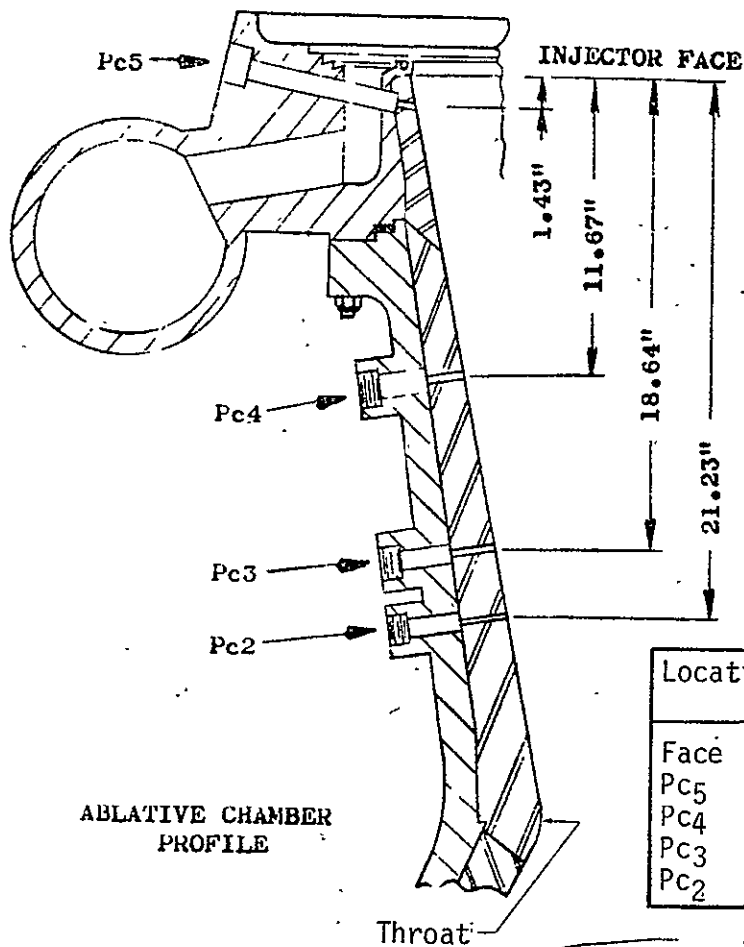
FIGURE C-2. PRESSURE TAP LOCATIONS
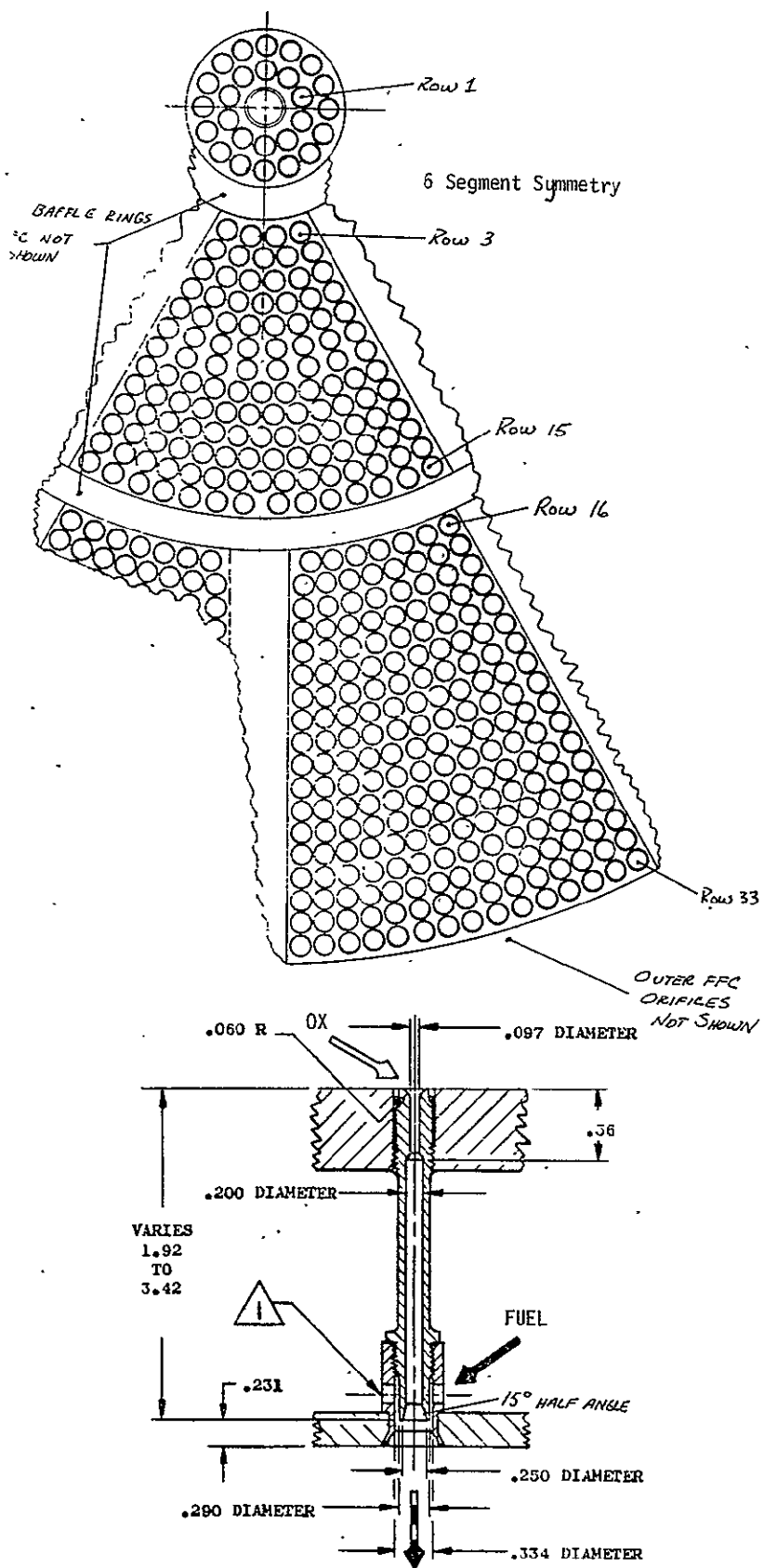
Row No.	Number of Orifices Req'd per Row
1	10
2	16
3	24
4	30
5	36
6	42
7	48
8	48
9	48
10	66
11	72
12	76
13	84
14	90
15	84
16	84
17	96
18	96
19	108
20	108
21	120
22	120
23	132
24	132
25	144
26	144
27	156
28	156
29	168
30	168
31	180
32	180
33	180

FIGURE C-3.   M-1 INJECTOR DESIGN

40.62
Dia.   38.31 Dia.

30.00 Dia.
Throat

43.1 Dia.

Injector
Face

5.79

23.96

URAD=31.98 in.

DRAD=3.2 in.

Chamber Pressure
Ports

FIGURE C-4. M-1 ABLATIVE CHAMBER FUEL TORUS ASSEMBLY

PARAMETER	ODK INPUT NAME	DESIGN VALUE
Chamber Radius, R_c	–	20.31 in.
Throat Radius, R_T	RSTAR	15.0 in.
Contraction Ratio	ECRAT	1.833 -
Inlet Angle, αu	THETAI	11.3°
Cylindrical Length, L_c	–	0.0 in.
Chamber Length, L_T	–	29.75 in.
Normalized Inlet Radius RWTU/R_T	RWTU	2.132
Normalized Outlet Radius RWTD/R_T	RWTD	.213
Expansion Angle, αD	THETA	29.9°
Exit Angle, αE	THE	29.9°
Exit Radius	–	21.55
Expansion Ratio	EPS	2.06:1

Figure C-5   M-1 Thrust Chamber Design Parameters

```
625,              18                                                              5
626.      .0           97.       2.016      1.4        .215E-05                  10
627.      .5          973.       3.024      1.389     1.039E-05                  20
628.     1.          1835.       4.032      1.356     1.819E-05                  30
629.     1.5         2611.       5.040      1.314     2.558E-05                  40
630.     2.4         3805.       6.853      1.261     3.809E-05                  50
631.     2.8         4260.       7.653      1.239     4.337E-05                  60
632.     3.2         4667.       8.444      1.219     4.830E-05                  70
633.     3.6         5021.       9.219      1.199     5.284E-05                  80
634.     4.0         5326.       9.973      1.183     5.692E-05                  90
635.     4.4         5579.      10.702      1.169     6.052E-05                 100
636.     4.8         5788.      11.404      1.157     6.366E-05                 110
637.     5.2         5957.      12.078      1.148     6.635E-05                 120
638.     5.6         6089.      12.721      1.142     6.858E-05                 130
639.     6.0         6190.      13.333      1.136     7.040E-05                 140
640.     7.0         6323.      14.726      1.130     7.337E-05                 150
641.     8.0         6344.      15.937      1.128     7.464E-05                 160
642.    10.0         6233.      17.930      1.129     7.462E-05                 170
643.    12.0         6053.      19.514      1.132     7.327E-05                 180
644.           1           1          0          10         3                   10
645.    23.874         .0      97.        2.016      1.4        4.05            30
646.      .05        120.        .08      4.05                                  40
647.   1295.9        29.75       1.833     11.29        .0         31.98        50
648.       INJECTION PROCESSES PROGRAM TASK IIB M=1 TEST DATA CORRELATION      110
649.       TEST 009 XMINDE=4.05
650.            0         3248          0          2          0                 120
651.            1            0          3          1                            130
652.     .087616        .231      .57265    -22.5        .0         .0          140
653.     .071221         .0      .021564     .0        97.         .0           160
654.     .428879     169.      -.049087 6000.         3.0553      .037854       170
655.       .0           .0      97.        2.016      1.4        4.05           180
656.   556.6         26.09      0.5        0.031      0.010      1.             190
657.     .2207          .0      600.                                           191
658.            1           11                                                  300
659.     1.           1.                                                        320
660.       .1           .1         .1          .1         .1          .1        330
661.       .1           .1         .1          .05        .05                   331
```

                                                                    12

                                                                    12

                                                                    12
                                                                    12
                                                                    12
                                                                    12

NOTE: FIRST 624 CARDS IDENTICAL TO
        SAMPLE CASE IN REF. 6

FIGURE C-6.   CICM INPUT DECK

```
  1.      .  STC INPUT FROM CICM PROGRAM CASE                                              10
  2.         TRAJECTION PROCESSES PROGRAM TASK IIB M-1 DATA ANALYSIS                       20
  3.         TEST 009 CONTRACT NAS 3-11214 NASA CR 72512                                   30
  4.         LAST SUM PERIOD    O/F=5.46  PC(FACE EST)=557 PSIA  1 ZONE ANALYSIS           40
  5.           0          1          0          0                                          50
  6.           0          0          0          0                                        5010
  7.        257          6         18         20                                         5020
  8.     .0       40.62      7.       37.825     15.       34.631                         5030
  9.   20.       32.634     25.469     31.238     29.75     30.612                        5040
 10.         O2/H2 GAS PROPERTIES FROM CICM INPUT                                        5100
 11.   .000000    .500000+00  .100000+01  .150000+01  .240000+01  .280000+01             5110
 12.   .320000+01  .360000+01  .400000+01  .440000+01  .480000+01  .520000+01            5120
 13.   .560000+01  .600000+01  .700000+01  .800000+01  .100000+02  .120000+02            5130
 14.   .970000+02  .973000+03  .183500+04  .261100+04  .380500+04  .426000+04            5210
 15.   .466700+04  .502100+04  .532600+04  .557900+04  .578800+04  .595700+04            5220
 16.   .608900+04  .619000+04  .632300+04  .634400+04  .623300+04  .605300+04            5230
 17.   .215000-05  .103900-04  .181900-04  .255800-04  .380900-04  .433700-04            5310
 18.   .483000-04  .528400-04  .569200-04  .605200-04  .636600-04  .663500-04            5320
 19.   .685000-04  .704000-04  .733700-04  .746400-04  .746200-04  .732700-04            5330
 20.   .140000+01  .158900+01  .135600+01  .131400+01  .126100+01  .123900+01            5410
 21.   .121900+01  .119900+01  .118300+01  .116900+01  .115700+01  .114800+01            5420
 22.   .114200+01  .113600+01  .113000+01  .112800+01  .112900+01  .113200+01            5430
 23.   .201600+01  .302400+01  .403200+01  .504000+01  .685300+01  .765300+01            5510
 24.   .844400+01  .921900+01  .997300+01  .107020+02  .114040+02  .120780+02            5520
 25.   .127210+02  .153330+02  .147260+02  .159370+02  .179300+02  .195140+02            5530
 26.   .225300+04  .585600+04  .701600+04  .756300+04  .794500+04  .800200+04            5610
 27.   .802000+04  .800900+04  .797200+04  .791400+04  .784000+04  .775400+04            5620
 28.   .765900+04  .755600+04  .728600+04  .702000+04  .655600+04  .618700+04            5630
 29.   .000000    .000000    .000000    .000000    .000000    .000000                    5710
 30.   .000000    .000000    .000000    .000000    .000000    .000000                    5720
 31.   .000000    .000000    .000000    .000000    .000000    .000000                    5730
 32.   .000000    .000000    .000000    .000000    .000000    .000000                    5740
 33.   .000000    .000000    .000000    .000000    .000000    .000000                    5810
 34.   .000000    .000000    .000000    .000000    .000000    .000000                    5820
 35.   .000000    .000000    .000000    .000000    .000000    .000000                    5830
 36.   .000000    .000000    .000000    .000000    .000000    .000000                    5840
 37.   .000000    .000000    .000000    .000000    .000000    .000000                    5910
 38.   .000000    .000000    .000000    .000000    .000000    .000000                    5920
 39.   .000000    .000000    .000000    .000000    .000000    .000000                    5930
 40.   .000000    .000000    .000000    .000000    .000000    .000000                    5940
 41.   .200000+03  .205000+03  .275000+03  .285000+03  .300000+03  .340000+03            6010
 42.   .400000+03  .600000+03  .120000+04  .180000+04  .240000+04  .300000+04            6020
 43.   .340100+04  .380000+04  .420000+04  .460000+04  .500000+04  .560000+04            6030
 44.   .600100+04  .640000+04  .000000    .000000    .000000    .000000                  6040
 45.   .940000+00  .940000+00  .550000+00  .430000+00  .356000+00  .286000+00            6110
 46.   .257000+00  .226000+00  .245000+00  .260000+00  .269000+00  .276000+00            6120
 47.   .280000+00  .264000+00  .288000+00  .292000+00  .295500+00  .301000+00            6130
 48.   .304000+00  .307000+00  .000000    .000000    .000000    .000000                  6140
 49.   .917000-05  .917000-05  .108000-04  .110500-04  .113000-04  .116700-04            6210
 50.   .158000-04  .161000-04  .277600-04  .350000-04  .402800-04  .444400-04            6220
 51.   .458300-04  .458100-04  .472200-04  .463900-04  .450000-04  .380600-04            6230
 52.   .191700-04  .000000    .000000    .000000    .000000    .000000                  6240
 53.   .000000    .000000    .000000    .000000    .201600+01  .201600+01               6510
 54.   .102000+03  .203000+03  .413000-01  .266000-01  .320000+02  .320000+02            6520
```
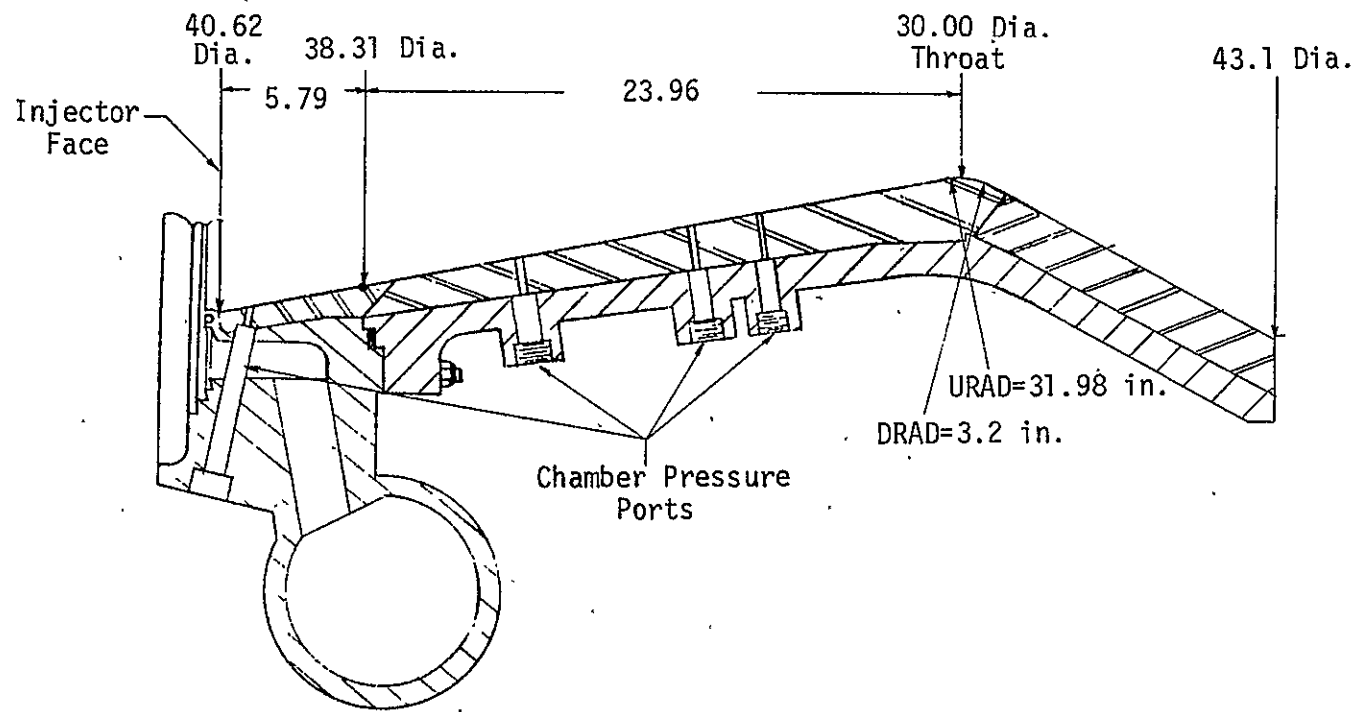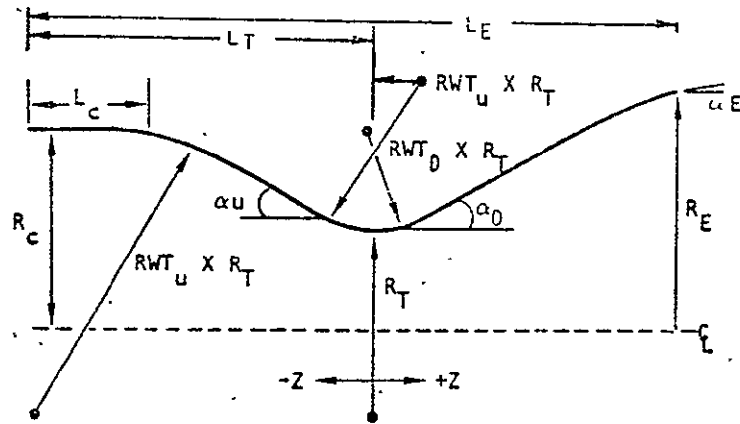
55.	.590000+02	.278600+03	.000000	.470000+02			6530
56.	1	3		0	1	25	25	6540
57.	.100000-01	.100000-01					6550
58.	.535331+03	.410000+01					6710
59.	12	1	1	1			6720
60.	.119349+04	.855539+03	.234864+01				7010
61.	.000000	.100000+03	.000000	.792941+02	.503127+03	.821732-02	7011
62.	.792941+02	.474381+03	.103349-01	.792941+02	.444035+03	.133125-01	7012
63.	.792941+02	.415481+03	.167956-01	.792941+02	.387979+03	.206571-01	7013
64.	.792941+02	.362692+03	.243797-01	.792941+02	.361542+03	.228146-01	7014
65.	.792941+02	.369399+03	.190233-01	.792941+02	.370694+03	.154398-01	7015
66.	.396470+02	.357409+03	.131637-01	.396470+02	.318678+03	.113274-01	7016

FIGURE C-7. STC INPUT DECK
(Sheet 2 of 2)

```
aXQT TDK
THERMO
    300.000  1000.000  5000.000
AR                    L 5/66AR  100  000  000   0G   300.000  5000.000        1
  0.25000000E 01 0.            0.            0.            0.                  2
 -0.74537502E 03 0.43660006E 01 0.25000000E 01 0.        0.                  3
  0.           0.            -0.74537498F 03 0.43660006E 01                  4
H                     J 9/65H   100  000  000   0G   300.000  5000.000        1
  0.25000000E 01 0.            0.            0.            0.                  2
  0.25471627E 05-0.46011763F 00 0.25000000F 01 0.        0.                  3
  0.           0.             0.25471627F 05-0.46011762E 00                  4
H2                    J 3/61H   20   00   00    0G  .300.000  5000.000        1
  0.31001901E 01 0.51119464E-03 0.52644210E-07-0.34909973E-10 0.36945345E-14 2
 -0.87738042E 03-0.19629421E 01 0.30574451F 01 0.26765200E-02-0.58099162E-05 3
  0.55210391E-08-0.18122739E-11-0.98890474E 03-0.22997056E 01               4
H20                   J 3/61H   20   100  000   0G   300.000  5000.000        1
 .0.27167633E 01 0.29451374E-02-0.80224374E-06 0.10226682E-09-0.48472145E-14 2
 -.29905826E 05 0.66305671E 01 0.40701275E 01-0.11084499E-02 0.41521180E-05 3
 -.29637404E-08 0.80702103E-12-0.30279722F 05-0.32270046E 00               4
N2                    J 9/65N   20   00   00    0G   300.000  5000.000        1
  0.28963194E 01 0.15154866E-02-0.57235277E-06 0.99807393E-10-0.65223555E-14 2
 -0.90586184E 03 0.61615148E 01 0.36748261F 01-0.12081500E-02 0.23240102E-05 3
 -0.63217559E-09-0.22577253E-12-0.10611588E 04 0.23580424E 01               4
0                     J 6/620   100  000  000   0G   300.000  5000.000        1
  0.25420596E 01-0.27550619E-04-0.31028033E-08 0.45510674E-11-0.43680515E-15 2
  0.29230803E 05 0.49203080E 01 0.29464287E 01-0.16381665E-02 0.24210316E-05 3
 -0.16028432E-08 0.38906964E-12 0.29147644F 05 0.29639949E 01               4
OH                    J12/700   1H   10   00    0G   300.000  5000.000        1
  0.29131230E+01 0.95418248E-03-0.19084325E-06 0.12730795E-10 0.24803941E-15 2
  0.39647060E+04 0.54288735E+01 0.38365518E+01-0.10702014E-02 0.94849757E-06 3
  0.20843575E-09-0.23384265E-12 0.36715807F+04 0.49805456E+00               4
02                    J 9/650   20   00   00    0G   300.000  5000.000        1
  0.36219535E 01 0.73618264E-03-0.19652228E-06 0.36201558E-10-0.28945627E-14 2
 -0.12019825E 04 0.36150960E 01 0.36255985F 01-0.18782184E-02 0.70554544E-05 3
 -0.67635137E-08 0.21555993E-11-0.10475226F 04 0.43052778E 01               4
END
TITLE H-1 ODK DATA TEST 009 INLET CONDS.  PC=517
PROBLEM ODE-ODK-TDK,NZONES=1,
REACTANTS
0 2.                                  99.519   -3027.  L 90.18  U
AR 1.                                  0.437   -2571.  L 90.18  O
N 2.                                   0.044   -2699.  L 90.18  U
H 2.                                 100.      -1837.  L 20.25  F

NAMELISTS
$ODE
RKT=.TRUE., PSIA=.TRUE.,
OF=.TRUE.,
P=517.,                            NOMINAL TEST  009 0/F
OFSKED(1)=5.46,
SUPAR(1)=2.064,
SUBAR(1)=1.833, ECRAT=1.833,
EQL=.TRUE., FROZ=.FALSE.,
PCP(1)=1.01,1.05,1.1,1.2,1.6,2.,5.,10.,20.,
IPTAB=1, IOFF=0, IPTBL=0,
$END
REACTIONS
H + H  = H2                ,A=6.4E17, N=1.0, B=0.0,
0 + 0  =02                 ,A=1.3E17, N=1.0, B=0.34,
H + OH = H2U               ,A=8.4E21, N=2.0, B=0.0,
```

FIGURE C-8.   TDK INPUT DECK (Sheet 1 of 2)

```
END TBR REAX
H2 + O  = H    + OH        ,A=1.8E10, N=-1.0, B=8.90,
O2 + H  = OH   + O         ,A=2.2E14, N=0.0, B=16.8,
H2 + OH = H2O  + H         ,A=2.20E13, N=0.0, B=5.15,
OH + OH = H2O  + O         ,A=6.30E12, N=0.0, B=1.0,
LAST REAX
INERTS N2,AR,END
THIRD BODY REAX RATE RATIOS
SPECIES AR,  1.0,1.0,1.0,
SPECIES H,   25.0,12.5,12.5,
SPECIES H2,  4.0,5.0,5.0,
SPECIES H2O, 20.0,5.0,17.0,
SPECIES N2,  1.5,4.0,3.0,
SPECIES OH,  25.0,12.5,12.5,
SPECIES O,   25.0,12.5,12.5,
SPECIES O2,  1.5,11.0,5.0,
LAST CARD
 $ODK
 RSTAR=15., RWTU=2.132, RWTD=.213, THETAI=11.29, RI=0.0,
 IWALL=1, THETA=29.9,
 EPS=2.064,
 $END
 $TRANS
 XM(1)=1.,
 $END
 $TDK
 $END
```

FIGURE C-8.   TDK INPUT DECK (Sheet 2 of 2)

```
ƏXQT BLIMP
30200623210212     M-1 ANALYSIS TEST 009 CONDS.
 $MISLIS
 NSP=2,  KS=19*1,
 NS=19, KR9=19*2,
 S(1)=.024,
 NETA=12, ETA=0.,.001,.006,.01,.025,.06,.15,.40,.70,1.,1.5,2.5,
 KAPPA=10, CBAR=0.95, KUNRFT=1, NPOINT=3, RATLIM=0.5,
 F2FIX=.0,.05,.12,.25,.35,.45,.60,.75,.85,.95,.98,1.,,
 GW=-671.,,
 RTM=1.25, PTET(1)=35.17, GE(1)=-590.1,,
 ELCON=0.4, YAP=-11.8, CLNUM=0.0168, SCT=0.9, PRT=-0.44,
 $END
 $INPUT
 N=81, NTH=27, IP=1,
 NP=2,4,6,10,16,19,22,24,25,26,27,36,44,51,53,54,55,57,60,64,68,72,
 77,81,
 XITAB(  1)=  -.19834+01, YITAB(  1)=  .13539+01, PITAB(  1)=  .93380+00,
 XITAB(  2)=  -.19199+01, YITAB(  2)=  .13412+01, PITAB(  2)=  .93087+00,
 XITAB(  3)=  -.18419+01, YITAB(  3)=  .13256+01, PITAH(  3)=  .92708+00,
 XITAB(  4)=  -.17658+01, YITAB(  4)=  .13101+01, PITAB(  4)=  .92301+00,
 XITAB(  5)=  -.16858+01, YITAB(  5)=  .12945+01, PITAB(  5)=  .91863+00,
 XITAB(  6)=  -.16077+01, YITAB(  6)=  .12789+01, PITAB(  6)=  .91390+00,
 XITAB(  7)=  -.15296+01, YITAB(  7)=  .12633+01, PITAB(  7)=  .90878+00,
 XITAB(  8)=  -.14516+01, YITAB(  8)=  .12477+01, PITAB(  8)=  .90324+00,
 XITAB(  9)=  -.13735+01, YITAB(  9)=  .12321+01, PITAB(  9)=  .89720+00,
 XITAB( 10)=  -.12955+01, YITAB( 10)=  .12166+01, PITAB( 10)=  .89063+00,
 XITAB( 11)=  -.12174+01, YITAB( 11)=  .12010+01, PITAB( 11)=  .88343+00,
 XITAB( 12)=  -.11393+01, YITAB( 12)=  .11854+01, PITAB( 12)=  .87554+00,
 XITAB( 13)=  -.10613+01, YITAB( 13)=  .11698+01, PITAB( 13)=  .86682+00,
 XITAB( 14)=  -.98322+00, YITAB( 14)=  .11542+01, PITAB( 14)=  .85717+00,
 XITAB( 15)=  -.90516+00, YITAB( 15)=  .11386+01, PITAB( 15)=  .84640+00,
 XITAB( 16)=  -.82710+00, YITAB( 16)=  .11231+01, PITAB( 16)=  .83430+00,
 XITAB( 17)=  -.74904+00, YITAB( 17)=  .11075+01, PITAB( 17)=  .82058+00,
 XITAB( 18)=  -.67098+00, YITAB( 18)=  .10919+01, PITAB( 18)=  .80484+00,
 XITAB( 19)=  -.59292+00, YITAB( 19)=  .10763+01, PITAB( 19)=  .78648+00,
 XITAB( 20)=  -.51486+00, YITAB( 20)=  .10607+01, PITAB( 20)=  .76454+00,
 XITAB( 21)=  -.43680+00, YITAB( 21)=  .10451+01, PITAB( 21)=  .73750+00,
 XITAB( 22)=  -.35874+00, YITAB( 22)=  .10304+01, PITAB( 22)=  .70738+00,
 XITAB( 23)=  -.28069+00, YITAB( 23)=  .10186+01, PITAB( 23)=  .67577+00,
 XITAB( 24)=  -.20263+00, YITAB( 24)=  .10097+01, PITAB( 24)=  .64290+00,
 XITAB( 25)=  -.12457+00, YITAB( 25)=  .10036+01, PITAB( 25)=  .60901+00,
 XITAB( 26)=  -.48107-01, YITAB( 26)=  .10005+01, PITAB( 26)=  .57511+00,
 XITAB( 27)=   .00000   , YITAB( 27)=  .10000+01, PITAB( 27)=  .50727+00,
 XITAB( 28)=   .30352-02, YITAB( 28)=  .10000+01, PITAB( 28)=  .48682+00,
 XITAB( 29)=   .62627-02, YITAB( 29)=  .10001+01, PITAB( 29)=  .46829+00,
 XITAB( 30)=   .96349-02, YITAB( 30)=  .10002+01, PITAB( 30)=  .45036+00,
 XITAB( 31)=   .13135-01, YITAB( 31)=  .10004+01, PITAB( 31)=  .43302+00,
 XITAB( 32)=   .16743-01, YITAB( 32)=  .10007+01, PITAB( 32)=  .41599+00,
 XITAB( 33)=   .20449-01, YITAB( 33)=  .10010+01, PITAB( 33)=  .39940+00,
 XITAB( 34)=   .24248-01, YITAB( 34)=  .10014+01, PITAB( 34)=  .38318+00,
 XITAB( 35)=   .28134-01, YITAB( 35)=  .10019+01, PITAB( 35)=  .36729+00,
 XITAB( 36)=   .32102-01, YITAB( 36)=  .10024+01, PITAB( 36)=  .35171+00,
 XITAB( 37)=   .36151-01, YITAB( 37)=  .10031+01, PITAB( 37)=  .33642+00,
 XITAB( 38)=   .40276-01, YITAB( 38)=  .10038+01, PITAB( 38)=  .32141+00,
 XITAB( 39)=   .44476-01, YITAB( 39)=  .10047+01, PITAB( 39)=  .30668+00,
 XITAB( 40)=   .48750-01, YITAB( 40)=  .10057+01, PITAB( 40)=  .29222+00,
 XITAB( 41)=   .53096-01, YITAB( 41)=  .10067+01, PITAB( 41)=  .27803+00,
 XITAB( 42)=   .57513-01, YITAB( 42)=  .10079+01, PITAB( 42)=  .26411+00,
 XITAB( 43)=   .62000-01, YITAB( 43)=  .10092+01, PITAB( 43)=  .25046+00,
```

STAGNATION ENTHALPY OF
O/F = 2.5 EDGE GAS

TDK 1 ZONE RESULTS
FOR CORE O/F OF 5.46:1

FIGURE C-9.   BLIMP INPUT DECK (Sheet 1 of 3)

C-13

C-14

```
XITAB( 44)=    .66557-01,  YITAB( 44)=    .10107+01,  PITAB( 44)=    .23709+00,
XITAB( 45)=    .71186-01,  YITAB( 45)=    .10122+01,  PITAB( 45)=    .22398+00,
XITAB( 46)=    .75884-01,  YITAB( 46)=    .10140+01,  PITAB( 46)=    .21115+00,
XITAB( 47)=    .80654-01,  YITAB( 47)=    .10159+01,  PITAB( 47)=    .19859+00,
XITAB( 48)=    .85493-01,  YITAB( 48)=    .10179+01,  PITAB( 48)=    .18632+00,
XITAB( 49)=    .90404-01,  YITAB( 49)=    .10201+01,  PITAB( 49)=    .17434+00,
XITAB( 50)=    .95387-01,  YITAB( 50)=    .10226+01,  PITAB( 50)=    .16265+00,
XITAB( 51)=    .10044+00,  YITAB( 51)=    .10252+01,  PITAB( 51)=    .15126+00,
XITAB( 52)=    .10557+00,  YITAB( 52)=    .10280+01,  PITAB( 52)=    .14018+00,
XITAB( 53)=    .11082+00,  YITAB( 53)=    .10310+01,  PITAB( 53)=    .13871+00,
XITAB( 54)=    .13157+00,  YITAB( 54)=    .10430+01,  PITAB( 54)=    .13729+00,
XITAB( 55)=    .15227+00,  YITAB( 55)=    .10549+01,  PITAB( 55)=    .13590+00,
XITAB( 56)=    .17303+00,  YITAB( 56)=    .10668+01,  PITAB( 56)=    .13445+00,
XITAB( 57)=    .19388+00,  YITAB( 57)=    .10788+01,  PITAB( 57)=    .13298+00,
XITAB( 58)=    .21485+00,  YITAB( 58)=    .10908+01,  PITAB( 58)=    .13148+00,
XITAB( 59)=    .23707+00,  YITAB( 59)=    .11036+01,  PITAB( 59)=    .12979+00,
XITAB( 60)=    .25414+00,  YITAB( 60)=    .11134+01,  PITAB( 60)=    .12822+00,
XITAB( 61)=    .27919+00,  YITAB( 61)=    .11278+01,  PITAB( 61)=    .12564+00,
XITAB( 62)=    .29605+00,  YITAB( 62)=    .11375+01,  PITAB( 62)=    .12367+00,
XITAB( 63)=    .31709+00,  YITAB( 63)=    .11496+01,  PITAB( 63)=    .12081+00,
XITAB( 64)=    .34457+00,  YITAB( 64)=    .11654+01,  PITAB( 64)=    .11584+00,
XITAB( 65)=    .37366+00,  YITAB( 65)=    .11822+01,  PITAB( 65)=    .11303+00,
XITAB( 66)=    .40203+00,  YITAB( 66)=    .11985+01,  PITAB( 66)=    .10991+00,
XITAB( 67)=    .42870+00,  YITAB( 67)=    .12138+01,  PITAB( 67)=    .10859+00,
XITAB( 68)=    .45532+00,  YITAB( 68)=    .12291+01,  PITAB( 68)=    .10739+00,
XITAB( 69)=    .48257+00,  YITAB( 69)=    .12447+01,  PITAB( 69)=    .10599+00,
XITAB( 70)=    .50989+00,  YITAB( 70)=    .12605+01,  PITAB( 70)=    .10441+00,
XITAB( 71)=    .53772+00,  YITAB( 71)=    .12765+01,  PITAB( 71)=    .10279+00,
XITAB( 72)=    .56591+00,  YITAB( 72)=    .12927+01,  PITAB( 72)=    .10111+00,
XITAB( 73)=    .59442+00,  YITAB( 73)=    .13091+01,  PITAB( 73)=    .99413-01,
XITAB( 74)=    .62332+00,  YITAB( 74)=    .13257+01,  PITAB( 74)=    .97680-01,
XITAB( 75)=    .65256+00,  YITAB( 75)=    .13425+01,  PITAB( 75)=    .95938-01,
XITAB( 76)=    .68218+00,  YITAB( 76)=    .13596+01,  PITAB( 76)=    .94186-01,
XITAB( 77)=    .71220+00,  YITAB( 77)=    .13768+01,  PITAB( 77)=    .92420-01,
XITAB( 78)=    .74265+00,  YITAB( 78)=    .13943+01,  PITAB( 78)=    .90639-01,
XITAB( 79)=    .77346+00,  YITAB( 79)=    .14121+01,  PITAB( 79)=    .88872-01,
XITAB( 80)=    .80478+00,  YITAB( 80)=    .14301+01,  PITAB( 80)=    .87083-01,
XITAB( 81)=    .81272+00,  YITAB( 81)=    .14346+01,  PITAB( 81)=    .86650-01,
$END
   3
H HYDROGEN      1.008       200.                265.                        11100   S
C  CARBON      12.01                             127.                       11201   S
O  OXYGEN      16.0          31.                  44.                       11202   S
      300.     1000.        5000.                                           11203   S
WALL GAS DUM       MAY 76H 2650   44C 127       S    300.       100.             1
                                                                                2
              -1000.                                                            3
                                                                                4
EDGE GAS DUM       MAY 76H 2000  31              S    300.       100.            1
                                                                                2
              -1000.                         -1000.                             3
                                                                                4
                                             -1000.
$ADD,P THERMO/DATA
                                                                    13 LAST
$STALIS
TW=5*2560.,2770.,3420.,3640.,11*3430.,
FLUXJ(2,1,1)=.00232,2*0.0,.00232,2*0.0,.00232,2*0.0,.00232,2*0.0,
```

O/F = 2.5
EDGE GAS

CHEMICAL FORMULA
FOR ABLATIVE WALL PYROLYSIS GAS

FIGURE C-9. BLIMP INPUT DECK (Sheet 2 of 3)

```
.00232,2*0.0,.00271,2*0.0,.00657,2*0.0,.01121,2*0.0
.02127,2*0.0,.02127,2*0.0,.02127,2*0.0,.02127,2*0.0,.02127,2*0.0
.02127,2*0.0,.02127,2*0.0,.02127,2*0.0,.02127,2*0.0,.02127,2*0.0
.02127,2*0.0,
SEND
```

LAST   S

FIGURE C-9. BLIMP INPUT DECK (Sheet 3 of 3)

APPENDIX D

STATIC PRESSURE PROFILE
DATA REDUCTION (REF. 15 PAPER)

An Experimental-Analytical Method to Study Steady Spray Combustion

FREDIANO V. BRACCO*

Guggenheim Laboratories, Princeton University, Princeton, N. J.

Theme

AN experimental-analytical method is presented by which the local combustion gas parameters and flux of liquid fuel drops resulting from the steady burning of a fuel spray in a gaseous oxidizer can be determined. The method does not require any knowledge of the droplet distribution function, drag and vaporization equations. Instead, it requires local static pressure measurements. Results from the application of this method to a liquid oxygen-ethanol rocket combustor are given. They relate mostly to the axial uniformity of the vaporization rate and of the combustion gas variables.

Content

This method is essentially a technique to obtain maximum information out of a set of static pressure measurements based on substituting the measured static pressure values into the conservation equations and in solving them for other unknown quantities. For clarity, the technique is here illustrated using a simplified set of equations which require more assumptions than are necessary. The necessary assumptions are listed after the technique has been introduced. Details about the technique and its extensive application to various configurations of a liquid oxygen-ethanol rocket motor can be found in the thesis referred to in the footnote.

Consider a constant cross-sectional area combustor in which a liquid fuel and a liquid oxidizer are injected. Assume that the oxidizer vaporizes much faster than the fuel and consider that part of the combustor where only gaseous oxidizer, combustion products, and liquid fuel drops exist. Further assume that the combustion is steady, that at the station of interest the flow is one dimensional (uniform through the cross section) and that there is no recirculation. Neglect heat transfer and viscosity effects. Temporarily assume also that all fuel drops have initially the same velocity and radius and that there are no collisions, breakups, or nucleations. The following equations, relating properties at the injector end to properties at any downstream station, can then be written

$$\rho u = -(W_F - W_{0_t}) + W_{0_\phi} \tag{1}$$

$$\rho u^2 = p_0 - p - (W_t u_F - W_{0_t} u_{xF}) + W_{0_t} u_{x\phi} \tag{2}$$

$$\rho u[h + (u^2/2)] = -[W_t(\Lambda_t + u^2_t/2 + h^0_t) - W_{0F}$$
$$(\Lambda_{0F} + u^2_{0t}/2 + h^0_t) - W_{0\phi}(\Lambda_{0\phi} + u^2_{0\phi}/2 + h_{0\phi})] \tag{3}$$

$$T = T(p, \rho, X_i) \tag{4}$$

$$h = h(p, \rho, X_i) \tag{5}$$

$$F_i(p, T, X_{1, 2, ..., I}, W_{0F}, W_{0_\phi}, W_F) = 0 \qquad i = 1, 2 ... I$$

$$W_F/r^3 = W_{0_t}/r_0^3 \tag{6}$$

$$u_t(du_F/dx) = \tfrac{3}{8} C_D \rho |u - u_F|(u - u_F)/r\rho_L \tag{7}$$

$$u_t(dr/dx) = -k[s + g R_e^q]/8r \tag{8}$$

Where ρ, u, p, T, h are the combustion gas density, velocity, pressure, temperature, and latent enthalpy respectively (p_0 is the value of p at the injector end). W_t (W_ϕ) is the local liquid fuel (oxidizer) flux and W_{0F} (W_{0_ϕ}) is its value at $x = 0$ (injector end). u_t (u_ϕ) is the liquid fuel (oxidizer) drop velocity, u_{0t}($u_{0\phi}$) is the injection velocity and u_{xt}($u_{x\phi}$) is its component in the x direction. $\Lambda_t(\Lambda_\phi)$ and h^0_t(h_ϕ^0) are the vaporization energy and the enthalpy of formation respectively. X_i are the number of moles of product i per mole of burned fuel. r is the local drop radius. ρ_L is the specific gravity of the liquid fuel. C_D and R_e are the drag coefficient and the Reynolds number respectively and k, s, g, q are properly selected constants. Equations (1–3) express mass, momentum, and energy conservation, respectively. Equation (4) is the thermal equation of state of the combustion products, and Eq. (5) is the caloric equation of state. F_i stands for a set of I equations which are necessary to relate the amount of vaporized propellants to the variables of the gas (they are as many as the chemical species of which the gas is assumed to be made up.) Equation (6) states the conservation of the drop number. Equations (7) and (8) are possible forms of the drag and vaporization equations for individual drops. If the conditions at the injector end and basic thermodynamic data are known, these $8 + I$ equations contain the following $8 + I$ unknowns: ρ, u, p, T, h, W_F, u_F, r, $X_{1, 2... t}$.

It is then observed that the first $5 + I$ equations could be solved if any two of the $7 + I$ unknowns appearing in them were given, in which case the last three equations could be dropped. Notice that the knowledge of two parameters allows the elimination of three equations since Eq. (6) contains the drop radius which appears in the last two equations but not in the first $5 + I$.

Actually, the measurement of just one parameter is sufficient to obtain useful solutions of the first $5 + I$ equations. Indeed the terms containing the liquid drop velocity (u_t) in Eqs. (2) and (3) are small so that the solution of the system is not very sensitive to its value. Accordingly, the ratio $0 < u_t/u \le 1$ was selected as one of the two parameters.

The selection of the parameter which is to be measured is dictated by the criterion that it must be easy to measure and the solution of the first $5 + I$ equations must be sensitive to its value. The static pressure (actually the loss of static pressure between the injector and any axial location), which meets those requirements, can be selected.

In conclusion, the first $5 + I$ equations can be solved, at various axial locations, for selected values of u_t/u and using static pressure measurements. All the gas variables and the liquid fuel flux are thus determined without any assumption about the droplet drag, and vaporization processes.

Typical results are presented in Figs. 1 and 2. They were obtained with an oxygen-ethanol rocket motor of constant cross sectional area (7.62 cm ID). The injector was made up of 16 impinging like-on-like doublets with a distance between injector units of 1.5 cm. Chamber pressure, nozzle entrance Mach number and injection mixture ratio (O/F) were 20 atm, 0.15 and 2.33, respectively. The static pressure difference between the injector and various downstream stations was measured accurately and repeatedly by water manometers and is given in Fig. 1 (this technique is feasible only for low chamber pressures and/or small nozzle entrance Mach numbers). The first $5 + I$ equations were then solved for p, u, T, h, W_t and the local concentrations of O, H, O_2, H_2, OH, CO, H_2O.

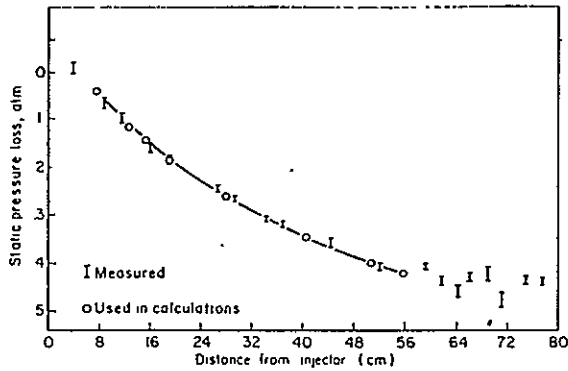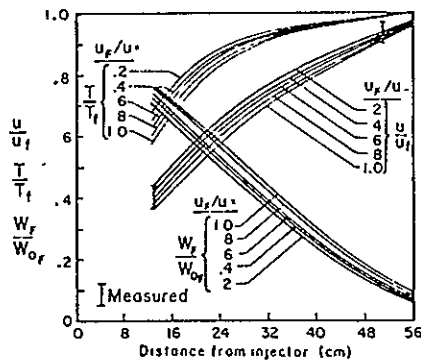Fig. 1. Measured loss of static pressure vs distance from the inector.

Fig. 2. Calculated dimensionless gas velocity, gas temperature, and liquid fuel flux vs distance from the injector.

and CO_2 ($I = 8$). The calculated local gas velocity, gas temperature, and flux of liquid fuel are given in Fig. 2 where u_f and T_f are the complete combustion values and W_o^f is the injection value. The validity of the approach and of the assumptions embodied in the first $5 + I$ equations were further checked by measuring the gas velocity (by streak photography) at two stations (vertical bars in Fig. 2). Of particular interest is the calculated dimensionless liquid fuel flux; a parameter which is important for both efficient and stable rocket chamber design.

A re-examination of the assumptions actually needed for the application of this method, leads to the conclusion that only two assumptions influence the results markedly. The first assumption is that of no recirculation at the station of interest (not everywhere between the injector and the station of interest). Near the injector, within distances of the order of the distance between injector units or of the jet break-up length, which ever is longer, recirculation can be expected to be active and the first 5 equations do not apply. Indeed in Fig. 2 no results are given for $x < 13$ cm. The second assumption is that which must be made to write out explicitly the F_i equations. In this study, instantaneous mixing and reaction of the vaporized fuel to equilibrium reaction products was assumed. Notice that the assumption that all fuel drops have initially the same velocity and radius and that there are no collisions, break-ups, or nucleations are not necessary as it is indicated by the relative insensitivity of the solution to the value of the parameter u_r/u.

The objective of this Synoptic has been the explanation of the method. However, the results which were obtained by its extensive application to the liquid oxygen-ethanol system are also of practical importance. They are discussed in the footnote and concern both optimal and steady combustion chamber design and research. The conclusions, which should be valid for liquid oxygen-hydrocarbon systems of practical interest, include: the assumption of chemical equilibrium of the reaction products appears to be a valid one (it simplifies considerably computations), the liquid fuel vaporizes and burns uniformly in the axial direction (see Fig. 2, for example) rather than actively near the injector and very slowly far from it (it limits the usefulness of the concentrated combustion models sometimes used in stability studies); the gas parameters are not axially uniform (as exemplified in Fig. 2, it explains why the observed longitudinal instability shock wave frequency is found to be close to the complete combustion acoustic chamber frequency); the energy source is not proportional to the mass source (a consequence of the chemical equilibrium of the reaction products, it complicates considerably stability studies); the initial momenta of the liquids are important in steady state computations (they account, for example, for the observed increase of static pressure near the injector, as shown in Fig 1).

APPENDIX E

NOMENCLATURE

NOMENCLATURE LIST

A   Area

B Drop size constant

B_A Drop size constant

C Constant

C_A Atomization rate constant

C_D Drag coefficient

D Diameter

$\bar{D}$ Mass median drop diameter

J_A Drop secondary breakup constant

K Mass transfer coefficient

L' Chamber length

$\dot{M}$ Flowrate

ODE   One dimensional equilibrium

O/F   Mixture ratio

Pc   Chamber pressure

Re_D Reynold's number

T Temperature

U Velocity

V Velocity

W_e Weber number

W_i Local mass flux

ZOM   Cold flow collection plane distance

Z Axial distance

Δ Difference

% C*   Characteristic exhaust velocity efficiency

η_{C*}	Same as % C*
α	Diffusion correction factor
σ	Surface tension, standard deviation
μ.	Viscosity
ρ	Density
ϵ	Chamber contraction ratio
α	Diffusion correction factor

Subscripts

a,s	Vapor pressure at droplet surface
BL	Boundary layer
C	Chamber
d	drop
D	Drop, diameter
eff	Effective throat stagnation pressure
f	Fuel
g	Gas
HL	Heat loss
HW	Hot wax
j	Jet
Kin	Kinetics
l	Liquid
MIX	Mixing
0	Oxidizer
OPP	Opposite orifice
PRED	Predicted
P	Propellant

Subscripts (cont.)

r	Relative
s	Surface, static pressure
T	Throat, total
TD	Two-Dimensional
Test	Test Value
V	Vapor
VAP	Vaporization

APPENDIX F

REFERENCES

REFERENCES

1. Pieper, J. L., _ICRPG Liquid Propellant Thrust Chamber Performance Evaluation Manual_, CPIA 178, September 1968

2. Combs, L. P., "Liquid Rocket Performance Computer Model with Distributed Energy Release", Final Report NASA CR-114462, 10 June 1972

3. _JANNAF Rocket Engine Performance Prediction and Evaluation Manual_, CPIA Publication 246, April 1975

4. Sutton, R. D., et. al., "Operating Manual for Coaxial Injection Combustion Model", NASA CR-129031, Rocketdyne, April 1974

5. _JANNAF Two Dimensional Kinetic (TDK) Reference Program_, Ultrasystems, Inc. Irvine, Ca., December 1973

6. Combs, L. P., "Liquid Rocket Performance Computer Model with Distributed Energy Release", DER Computer Program Documentation and User's Guide Vol. I, 15 December 1971, Revised Edition, 1 January 1974

7. Bracco, F. V., "Application of Steady-State Spray Equations to Combustion Modeling", AIAA Journal Vol. 12, No. 11, 1974

8. Barsotti, R. J., et. al., _Development of Liquid Oxygen/Liquid Hydrogen Thrust Chamber for the M-1 Engine_, NASA CR-54813, Contract NAS 3-2555, 15 May 1968

9. Kovach, R. J., et. al., _Large Hydrogen-Oxygen Ablative Chamber Test Program_, NASA CR 72512, Contract NAS 3-11214, 14 March 1969

10. Evans, R. M., _Boundary Layer Integral Matrix Procedure, BLIMP-J User's Manual_, Contract NAS8-30930, Aerotherm UM-75-64, July 1975

11. Calhoon, D. F., et. al., _Investigation of Gaseous Propellant Combustion and Associated Injector/Chamber Design Guidelines_, NASA CR 121234, 31 July 1973

12. _JANNAF Rocket Engine Performance Test Data Acquisition and Interpretation Manual_, CPIA Publication 245, April 1975

13. Ingebo, R. D., "Maximum Drop Diameters for the Atomization of Liquid Jets Injected Concurrently into Accelerating or Decelerating Gas Streams", NASA TN D-4640, July 1968

14. Ito, J. I., "Development Test Report OMS Injector Subscale Pattern Evaluation", Contract M4J7XMA-483030H, Report No. 6673:207, (PDRD TMO5-25), Aerojet Liquid Rocket Co., March 1976

15. Bracco, F. Y., "An Experimental Analytical Method to Study Steady Spray Combustion", Journal of Spacecraft and Rockets, Vol. 10, No. 6, June 1973, pp. 353-354.

16. Ingebo, R. D., "Vaporization Rates and Drag Coefficients for Isoctane Sprays in Turbulent Air Streams", NACA TN 3265, October 1954

17. Priem, R. J. and Heidmann, M. F., "Propellant Vaporization as a Design Criterion for Rocket Engine Combustion Chambers", NASA TR-R-67, 1960

18. Lawver, B. R., High Performance N_2O_4/Amine Elements - "Blowapart", Contract NAS9-14186, Final Report, ALRC, to be published.

19. Falk, A. Y., High Performance N_2O_4/Amine Elements , Final Report, Contract NAS9-14126, Rocketdyne, March 1976

20. Salmon, J. W. and Pieper, J. L., Design Analysis Procedures Using the JANNAF Distributed Energy Release Computer Program, 11th JANNAF Combustion Meeting, 9-13 September 1974 .

21. Kushida, R., "Application of the Distributed Energy Release (DER) Computer Program to Rocket Engine Performance Analysis II" 10th JANNAF Combustion Meeting, CPIA Publication 243, Volume III, 6-10, August 1973

22. Combs, L. P., "Catalog of Injector Spray Correlations", Contract NAS 7-746, Rocketdyne, 22 June 1972

23. Hines, W. S., et. al., "Extension of a Thrust Chamber Compatibility Model", Final Report AFRPL-TR-72-19, March 1972

24. Dickerson, R. A., et. al., Correlation of Spray Injector Parameters with Rocket Engine Performance, Final Report AFRPL-TR-68-147, Rocketdyne, June 1968

25. Falk, A. Y., et. al., Space Storable Propellant Performance Study, Final Report, NASA CR-72487, Contract NAS 3-11199, Rocketdyne, 24 November 1968

26. Weiss, Malcolm, A., and Worsham, Charles, H., "Atomization in High Velocity Air-Streams", ARS J., Vol. 29, No. 4, April 1959, pp. 252-259

27. Ingebo, R. D., and Foster, H. H., "Drop-Size Distribution for Crosscurrent Breakup of Liquid Jets in Airstreams", NACA TN 4087, 1957

28. Nukiyama, Shiro; and Tanasawa, Yasusi (E. Hope, trans.): Experiments on the Atomization of Liquids in Airstreams, Ref. No. 3, On the Droplet Size Distribution in an Atomized Jet, Defense Res. Board, Dept. Nat. Defense, Ottawa (Canada), Mar. 18, 1950; (Trans from Trans. Soc. Mech. Engr (Japan), Vol. 5, No. 18, Feb. 1939, pp. 62-67)

29. Eisenklam, S. A., et. al., "Evaporation Rates and Drag Resistance on Burning Drops", 11th Symposium on Combustion, 1966, pp. 715-728.

30. El Wakil, M. M., et. al., "Experimental and Calculated Temperature and Mass Histories of Vaporizing Fuel Drops", NACA TN 3490, January 1956

31. Rabin, E., et. al., "Displacement and Shatting of Propellant Droplets", AFOSR-TR-60-75, Rocketdyne, 1960

32. Cramer, F. B., and Baker, P. D., Combustion Processes in a Bipropellant Liquid Rocket Engine, A Critical Review, JPL Report 900-2, 15 Jan. 1967

33. Schuman, M. D., "Distributed Energy Release (DER) Computer Program", Contract F04611-75-C-0055, 2nd Monthly Report, 7 August 1975

34. Breen, B. P., and Beltran, M. R., Steady-State Droplet Combustion with Decomposition: Hydrazine/NTO, presented at AIChE 61st National Meeting, Houston, Texas, February 19-23, 1967

35. Tarifa, C. S. and P. O., del Notario, An Experimental Investigation of The Combustion of Monopropellant Droplets, AFOSR-TN-628, AD 217-813, 1959

36. Sawyer, R. F., The Homogeneous Gas Kinetics of Reaction in the Hydrazine-Nitrogen Tetroxide Propellant System, Princeton Univ. Department of Aerospace and Mechanical Sciences, Tech. Report No. 761, 1965.

37. Webber, W. T., et. al., Plume Contamination Effects Prediction, Final Report, and Program User's Manual, AFRPL-TR-71-109, December 1971

38. Rousar, D. C., Combustion Effects on Film Cooling, Final Report Contract NAS3-17813, Aerojet Liquid Rocket Company, to be published.

39. O'Hara, J. C., et. al., "Analysis of Rocket Combustion Chamber Turbulence Levels from Diffusion Data", Combustion and Flame, Vol. 25, 1975, pp. 161-176.